Metodología para comparar tecnologías solares fotovoltaicas considerando el desempeño eléctrico en condiciones de exterior

César David Londoño Montoya

Trabajo de investigación presentado para optar al título de Magíster en Ingeniería

Director
PhD. Esteban Velilla Hernández
Codirector
PhD. Juan Bernardo Cano Quintero

Universidad de Antioquia
Facultad de Ingeniería
Maestría en Ingeniería
Medellín, Antioquia, Colombia
2023

Cita	(Londoño Montoya, 2023)
Referencia **Estilo APA 7 (2020)**	Londoño Montoya, C. (2023). *Metodología para comparar tecnologías solares fotovoltaicas considerando el desempeño eléctrico en condiciones de exterior, 2021 - 2023* [Tesis de maestría]. Universidad de Antioquia, Medellín, Colombia.

Maestría en Ingeniería, Energética.

Grupo de Investigación Manejo Eficiente de la Energía (GIMEL).

Sede de Investigación Universitaria (SIU).

Centro de Documentación Ingeniería (CENDOI)

Repositorio Institucional: http://bibliotecadigital.udea.edu.co

Universidad de Antioquia - www.udea.edu.co

Agradecimientos

A los profesores del departamento de ingeniería eléctrica de la universidad de Antioquia Esteban Velilla, Juan Bernardo Cano y Jaime Alejandro Valencia por su invaluable apoyo, acompañamiento y mentoría a lo largo de todo este proceso.

A mi familia y en especial a mi compañera de vida Susana Gallón por su paciencia, comprensión y apoyo incondicional.

A amigos y compañeros de trabajo y estudio que siempre mostraron interés y proporcionaron su ayuda y consejo cuando lo necesité. En especial a Santiago Restrepo por estar siempre pendiente y dispuesto a ayudarme y apoyarme en todo momento.

Tabla de contenido

Resumen 7

Abstract 8

1. Introducción 9

2. Planteamiento del problema 14

3. Objetivos 20

3.1 Objetivo general 20

3.2 Objetivos específicos 20

4. Cumplimiento de los objetivos 21

5. Resultados 23

6. Conclusiones 26

7. Trabajos futuros 28

Referencias 29

Anexos 32

Anexo 1: Capacitive tracer design to mitigate incomplete I-V curves in outdoor tests https://doi.org/10.1016/j.solener.2022.08.021 32

Anexo 2: Supporting information of Capacitive tracer design to mitigate incomplete I-V curves in outdoor tests 42

Anexo 3: Outdoor and synthetic performance data for PV devices concerning the weather conditions and capacitor values of I-V tracer https://doi.org/10.1016/j.dib.2023.109007 52

Anexo 4: Photovoltaic performance assess by correcting the I-V curves in outdoor tests https://doi.org/10.1016/j.solener.2022.03.064 65

Anexo 5: Supporting information of Photovoltaic performance assess by correcting the I-V curves in outdoor tests 74

Anexo 6: Photovoltaic Modules Series Resistance Estimation In Outdoor Conditions Using I-V Curves Data (Borrador) 85

Lista de tablas

Tabla I Condiciones de prueba definidas (PRC) en IEC 61853-1, 2011. 15

Lista de figuras

Figura 1. (a) – Distribución de fuentes de generación de energía eléctrica para el año 2030 y 2050 considerando un escenario para lograr mantener el aumento de la temperatura global por debajo de 1.5°C (IRENA - International Renewable Energy Agency, 2022). (b) – Distribución del mercado comercial de paneles solares por tecnología (Ogbomo et al., 2017). 10
Figura 2. Capacidad de energía solar instalada por países y regiones entre el 2010 y 2020 (REN21, 2022)..... 11
Figura 3.Algunas instalaciones para caracterización en exteriores de tecnologías de paneles solares fotovoltaicos (a) (Makrides et al., 2008), (b) (Karami et al., 2017), (c) (Guenounou et al., 2016) y (d) (Visa et al., 2016). 12
Figura 4. Diferentes condiciones de operación entre las 06:00 y las 18:00 horas en Medellín, Colombia. (a) Irradiancia y (b) temperatura ambiente y del panel (línea discontinua). 14
Figura 5. (a) Radiación solar global promedio anual (UPME, 2005) y (b) temperatura promedio anual de Colombia (IDEAM, 2014). 16
Figura 6. Condiciones de operación para la ciudad de Medellín, Colombia, entre las 06:00 y las 19:00 horas durante aproximadamente 18 meses (octubre de 2021 a febrero de 2023). (a) Radiación solar global perpendicular a un plano horizontal (b) temperatura ambiente y del panel. Las líneas oscuras corresponden a la mediana y las áreas sombreadas corresponden a una desviación estándar respecto a la mediana. Los paneles de la derecha corresponden a la distribución de los datos. 17
Figura 7. HSP por mes para la ciudad de Medellín, Colombia, considerando información de aproximadamente 18 meses (octubre de 2021 a febrero de 2023). El panel derecho corresponde a la distribución de los datos de cada uno de los meses. 18
Figura 8. (a) - Curva I-V para STC (SHARP Energy Solutions) y (b) - curvas I-V medidas experimentalmente. 19
Figura 9. Resumen gráfico del trabajo de investigación realizado. 25

Resumen

Este trabajo presenta los resultados de investigación sobre el desempeño de paneles fotovoltaicos en condiciones reales de operación. En una primera etapa se propuso una metodología para el dimensionamiento del capacitor involucrado en el prototipo electrónico para trazar la curva I-V de dispositivos fotovoltaicos. Esta metodología permitió mitigar la obtención de curvas incompletas al considerar la dinámica del capacitor, relés del trazador y sus características, así como del panel en evaluación según el rango objetivo de irradiancia definido. La metodología fue validada con paneles comerciales de diferentes tecnologías mediante curvas I-V simuladas con el programa OpenModelica y curvas I-V obtenidas experimentalmente que consideraron variaciones de irradiancia y temperatura. Los datos experimentales fueron obtenidos en las instalaciones de la Sede de Investigación Universitaria de la Universidad de Antioquia en la ciudad de Medellín, Colombia. Estos registros permitieron validar los rangos teóricos de operación del trazador en función de la irradiancia y capacitancia. Las curvas I-V experimentales fueron el insumo para la segunda etapa del proyecto, la cual consistió en la implementación de una metodología computacional para la estimación del desempeño eléctrico de los paneles. En este sentido, se propuso la metodología de la traslación de curvas I-V para estimar el desempeño del panel en una condición especifica de irradiancia y temperatura a partir de tres curvas medidas a diferentes condiciones atmosféricas considerando la norma IEC 60891. Este procedimiento se hizo de manera extensiva y fue validado considerando registros de medición cada minuto. La técnica de traslación permitió calcular los coeficientes de temperatura de los paneles fotovoltaicos evaluados y verificar los valores dados por los fabricantes en las hojas de datos. Luego, utilizando el método de traslación propuesto, se realizó la estimación y comparación del desempeño eléctrico de cinco paneles fotovoltaicos que fueron evaluados durante aproximadamente 10 meses. Por último, se propone una metodología para la estimación de la resistencia serie de paneles fotovoltaicos a partir de curvas I-V, utilizando como insumo la técnica de traslación y la metodología de Suns V_{oc}. Las técnicas de traslación y resistencia serie pueden ser utilizadas para calcular la degradación de los dispositivos.

Palabras clave — **Pruebas en exteriores, desempeño de paneles fotovoltaicos, curvas I-V, medidores capacitivos de curvas I-V, condiciones atmosféricas, condiciones reales de operación.**

Abstract

This work presents the research results on the performance of photovoltaic panels under real operating conditions. In the first stage, a methodology was proposed for sizing the capacitor involved in the electronic prototype for tracing the I-V curve of photovoltaic devices. This methodology allowed mitigating the obtaining of incomplete curves by considering the dynamics of the capacitor, tracer relays and their characteristics, as well as the panel under evaluation and according to the defined irradiance range objective. The methodology was validated with commercial panels of different technologies by I-V curves simulated with the OpenModelica program and real I-V curves that considered variations of irradiance and temperature. Real information was obtained at the Sede de Investigación Universitaria of the Universidad de Antioquia in Medellin, Colombia. These records allowed validating the theoretical operating ranges of the tracer based on irradiance and capacitance. The real I-V curves were the input for the second stage of the project, which consisted of the implementation of a computational methodology for the estimation of the panel's electrical performance. In this sense, the I-V curve translation methodology was proposed to estimate the panel performance in a specific condition of irradiance and temperature from three measured curves at different atmospheric conditions based on the IEC 60891 standard. This procedure was done extensively and validated considering measurement records every minute. The translation technique allowed the calculation of the temperature coefficients of the evaluated photovoltaic panels and to verify the values given by the manufacturers in the data sheets. Then, using the proposed translation method, the electrical performance estimation and comparison of five photovoltaic panels were carried out, which were evaluated for approximately 10 months. Finally, a methodology is proposed for the estimation of the series resistance of photovoltaic panels from I-V curves, using the translation technique and the Suns Voc methodology as inputs. The translation and series resistance techniques can be used to observe the performance evolution over time and thus calculate the degradation of the devices.

Keywords — **Outdoor tests, Photovoltaic device performance, I-V curves, Capacitive I-V tracers, Weather conditions, Outdoor conditions.**

1. Introducción

Los paneles solares son dispositivos que transforman la energía solar en energía eléctrica mediante celdas solares compuestas por diferentes materiales fotovoltaicos y estructuras de diseño. A lo largo de los años, se ha investigado y desarrollado diversas tecnologías de paneles solares, que generalmente se clasifican en tres categorías principales (Mussard and Amara, 2018):

1. **Primera generación:** Conformada por dispositivos elaborados con silicio, en su estructura monocristalina y policristalina. Estos dispositivos son los que presentan mayor madurez tecnológica y los que mayor cuota de mercado tienen e igualmente han sido usados y probados durante muchos años. Se caracterizan por tener un periodo de vida útil importante (entre 20 y 25 años) y que su materia prima es abundante, pero de alta complejidad para su obtención y fabricación.

2. **Segunda generación:** Conformada por paneles de película delgada (*thin film*) que presentan grandes ventajas respecto a la primera generación como menor consumo de materias primas para su fabricación, fácil integración con edificaciones, fabricación más fácil y menor efecto de la temperatura para su funcionamiento.

3. **Tercera generación:** Compuesta por dispositivos de celdas solares sensibilizadas por colorantes (*Dye-sensitized solar cells*) las cuales son elaboradas con materiales foto-electro-químicos mezclados con materiales semiconductores. Por el momento estos dispositivos a gran escala presentan menores eficiencias a comparación otras tecnologías, pero existe gran interés por parte de empresas y academias y se encuentran en fases de investigación y desarrollo.

Algunas de las mayores eficiencias, según su tecnología, alcanzadas para paneles fotovoltaicos hasta la fecha son: 24.4 % para silicio cristalino, 20.4 para silicio multicristalino, 19.2 % para CIGS, 12.3 % para silicio amorfo, 17.9 % para perovskite y 8.7 % para orgánicas (Green et al., 2023). Lo anterior muestra que existe una gran variedad de eficiencias según la tecnología o materiales semiconductores utilizados en la fabricación. Por tanto, es de esperar que el desempeño

eléctrico de cada tecnología dependa de las condiciones atmosféricas y características geográficas del lugar donde sean instaladas.

En la Figura 1 (a) se muestra la proporción de los tipos de generación de energía eléctrica para el año 2030 y 2050 a nivel mundial con los que se lograría cumplir la meta de mantener el aumento de la temperatura global del planeta por debajo de los 1.5°C, donde se evidencia el papel importante que se espera tengan los paneles solares fotovoltaicos para suplir la demanda de energía eléctrica. De las diferentes tecnologías de paneles solares se tiene que la primera generación conformada por módulos de silicio en su forma monocristalina y policristalina dominan el mercado, ya que como se observa en la Figura 1 (b), aproximadamente el 74 % corresponden a paneles de estos materiales, donde las demás tecnologías y generaciones se distribuyen el porcentaje restante.

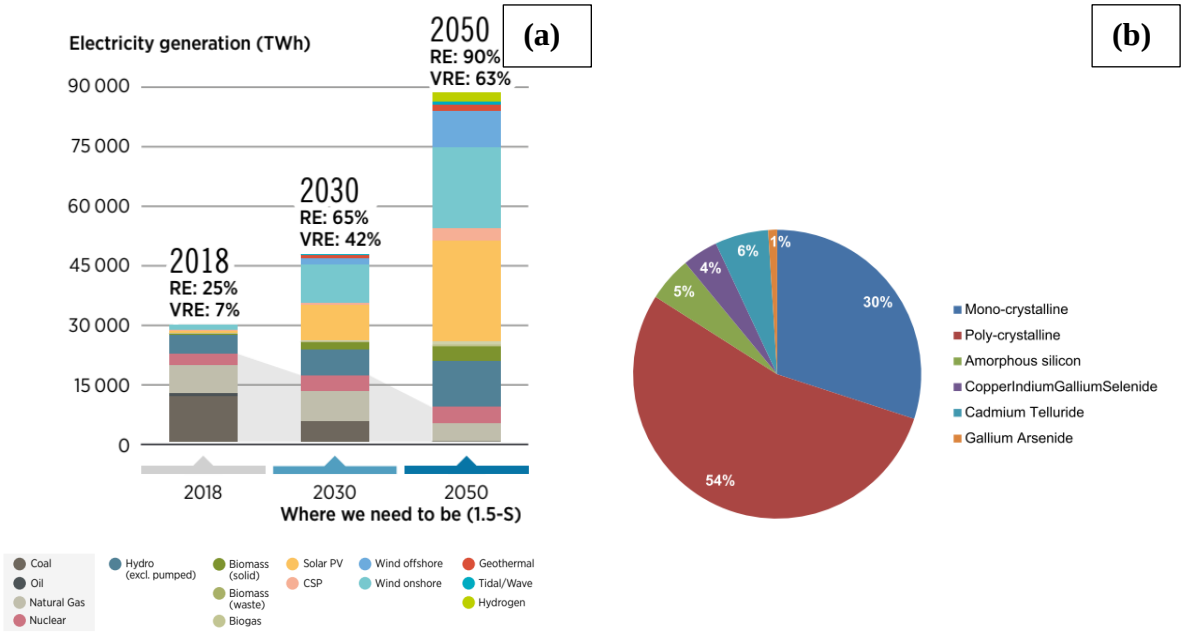

Figura 1. (a) – Distribución de fuentes de generación de energía eléctrica para el año 2030 y 2050 considerando un escenario para lograr mantener el aumento de la temperatura global por debajo de 1.5°C (IRENA - International Renewable Energy Agency, 2022). (b) – Distribución del mercado comercial de paneles solares por tecnología (Ogbomo et al., 2017).

La distribución de la capacidad instalada de generación de energía mediante paneles solares a nivel global se centra principalmente en algunos países y regiones, como se muestra en la Figura 2, donde China, Estados Unidos, Japón, India y la Unión Europea concentran el mayor porcentaje

de esta capacidad, pero donde se observa que el resto de países del mundo han ido tomando una mayor relevancia en los últimos años.

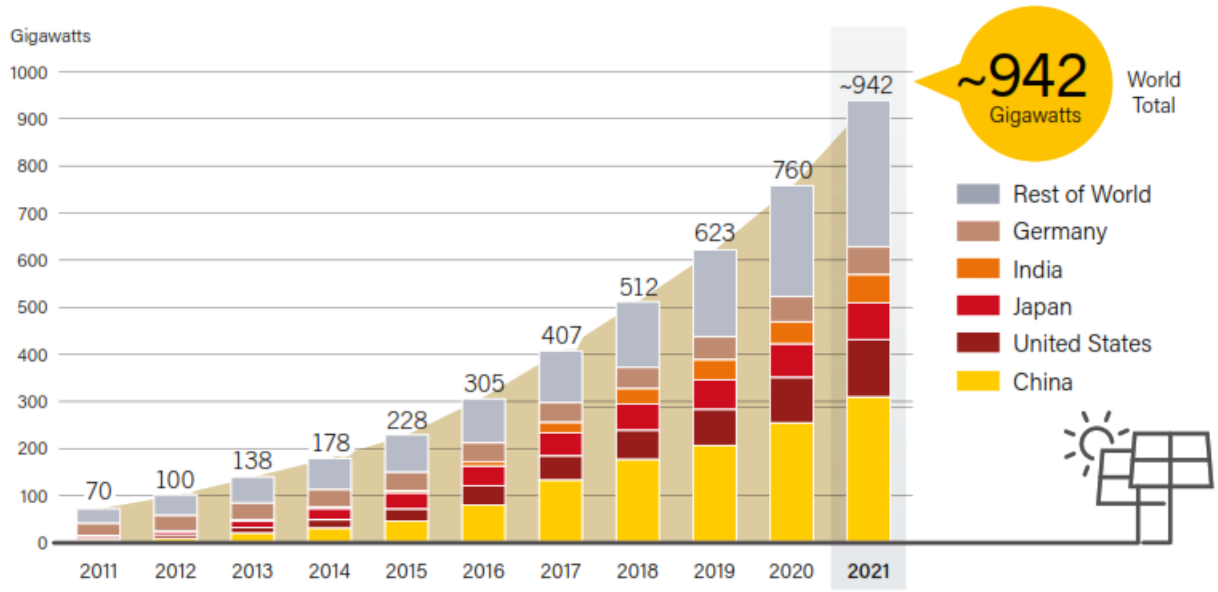

Figura 2. Capacidad de energía solar instalada por países y regiones entre el 2010 y 2020 (REN21, 2022).

El desempeño eléctrico de dispositivos fotovoltaicos (celdas y módulos), tradicionalmente se evalúa en laboratorios utilizando simuladores solares y condiciones atmosféricas controladas como las especificadas en las hojas de datos de los dispositivos conocidas como condiciones estándar de prueba (STC, por sus siglas en inglés). Sin embargo, este enfoque conlleva costos elevados debido a la necesidad de equipos especializados de medición y simulación de condiciones ambientales específicas.

Una limitación importante de las pruebas en laboratorio es que las condiciones simuladas pueden no representar completamente el entorno real al que los paneles solares están expuestos. En condiciones reales de operación, los paneles solares están sujetos a variaciones climáticas, como la intensidad y dirección de la radiación solar, la temperatura ambiente, la humedad y otros factores ambientales, que pueden afectar su desempeño eléctrico de manera significativa.

Para abordar esta limitación, las evaluaciones de paneles fotovoltaicos en condiciones reales se realizan generalmente en el ámbito académico en instalaciones de universidades y centros de

investigación, lo que presenta un desafío adicional. Estos dispositivos no son sometidos a las mismas condiciones atmosféricas y ambientales que se encuentran en laboratorios con simuladores solares, lo que puede generar discrepancias en los resultados obtenidos.

A pesar de estos desafíos, las evaluaciones en condiciones reales son importantes para comprender el verdadero desempeño de los dispositivos fotovoltaicos y su adecuación para aplicaciones prácticas. Estos estudios permiten proporcionar datos más representativos de la eficiencia y el comportamiento de los paneles solares en situaciones reales, lo que ayuda a mejorar la precisión de las predicciones de rendimiento y a optimizar su diseño y funcionamiento en aplicaciones.

En la Figura 3 se muestran algunas instalaciones donde se han caracterizado y monitoreado tecnologías de paneles solares, donde se observan los diferentes colores y materiales usados para la construcción de los módulos, y que generalmente se disponen los paneles bajo las mismas configuraciones de ángulo y orientación.

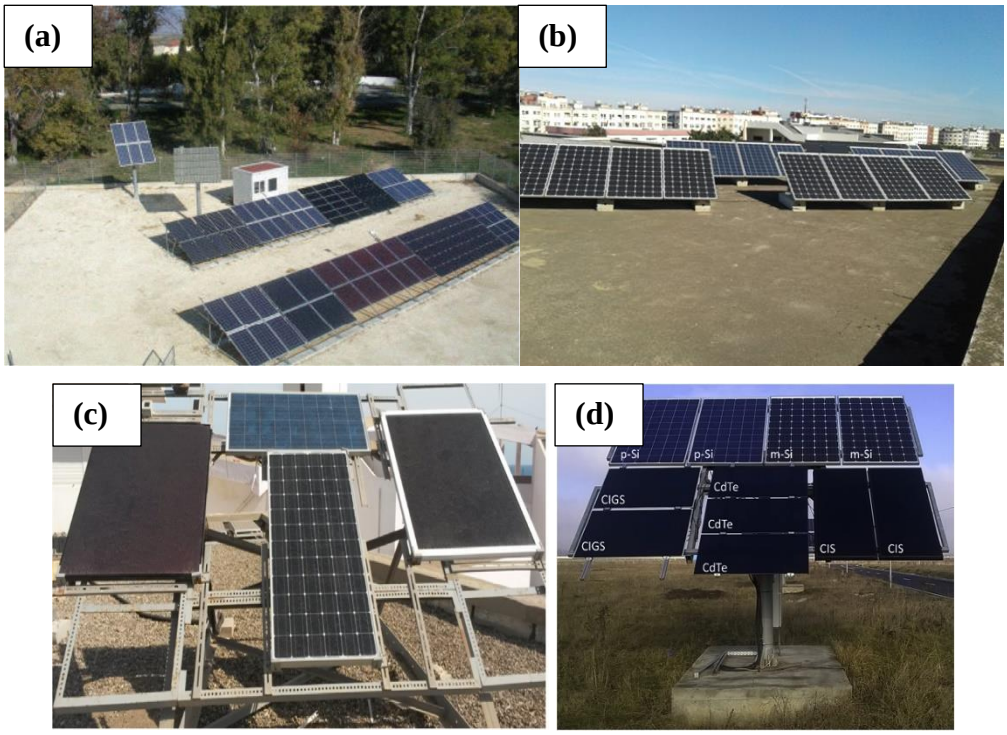

Figura 3.Algunas instalaciones para caracterización en exteriores de tecnologías de paneles solares fotovoltaicos (a) (Makrides et al., 2008), (b) (Karami et al., 2017), (c) (Guenounou et al., 2016) y (d) (Visa et al., 2016).

Al momento de caracterizar paneles solares en condiciones de exterior se pueden presentar los siguientes retos y problemas:

- Simultaneidad y sincronización de la información experimental para poder hacer comparaciones directas (Gaglia et al., 2017; Katsaounis et al., 2019; Louwen et al., 2017; Wang et al., 2018).
- Calidad de las curvas I-V registradas (Balaska et al., 2017; Park et al., 2019; Wang et al., 2018).
- Ubicación geográfica y sus condiciones atmosféricas asociadas (Kaaya et al., 2019; Wang et al., 2018).
- Acumulación de materiales sobre los paneles (Nieve, suciedad, contaminación, entre otros) (Kaaya et al., 2019; Wang et al., 2018).
- Métodos de medición rápidos que garanticen condiciones estables (Akhmad et al., 1997).
- Métricas para comparar su desempeño (Eke et al., 2017; Elibol et al., 2017).
- Frecuencia de obtención de la información experimental (Dunlop and Halton, 2006; Eke et al., 2017; Wang et al., 2018)

2. Planteamiento del problema

Para caracterizar el desempeño paneles fotovoltaicos, tradicionalmente se han utilizado condiciones de prueba estándar o STC por sus siglas en inglés, las cuales son mediciones realizadas bajo condiciones controladas, generalmente en laboratorios a través de simuladores solares, donde se utiliza una temperatura del módulo de 25°C, una irradiancia de 1000W/m^2, una masa de aire 1.5 (AM1.5) y 0 velocidad del viento (IEC 60904-3, 2019). Las condiciones de STC no son condiciones reales a las que son expuestos estos dispositivos para su operación continua durante sus años de funcionamiento (Figura 4), por lo que no se puede comparar directamente su rendimiento con los valores reportados por los fabricantes, que generalmente lo reportan para condiciones STC.

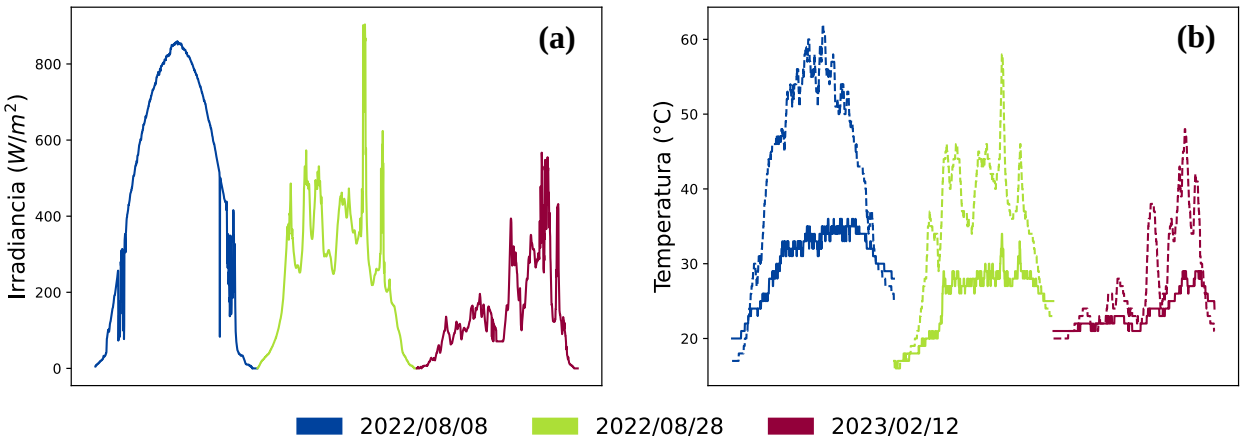

Figura 4. Diferentes condiciones de operación entre las 06:00 y las 18:00 horas en Medellín, Colombia. (a) Irradiancia y (b) temperatura ambiente y del panel (línea discontinua).

Se han definido otras condiciones de prueba para los paneles fotovoltaicos con el fin de caracterizar su desempeño eléctrico en diferentes condiciones, logrando con esto un mayor rango de caracterización y cubriendo condiciones más probables para su operación real (IEC 61853-1, 2011), estas condiciones también se conocen como *Power Rating Conditions* o *PRC*. Estas condiciones son definidas en la sección 7. Es de resaltar que hasta el momento es la única norma que se tiene para realizar evaluación de paneles solares fotovoltaicos bajo condiciones de exterior. Principalmente consisten en evaluar los paneles valores específicos de irradiancia y temperatura de operación del dispositivo, y donde no se define cuanto tiempo mínimo es necesario para la

caracterización bajo estas condiciones, solo se debe cumplir con tener las condiciones allí requeridas, lo que desencadena que muchas otras condiciones no sean tenidas en cuenta para la caracterización del desempeño de estos dispositivos. En la Tabla I se presentan las características definidas para la medición en cada condición.

Tabla I
Condiciones de prueba definidas (PRC) en IEC 61853-1, 2011.

Nombre	Abreviación	Irradiancia [W/m^2]	Temperatura del módulo [°C]
Hight Temperature Conditions	HTC	1000	75
Low Irradiance Conditions	LIC	200	25
Low Temperature Conditions	LTC	500	15
Normal Operating Cell Temperature	NOCT	800	20 (ambiente)
Standard Test Conditions	STC	1000	25

Las condiciones descritas en la Tabla I abarcan diferentes temperaturas e irradiancias, pero representan condiciones de medición específicas que generalmente se logran de forma más fácil en ambientes controlados. Debido a que las variables atmosféricas bajo las cuales operan los paneles fotovoltaicos presentan variaciones durante el día, la época del año y la ubicación geográfica, no es posible caracterizar el desempeño para un rango real de condiciones de operación únicamente con este tipo de métricas, lo que por consecuencia tampoco permite determinar completamente qué tipo de tecnología presentará un mejor desempeño para las características bajo las cuales va a ser instalada o si el dispositivo cumple con las información entregada por su fabricante.

En la Figura 5 se presentan los mapas de radiación solar y temperatura promedio anual para el territorio colombiano, donde se puede observar que existe diversidad de zonas con diferentes comportamientos y valores, lo que podrá representar que existan tecnologías que se desempeñen de forma diferente según las características de cada zona, por lo que la selección adecuada de esta tendrá un papel fundamental, teniendo como objetivo principal optimizar de mejor forma los recursos y con esto tener un mejor desempeño de las instalaciones y proyectos.

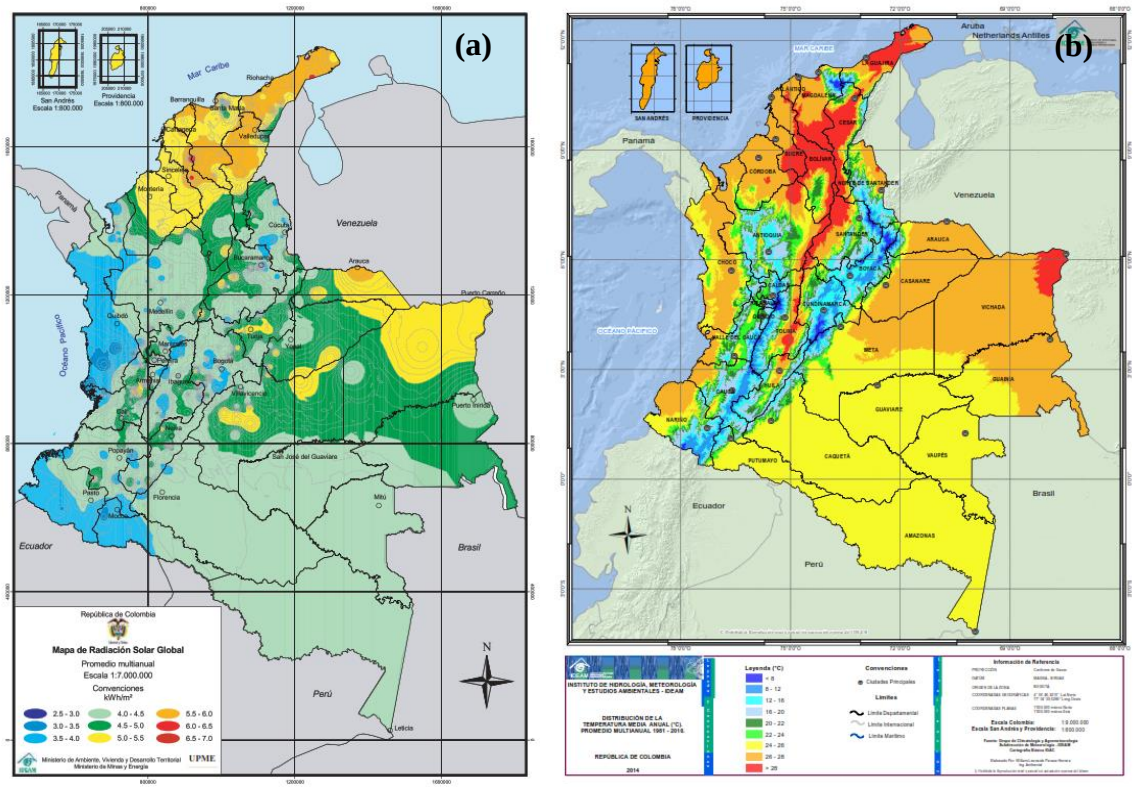

Figura 5. (a) Radiación solar global promedio anual (UPME, 2005) y (b) temperatura promedio anual de Colombia (IDEAM, 2014).

En la Figura 6 se presenta el comportamiento de tres variables atmosféricas que influyen en el desempeño de dispositivos fotovoltaicos medidas en el laboratorio de caracterización de dispositivitos fotovoltaicos en condiciones de exterior del grupo GIMEL de la Universidad de Antioquia. Se observa que estas variables toman un rango de valores a lo largo del día, lo que complementa lo observado en la Figura 5, donde se mostraba un comportamiento promedio global anual. Por lo que se observa que se presentan variaciones en estas variables según su ubicación geográfica y que para cada lugar también existen variaciones a lo largo del día. Estas condiciones muestran la importancia de contar con una metodología para estimar el rendimiento de los dispositivos en condiciones reales de operación, ya que no son condiciones constantes y se debe estandarizar o tomar un punto de referencia para evaluar o estimar su rendimiento a lo largo del tiempo.

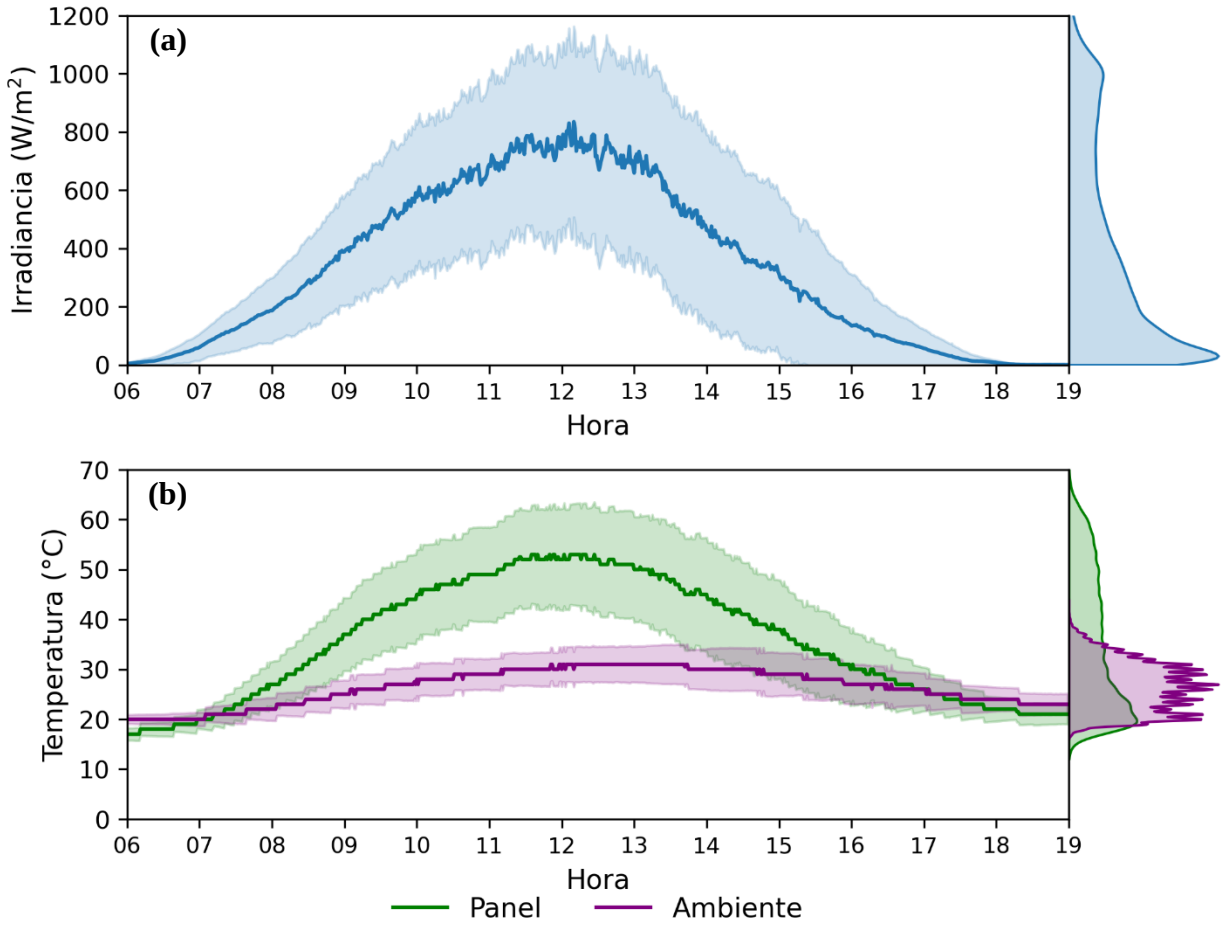

Figura 6. Condiciones de operación para la ciudad de Medellín, Colombia, entre las 06:00 y las 19:00 horas durante aproximadamente 18 meses (octubre de 2021 a febrero de 2023). (a) Radiación solar global perpendicular a un plano horizontal (b) temperatura ambiente y del panel. Las líneas oscuras corresponden a la mediana y las áreas sombreadas corresponden a una desviación estándar respecto a la mediana. Los paneles de la derecha corresponden a la distribución de los datos.

En Figura 7 se muestran las HSP para cada mes del año calculadas para Medellín, Colombia en el laboratorio solar del grupo GIMEL de la Universidad de Antioquia. Se observa que está ubicación presenta variaciones en cuanto al desempeño solar a lo largo del año pero que por su ubicación cuenta con un buen comportamiento de radiación solar durante todo el año, con un promedio diario anual de 4.6 HSP.

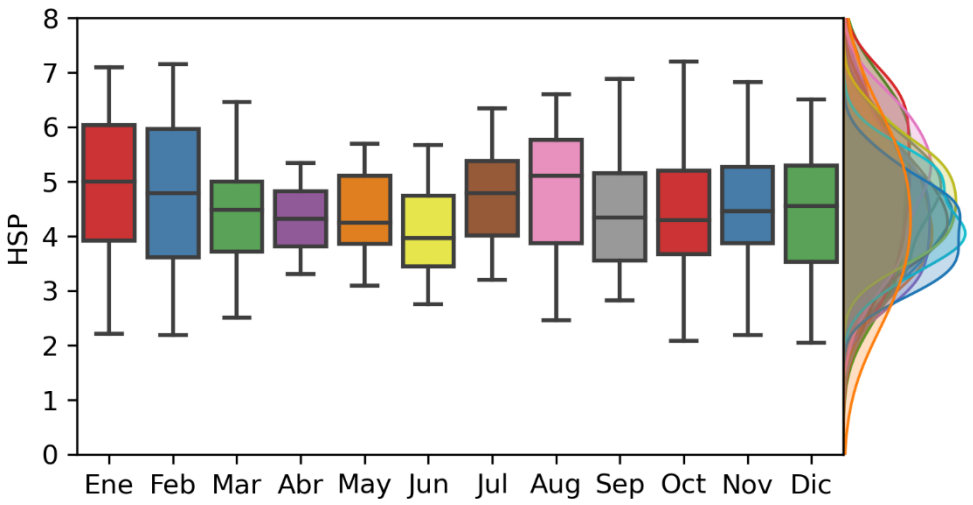

Figura 7. HSP por mes para la ciudad de Medellín, Colombia, considerando información de aproximadamente 18 meses (octubre de 2021 a febrero de 2023). El panel derecho corresponde a la distribución de los datos de cada uno de los meses.

Un reto en la caracterización de paneles fotovoltaicos en condiciones reales de funcionamiento es el método que se usa para la obtención de los datos eléctricos de operación y la velocidad que se necesita para el registro de información, ya que se busca que esta sea lo más rápida posible con el fin de garantizar condiciones atmosféricas constantes mientras la captura de los registros. En la Figura 8 se muestran curvas I-V de un panel fotovoltaico Sharp NU-RC290, donde la curva (a) corresponde a la reportada por el fabricante en su hoja de datos para condiciones STC y las curvas de la imagen de (b) corresponden a curvas registradas de forma experimental, obtenidas mediante la técnica de medición capacitiva, donde según el área que cubren las curvas se puede concluir que el panel estuvo expuesto a diferentes condiciones atmosféricas. Se observa además que al utilizar la técnica de medición de curvas I-V a través del método capacitivo se puede llegar a perder información, debido principalmente a la capacitancia utilizada y a las características electrónicas (tiempos, frecuencia de medición, entre otros) del equipo caracterizador. Sin embargo, esta técnica es una de las más utilizadas para condiciones de exterior ya que es económica, fácil de implementar y permite tener tiempos cortos de medición con el fin de realizar la captura de las curvas bajo las mismas condiciones atmosféricas (Velilla et al., 2019).

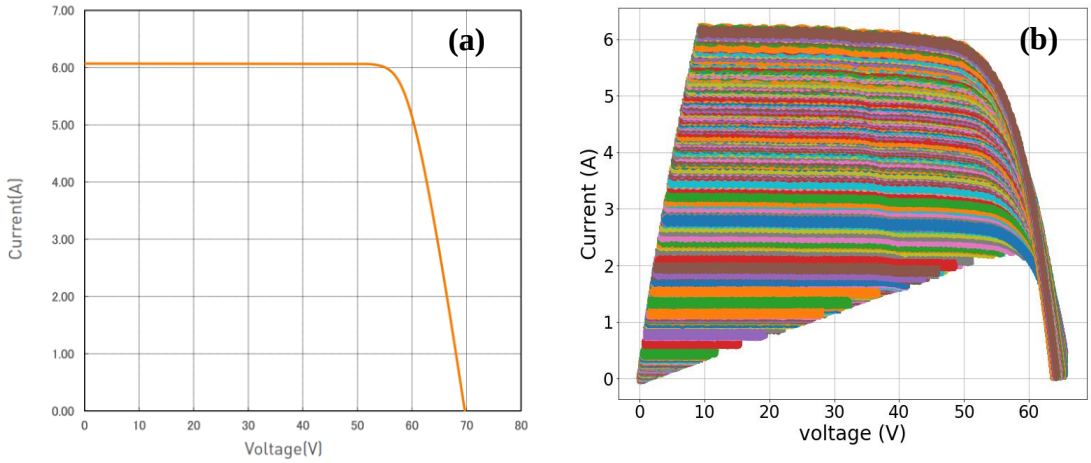

Figura 8. (a) - Curva I-V para STC (SHARP Energy Solutions) y (b) - curvas I-V medidas experimentalmente.

En condiciones de exterior se han planteado en la literatura diferentes métodos para estimar y calcular el desempeño de paneles fotovoltaicos, tanto para horizontes de tiempo cortos como largos pero no se tiene un consenso general, ya que este no es un proceso simple debido a que intervienen factores como la calidad de información medida, su procesamiento y las metodologías usadas para esto, lo que incluso puede ocasionar que partiendo de la misma información se obtengan resultados diferentes (Jordan et al., 2017). Por este motivo es importante contar con un procedimiento robusto que permita realizar la evaluación y comparación del desempeño eléctrico para condiciones de exterior de dispositivos solares fotovoltaicos.

3. Objetivos

3.1 Objetivo general

Implementar computacionalmente una metodología para comparar el desempeño eléctrico de tecnologías solares fotovoltaicas evaluadas en condiciones de exterior, considerando estándares internacionales aplicables.

3.2 Objetivos específicos

1. Estudiar el impacto de variables atmosféricas como irradiancia y temperatura en el desempeño eléctrico bajo condiciones de exterior de las tecnologías solares fotovoltaicas seleccionadas.

2. Investigar modelos, procedimientos y/o metodologías computacionales que puedan ser usados para la comparación de tecnologías solares fotovoltaicas evaluadas en condiciones de exterior considerando el impacto de variables atmosféricas en el desempeño eléctrico de los módulos.

3. Implementar computacionalmente metodología para la comparación del desempeño eléctrico de tecnologías solares fotovoltaicas en condiciones de exterior y validarla respecto al(los) modelo(s) y/o criterio(s) seleccionado(s) utilizando datos reales de desempeño eléctrico y condiciones específicas del lugar de instalación.

4. Cumplimiento de los objetivos

Este trabajo de investigación se ha estructurado como la compilación de tres artículos que son el resultado del proceso académico y de investigación desarrollado. Mediante estos artículos se da cumplimiento a los objetivos propuestos en la sección 3. Los artículos y los *supporting information* asociados a estos se encuentran anexos al final de este documento.

Mediante los artículos *Capacitive tracer design to mitigate incomplete I-V curves in outdoor tests* y *Outdoor and synthetic performance data for PV devices concerning the weather conditions and capacitor values of I-V tracer* (Londoño et al., 2022) se abordan los objetivos específicos 1 y 2 ya que se estudia el efecto de variables atmosféricas como la irradiancia sobre el comportamiento de los parámetros eléctricos derivados de la curva I-V como por ejemplo Voc e Isc de tres paneles fotovoltaicos de diferentes tecnologías y se identifica y soluciona el problema de la calidad de las curvas I-V mediante la propuesta de una metodología adecuada de dimensionamiento de la capacitancia, la cual es comprobada de forma experimental y teórica a través de datos experimentales y simulados respectivamente.

El objetivo específico 3 es abordado en el artículo llamado *Photovoltaic performance assess by correcting the I-V curves in outdoor tests* (Padilla et al., 2022) en el cual se propone e implementa computacionalmente una metodología de traslación de parámetros eléctricos de paneles fotovoltaicos que permite estimar el desempeño de estos dispositivos para una misma condición de temperatura irradiancia y con esto poder llevar a cabo una comparación evaluación del desempeño de estos en condiciones reales de operación.

Adicionalmente, para el cumplimento del objetivo específico 3, se ha desarrollado una metodología para la estimación y seguimiento de la resistencia serie de dispositivos fotovoltaicos en condiciones de exterior. Estos resultados se están compilando para una nueva publicación, se anexa una versión borrador de dicha metodología en el *Anexo 6: Photovoltaic Modules Series Resistance Estimation In Outdoor Conditions Using I-V Curves Data (Borrador)*.

Después de completar los objetivos específicos, se logra dar complimiento al objetivo general propuesto, ya que se propuso e implementó la metodología de traslación de parámetros eléctricos de dispositivos fotovoltaicos instalados en condiciones de exterior, la cual entre sus principales ventajas y aplicaciones se encuentran:

- Comprobación del desempeño eléctrico informado por los fabricantes.
- Estimación de parámetros eléctricos para condiciones específicas de operación.
- Cálculo de los coeficientes de temperatura.
- Medición de la degradación.
- Detección de fallas de los dispositivos.
- Seguimiento en línea del desempeño.
- Disminución de la dispersión en la estimación de los parámetros eléctricos.

A través de esta técnica se realiza una estimación y comparación del desempeño de diferentes tecnologías fotovoltaicas a través del cálculo de la potencia máxima y de la resistencia serie para condiciones específicas de temperatura e irradiancia, pudiendo observar con estas condiciones fijas la evolución de estos parámetros en el tiempo de evaluación de los dispositivos. Lo anterior puede ser observado en la Figura 9.

5. Resultados

En la Figura 9 se muestra de forma gráfica un resumen del trabajo de investigación realizado y los principales resultados obtenidos. A continuación, se describe cada una de las secciones de esta figura:

Sección superior izquierda: Esta sección corresponde con la obtención y manejo de información, allí se capturó el desempeño de diferentes tecnologías de paneles solares a través de curvas I-V (Velilla et al., 2019) medidas cada minuto y de forma simultánea para todos los paneles durante las horas de luz día y variables atmosféricas como irradiancia y temperatura utilizando el laboratorio de evaluación y caracterización de tecnologías fotovoltaicas del grupo GIMEL de la Universidad de Antioquia, el cual se encuentra ubicado en la Sede de Investigación Universitaria en la ciudad de Medellín, Colombia. Adicionalmente se abordó el reto de mejorar la calidad de las curvas I-V medidas, ya que en algunas condiciones estas quedaban incompletas, a través de la propuesta de una metodología de dimensionamiento adecuada del capacitor (Londoño et al., 2022) y con esto mejorar el desempeño de los demás análisis y metodologías realizadas a partir de la información en condiciones de exterior (Londoño et al., 2023).

Sección inferior izquierda: Está sección aborda el reto y objetivo del desarrollo de una metodología computacional a través de la cual se pueda realizar una comparación del desempeño de paneles fotovoltaicos en condiciones reales de operación. Para esto, se propuso e implementó un método aleatorio e iterativo para estimar diferentes parámetros eléctricos de los paneles dada una condición especifica de temperatura y nivel de radiación solar (Padilla et al., 2022).

Sección derecha: Esta sección corresponde a los resultados finales después de haber aplicado los procedimientos desarrollados en las dos secciones anteriores (azul y verde). Para esto se parte de datos de desempeño de paneles fotovoltaicos en condiciones de exterior (curvas IV, irradiancia y temperatura), con estos datos se realiza la metodología de traslación propuesta para estimar los parámetros para una condición especifica (STC) y finalmente se obtiene el desempeño eléctrico de estos (P_{max}). Estos mismos datos experimentales son utilizados para la estimación de la resistencia serie y su evolución en el tiempo aplicando la metodología de cálculo de resistencia

serie que se propone como resultado adicional de este trabajo de investigación. En total se evaluó y comparó el desempeño de cinco paneles fotovoltaicos durante aproximadamente 10 meses, según como se muestra en la imagen de esta sección.

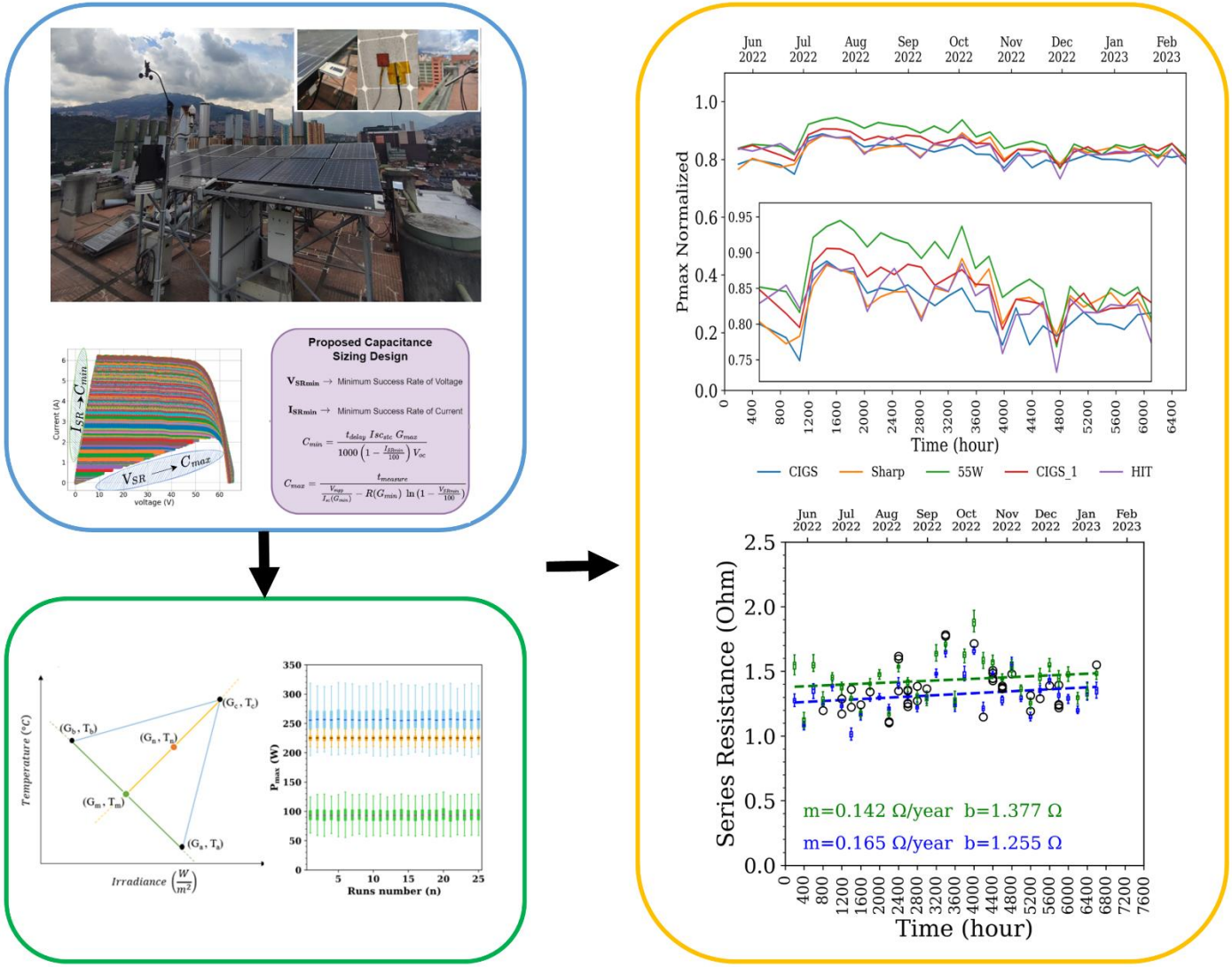

Figura 9. Resumen gráfico del trabajo de investigación realizado.

6. Conclusiones

Se desarrolló una metodología que permite comparar de forma simultánea diferentes tecnologías de paneles solares fotovoltaicos bajo condiciones reales de operación, la cual también puede ser usada para realizar análisis de degradación y detección de fallas en estos equipos, facilitando la implementación de medidas de mantenimiento preventivo y correctivo, contribuyendo así a prolongar la vida útil de los sistemas y maximizar su rendimiento a lo largo del tiempo. Al proporcionar una evaluación simultánea, esta metodología permite a investigadores y profesionales del área comprender mejor el rendimiento de cada dispositivo en relación con las condiciones específicas de operación, lo que resulta valioso en un entorno donde la tecnología solar está en constante evolución y se busca maximizar la producción de energía y la rentabilidad de los sistemas fotovoltaicos. La metodología fue aplicada a datos experimentales de curvas I-V obtenidas de forma simultánea para cinco paneles fotovoltaicos de diferentes tecnologías instalados en la ciudad de Medellín, Colombia.

Se realizó el registro de forma simultánea de las curvas I-V de cinco paneles fotovoltaicos de diferentes tecnologías, utilizando caracterizadores electrónicos de paneles desarrollados por el grupo GIMEL, los cuales se basan en la técnica capacitiva para la adquisición de las curvas. La sincronización en la medición permitió garantizar que los paneles fueran evaluados bajo las mismas condiciones atmosféricas, ya que la adquisición de las curvas era al mismo tiempo para todos. Las curvas I-V registradas fueron el insumo principal para los demás análisis y metodologías que se implementaron.

Se desarrolló una metodología de dimensionamiento de la capacitancia para medición de curvas I-V bajo condiciones de exterior considerando dos índices de desempeño (V_{SR} e I_{SR}), las características del equipo de medición de la curva y del panel fotovoltaico a evaluar. Esta metodología fue validada con datos teóricos, simulados y experimentales. Los resultados de estas validaciones demostraron que las consideraciones y simplificaciones de diseño propuestas son apropiadas, permitiendo ajustar el dimensionamiento del capacitor para diferentes escenarios de medición, mitigando así las curvas I-V incompletas obtenidas en condiciones de exterior.

Se demostró la relevancia en el proceso de diseño del retardo de la conmutación en los relés del equipo trazador de curvas I-V mediante la metodología capacitiva, que juega un papel importante al inicio del proceso de carga del capacitor afectando la región de I_{sc}. Esto indica que se deben usar dispositivos de conmutación rápida para el desarrollo de trazadores I-V con el fin de no disminuir la calidad de las curvas I-V medidas.

Se mitigó la perdida de datos en los extremos de las curvas I-V (zonas de V_{oc} e I_{sc}) de las curvas experimentales registradas en las instalaciones del laboratorio solar del grupo GIMEL al utilizar la metodología de dimensionamiento de la capacitancia y los índices de desempeño propuestos (V_{SR} e I_{SR}) para seleccionar el capacitor acorde con las características del equipo de medición (trazador de curvas I-V), del panel solar y el rango objetivo de irradiancia.

Se propuso e implementó una metodología computacional que permite estimar el desempeño de dispositivos fotovoltaicos en condiciones de exterior, utilizando un proceso aleatorio para la selección de los puntos que se consideran para hacer la traslación y de allí estimar según condiciones específicas de temperatura e irradiancia el valor de los principales parámetros eléctricos de estos dispositivos y finalmente con esto realizar una comparación entre diferentes tecnologías de paneles fotovoltaicos.

Adicionalmente, la metodología de traslación desarrollada fue utilizada para la estimación de los coeficientes de temperatura de los paneles fotovoltaicos evaluados, permitiendo calcular estos de forma práctica y obteniendo resultados en el rango de los valores reportados por los fabricantes y del comportamiento esperado de estos dispositivos.

Se propone una metodología para realizar la estimación y seguimiento de la resistencia serie de dispositivos fotovoltaicos en condiciones de exterior la cual parte de las curvas I-V y de la temperatura de operación del dispositivo, y a través de la técnica de traslación y el método Suns V_{oc} permite el cálculo de esta variable. Esta metodología complementa el seguimiento del desempeño de estos dispositivos, ya que permite realizar análisis de degradación y detección de fallas según el comportamiento de esta variable.

7. Trabajos futuros

En esta sección se presentan los posibles trabajos futuros que pueden ser planteados a partir de la temática y los resultados obtenidos del presente trabajo de investigación:

- Aplicar la metodología de traslación a información recolectada a lo largo de varios años, para otras tecnologías y para otras ubicaciones geográficas.
- Implementar modelos que utilicen la metodología de traslación para realizar predicción de desempeño e identificación de degradaciones tempranas.
- Implementar metodologías basadas en la traslación para estimar la degradación de los paneles fotovoltaicos.
- Evaluar el desempeño de MPPTs e inversores a partir de la metodología de traslación.
- Mejorar la metodología de dimensionamiento del capacitor utilizando bancos de capacitancia variable.
- Mejorar el desempeño de los trazadores de las curvas I-V al utilizar relés de conmutación mucho más rápida.
- Realizar estudios comparativos para analizar cómo la variación de la resistencia serie afecta el rendimiento general de los paneles solares y su eficiencia en diferentes entornos.

Referencias

Akhmad, K., Kitamura, A., Yamamoto, F., Okamoto, H., Takakura, H., Hamakawa, Y., 1997. Outdoor performance of amorphous silicon and polycrystalline silicon PV modules. Sol. Energy Mater. Sol. Cells 46, 209–218. https://doi.org/10.1016/S0927-0248(97)00003-2

Balaska, A., Tahri, A., Tahri, F., Stambouli, A.B., 2017. Performance assessment of five different photovoltaic module technologies under outdoor conditions in Algeria. Renew. Energy 107, 53–60. https://doi.org/10.1016/j.renene.2017.01.057

Dunlop, E.D., Halton, D., 2006. The performance of crystalline silicon photovoltaic solar modules after 22 years of continuous outdoor exposure. Prog. Photovoltaics Res. Appl. 14, 53–64. https://doi.org/10.1002/pip.627

Eke, R., Betts, T.R., Gottschalg, R., 2017. Spectral irradiance effects on the outdoor performance of photovoltaic modules. Renew. Sustain. Energy Rev. 69, 429–434. https://doi.org/10.1016/j.rser.2016.10.062

Elibol, E., Özmen, Ö.T., Tutkun, N., Köysal, O., 2017. Outdoor performance analysis of different PV panel types. Renew. Sustain. Energy Rev. 67, 651–661. https://doi.org/10.1016/j.rser.2016.09.051

Gaglia, A.G., Lykoudis, S., Argiriou, A.A., Balaras, C.A., Dialynas, E., 2017. Energy efficiency of PV panels under real outdoor conditions–An experimental assessment in Athens, Greece. Renew. Energy 101, 236–243. https://doi.org/10.1016/j.renene.2016.08.051

Green, M.A., Dunlop, E.D., Siefer, G., Yoshita, M., Kopidakis, N., Bothe, K., Hao, X., 2023. Solar cell efficiency tables (Version 61). Prog. Photovoltaics Res. Appl. 31, 3–16. https://doi.org/10.1002/pip.3646

Guenounou, A., Malek, A., Aillerie, M., 2016. Comparative performance of PV panels of different technologies over one year of exposure: Application to a coastal Mediterranean region of Algeria. Energy Convers. Manag. 114, 356–363. https://doi.org/10.1016/j.enconman.2016.02.044

IDEAM, 2014. Distribución de la temperatura media anual (°C). Promedio multianual 1981-2010. 1.

IEC 61853-1, 2011. 61853-1 13.

IRENA - International Renewable Energy Agency, 2022. World Energy Transitions Outlook:

1.5°C Pathway, International Renewable Energy Agency.

Jordan, D.C., Deline, C., Kurtz, S.R., Kimball, G.M., Anderson, M., 2017. Robust PV Degradation Methodology and Application. IEEE J. Photovoltaics 8, 525–531. https://doi.org/10.1109/JPHOTOV.2017.2779779

Kaaya, I., Koehl, M., Mehilli, A.P., De Cardona Mariano, S., Weiss, K.A., 2019. Modeling Outdoor Service Lifetime Prediction of PV Modules: Effects of Combined Climatic Stressors on PV Module Power Degradation. IEEE J. Photovoltaics 9, 1105–1112. https://doi.org/10.1109/JPHOTOV.2019.2916197

Karami, E., Rafi, M., Haibaoui, A., Ridah, A., Hartiti, B., Thevenin, P., 2017. Performance Analysis and Comparison of Different Photovoltaic Modules Technologies under Different Climatic Conditions in Casablanca. J. Fundam. Renew. Energy Appl. 07, 3–8. https://doi.org/10.4172/2090-4541.1000231

Katsaounis, T., Kotsovos, K., Gereige, I., Basaheeh, A., Abdullah, M., Khayat, A., Al-Habshi, E., Al-Saggaf, A., Tzavaras, A.E., 2019. Performance assessment of bifacial c-Si PV modules through device simulations and outdoor measurements. Renew. Energy 143, 1285–1298. https://doi.org/10.1016/j.renene.2019.05.057

Londoño, C.D., Cano, J.B., Jaramillo, F., Valencia, J.A., Velilla, E., 2023. Outdoor and synthetic performance data for PV devices concerning the weather conditions and capacitor values of I-V tracer. Data Br. 47. https://doi.org/10.1016/j.dib.2023.109007

Londoño, C.D., Cano, J.B., Velilla, E., 2022. Capacitive tracer design to mitigate incomplete I-V curves in outdoor tests. Sol. Energy 243, 361–369. https://doi.org/10.1016/j.solener.2022.08.021

Louwen, A., de Waal, A.C., Schropp, R.E.I., Faaij, A.P.C., van Sark, W.G.J.H.M., 2017. Comprehensive characterisation and analysis of PV module performance under real operating conditions. Prog. Photovoltaics Res. Appl. 25, 218–232. https://doi.org/10.1002/pip.2848

Makrides, G., Zinsser, B., Georghiou, G.E., Schubert, M., Werner, J.H., 2008. Outdoor efficiency of different photovoltaic systems installed in Cyprus and Germany. Conf. Rec. IEEE Photovolt. Spec. Conf. 7–12. https://doi.org/10.1109/PVSC.2008.4922830

Mussard, M., Amara, M., 2018. Performance of solar photovoltaic modules under arid climatic conditions: A review. Sol. Energy 174, 409–421. https://doi.org/10.1016/j.solener.2018.08.071

Ogbomo, O.O., Amalu, E.H., Ekere, N.N., Olagbegi, P.O., 2017. A review of photovoltaic module technologies for increased performance in tropical climate. Renew. Sustain. Energy Rev. 75, 1225–1238. https://doi.org/10.1016/j.rser.2016.11.109

Padilla, A., Londoño, C., Jaramillo, F., Tovar, I., Cano, J.B., Velilla, E., 2022. Photovoltaic performance assess by correcting the I-V curves in outdoor tests. Sol. Energy 237, 11–18. https://doi.org/10.1016/j.solener.2022.03.064

Park, H., Chang, S., Park, S., Kim, W.K., 2019. Outdoor performance test of bifacial n-type silicon photovoltaic modules. Sustain. 11. https://doi.org/10.3390/su11226234

REN21, 2022. Renewables 2022 Global Status, Global Status Report for Buildings and Construction: Towards a Zero-emission, Efficient and Resilient Buildings and Construction Sector.

UPME, 2005. Mapas de Radiación Solar Global Sobre una Superficie Plana. Atlas Radiac. Sol. Colomb. 23–40.

Velilla, E., Cano, J.B., Jaramillo, F., 2019. Monitoring system to evaluate the outdoor performance of solar devices considering the power rating conditions. Sol. Energy 194, 79–85. https://doi.org/10.1016/J.SOLENER.2019.10.051

Visa, I., Burduhos, B., Neagoe, M., Moldovan, M., Duta, A., 2016. Comparative analysis of the infield response of five types of photovoltaic modules. Renew. Energy 95, 178–190. https://doi.org/10.1016/j.renene.2016.04.003

Wang, M., Ma, X., Huang, W.-H., Liu, J., Curran, A.J., Schnabel, E., Köhl, M., Davis, K.O., Brynjarsdóttir, J., Braid, J.L., Braid, J.L., French, R.H., 2018. Evaluation of Photovoltaic Module Performance Using Novel Data-driven I-V Feature Extraction and Suns-VOC Determined from Outdoor Time-Series I-V Curves, in: 2018 IEEE 7th World Conference on Photovoltaic Energy Conversion, WCPEC 2018 - A Joint Conference of 45th IEEE PVSC, 28th PVSEC and 34th EU PVSEC. pp. 778–783. https://doi.org/10.1109/PVSC.2018.8547772

Anexos

Anexo 1:

Capacitive tracer design to mitigate incomplete I-V curves in outdoor tests

https://doi.org/10.1016/j.solener.2022.08.021

Solar Energy 243 (2022) 361–369

Contents lists available at ScienceDirect

Solar Energy

journal homepage: www.elsevier.com/locate/solener

Capacitive tracer design to mitigate incomplete I-V curves in outdoor tests

C.D. Londoño [a], J.B. Cano [a,*], E. Velilla [a,b]

[a] Grupo en Manejo Eficiente de la Energía, GIMEL, Universidad de Antioquia UdeA, Calle 70 No. 52-21, Medellín, Colombia
[b] Centro de Investigación, Innovación y Desarrollo de Materiales – CIDEMAT, Universidad de Antioquia UdeA, Calle 70 No. 52-21, Medellín, Colombia

ARTICLE INFO

Keywords:
Capacitance sizing
Capacitive tracer
I-V curves
Outdoor tests
Photovoltaic device

ABSTRACT

The capacitance technique is the most straightforward and low-cost technique to trace the I-V curve of photovoltaic (PV) modules. Nevertheless, the sweep speed and number of samples to measure the I-V curve depend on the device under test (DUT), capacitance size, switching dynamic, lighting conditions, Etc. Therefore, two performance indexes were proposed to evaluate the I-V curve quality. The indexes were estimated from a circuital model considering the transient capacitance charging process as a function of the target irradiance levels and parameters of the DUT and tracer. In this way, a capacitance range is estimated to mitigate the likelihood of measuring incomplete curves in the I_{sc} and V_{oc} regions. Finally, the capacitance sizing design in terms of both indexes for monitoring PV technologies was validated in outdoor tests.

1. Introduction

The performance of Photovoltaic (PV) devices is described by the short-circuit current (I_{sc}), open-circuit voltage (V_{oc}), fill factor (FF), maximum power (P_{max}), voltage and current at the maximum power point (V_{mpp}, I_{mpp}) and efficiency. These parameters are typically estimated from the I-V curve regarding light and temperature conditions (Velilla et al., 2017). In this context, the capacitance technique could be considered the most straightforward and low-cost technique to trace the I-V curve of PV modules. Nevertheless, it is possible to measure incomplete I-V curves and estimate inappropriate parameters concerning the performance because the sweep speed and the number of samples are functions of the device under test (DUT), capacitance value, switching dynamic, lighting conditions, Etc. These issues could be more relevant in outdoors because of the irradiance level changes, increasing the likelihood of measuring incomplete curves, highlighting the importance of measuring proper curves to improve the performance estimation.

The I-V curve is conventionally measured by scanning the device operating points starting at the short-circuit current point (0, I_{sc}), crossing the maximum power point (V_{mpp}, I_{mpp}) and ending at the open-circuit voltage point (V_{oc}, 0). Hence, several I-V tracers have been reported in the literature depending on the sensors and data-acquisition systems (Zhu and Xiao, 2020), which currently demonstrate more capabilities and lower cost. Thus, properties such as flexibility, fidelity, cost, fast-response, modularity, among other parameters, have been considered to evaluate the tracer performance (Duran et al., 2008).

Accordingly, the four-quadrant power supply, DC-DC converters and bidirectional power inverters coupled to DC/DC converters have been employed to trace the I-V curve by facilitating different sweep speeds and scan directions (forward and reverse), allowing testing the devices under dark or light conditions (Morales-Aragonés et al., 2021). On the other hand, resistive and capacitive load tracers have been widely used under light conditions because of the simplicity for measuring the curve regardless of the power dissipation drawbacks. However, the capacitance load or capacitance technique is the most straightforward technique to be implemented in the tracers because the dynamic behavior to scan the curve is inherent to the capacitor charging process. Therefore, the controllability and adaptability of the capacitance technique to scan the device operating points, facilitates for testing PV and arrays (Chen et al., 2018; García-Valverde et al., 2016), enables to design tracers with adaptive sampling period (Chen et al., 2020), tracers for estimation of the parameters of PV devices (Padilla et al., 2022; Velilla et al., 2021, 2019a; Velilla Hernández et al., 2022) or multi-module capacitive tracers for PV systems (Reischauer and Rix, 2019).

The capacitive technique requires large-high-quality capacitors (minor series resistance) to measure a proper I-V curve concerning light conditions. Accordingly, different approaches have been proposed for capacitance sizing. Most of them are based on the “fill factor one” or constant current approximation (Warner and Cox, 1982). Herein, the solar panel is modeled as an ideal current source with a magnitude value of I_{sc}. In this way, the current source charges the capacitor increasing the

* Corresponding author.
E-mail address: bernardo.cano@udea.edu.co (J.B. Cano).

https://doi.org/10.1016/j.solener.2022.08.021
Received 18 May 2022; Received in revised form 30 July 2022; Accepted 8 August 2022
Available online 13 August 2022

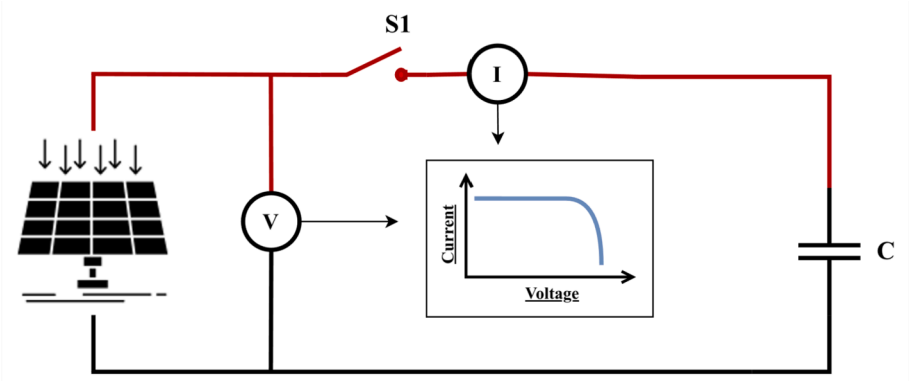

Fig. 1. Scheme of the capacitance technique to trace the I-V curve. The voltage and current signals are measured by the sensors V and I respectively.

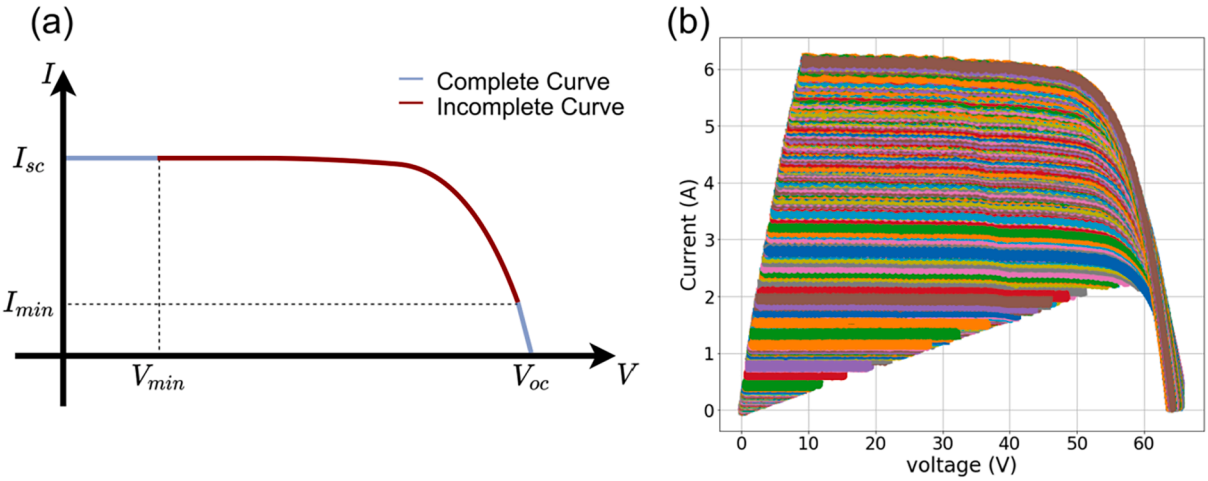

Fig. 2. I-V curve. Panel (a) corresponds to description of complete and incomplete I-V curve. Panel (b) corresponds to recorded I-V curves in outdoor tests to illustrate the regions affected by missing data because of the capacitor sizing and weather conditions.

voltage until the open-circuit voltage (V_{oc}). This charging process is considered by Eq. (1), indicating the relationship between the capacitance size (C), the DUT characteristics (I_{sc} and V_{oc}) and the charging time (t_s).

$$C = t_s \frac{I_{sc}}{V_{oc}} \tag{1}$$

Intended to generalize the fill factor approach modeling, a proportionality factor (k) value of 0.5 was included in Eq. (1) to consider the maximum sweep speeds (Mahmoud, 2006). Moreover, empirical k values ranging between 0.5 and 0.9090 were recommended depending on the application type (module or array of modules) (Sayyad and Nasikkar, 2020). Another approach for sizing the capacitance was proposed using a two-steps model to consider the transient effects in the charging process (Spertino et al., 2015). In this approach, the first step is modeled using a current source of value I_{sc} to produce a constant current charge, obtaining the I-V curve behavior close to I_{sc} value. Then, the second step is modeled as a voltage source (V_{oc}) in series with an equivalent resistance for obtaining the I-V curve behavior close to V_{oc} value. In this case, the charging time can be estimated using the 5RC criterion. Besides, this approach was modified to adjust the sampling period according to the irradiance changes using additional hardware (Chen et al., 2020).

It is worth noting that the approaches are only based on the total time required to charge the capacitor and do not consider specific characteristics of the data-acquisition system as the commutation delay of switches. Therefore, the transient behavior at the beginning of the I-V curve (close to I_{sc}) is not considered. Besides, the capacitance sizing is conventionally calculated considering only one irradiance condition, i.e., Standard Test Conditions (STC) or Nominal Operative Cell Temperature (NOCT) commonly reported in the datasheet of PV modules, thus, the dependence of the DUT parameters with irradiance is not considered. In this context, incomplete I-V curves and uncertainty in the estimated parameters are expected for evaluating PV modules in outdoor tests considering only one capacitance value, because the capacitor charging time also depends on the weather conditions according to Eq. (1). Therefore, this work proposes an alternative approach by proposing two performance indexes to verify the I-V curve completeness and estimate a capacitance range for the tracer concerning the target irradiance levels, panel characteristics, and acquisition system parameters.

2. Capacitance technique

The capacitance technique traces the I-V curve by measuring and recording the current (I) and voltage (V) signals when the switch (S1) is closed to connect the capacitor (C) to the DUT or solar module, Fig. 1. In this case, it is expected to trace complete I-V curves from voltages values approaching zero (correlated to the short-circuit point) to the open-circuit voltage (V_{oc}) during the capacitor charging process, Fig. 2. Nevertheless, it is possible to obtain incomplete curves close to V_{oc} depending on the maximum measurement time or tolerance in the current measurement (uncertainty), or close to I_{sc} depending mainly on the switching behavior (transient effects). Therefore, it highlights the principal role of the switch operation in this technique, which must be

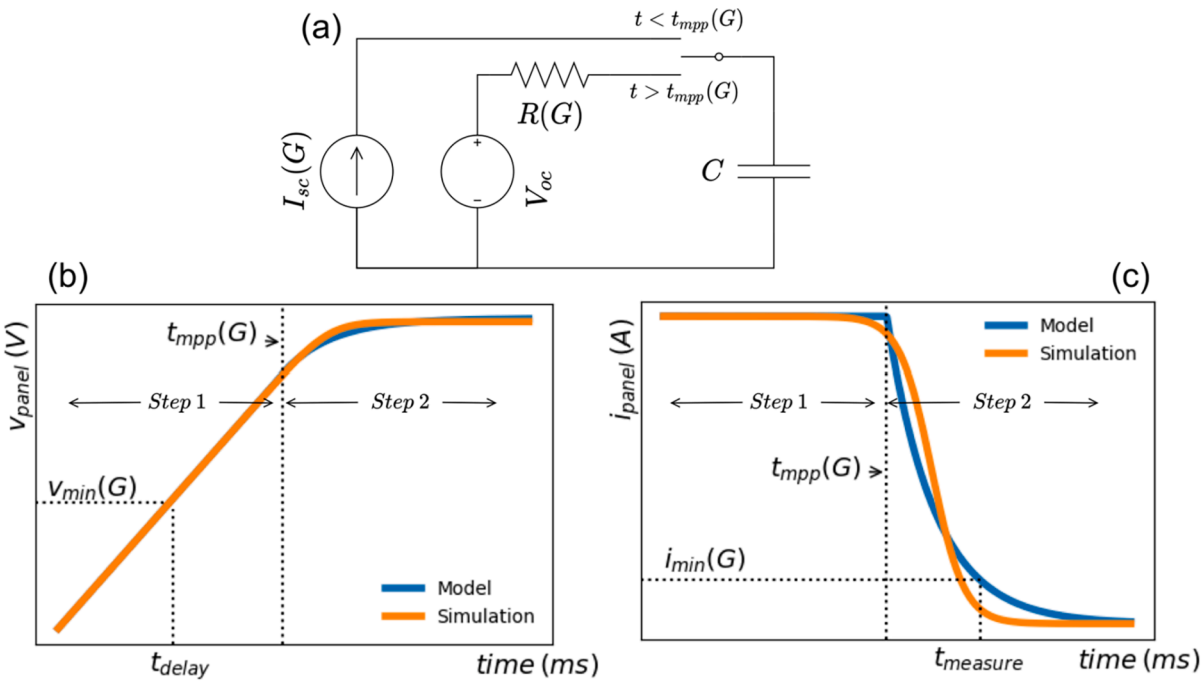

Fig. 3. Transient Charging Circuital Model. Panel (a) corresponds to the equivalent circuit. Panel (b) corresponds to the voltage comparison between the two-Step model (blue line) and one-diode model simulation (orange line). Panel (c) corresponds to the current comparison. The Two Step model is divided in two regions to show the starting capacitance charging process (Step 1) and the exponential current behavior at the end of the capacitance charging process (Step 2). Adapted from (Spertino et al., 2015) and (Chen et al., 2020). (For interpretation of the references to colour in this figure legend, the reader is referred to the web version of this article.)

programmed and synchronized with the data acquisition systems to mitigate the transient effects when the switch is closed and properly record the voltage and current signals during the test.

In a nutshell, a I-V tracer equipment that implements the capacitance technique includes the capacitor, switch, sensors, data acquisition system and control system to perform the tasks. From the hardware point of view, this technique only involves a few elements (switch and capacitor at least), demonstrating the simplicity of performing the I-V curve. From the software point of view, few steps are required to record the data. Moreover, it is possible to include an external resistance (R) to discharge the capacitor and reduce the death time between measurements. In this case, another switch is required and taken into account in the logical process (switches sequence) to trace the I-V curve (Velilla et al., 2019a; Velilla Hernández et al., 2022). Therefore, these advantages allow observing why this technique is a simplest and low-cost technique to trace the I-V.

3. Design methodology for capacitance sizing

This section shows the impact of the capacitance value in the I-V curves to determine the variables and models required for sizing the capacitive tracer concerning light condition and DUT parameters.

3.1. Impact of light conditions on the I-V curve behavior

Fig. 2a shows in a general way the distinction between a complete and incomplete I-V curve. This distinction is highlighted considering the minimum voltage measured (V_{min}) and the minimum current measured (I_{min}), in this case, an appropriate I-V curve is recorded as both parameters tend to zero. Thus, the transient effects due to the switching dynamic and commutation delay involved in the technique could be correlated to the missing or dirty data close to the I_{sc} region. Hence, V_{min} close to zero indicates a quasi-ideal curve and V_{min} close to V_{oc} indicates a poor-quality curve. On the other hand, an insufficient time to fully charge the capacitor or shorter available time for the measurement could be correlated to missing data correlated to the V_{oc} region. Hence, I_{min} close to zero indicates a successful measurement of the V_{oc} while I_{min} close to I_{sc} indicates an incomplete charging process of the capacitor.

Fig. 2b shows the impact of light conditions (G) on both regions (I_{sc} and V_{oc}) of the I-V curve recorded in outdoor tests considering a fixed capacitance value. Here, the behavior close to V_{oc} can be explained regarding Eq. (1), because the DUT parameters (I_{sc} and V_{oc}) depend on weather conditions. Thus, the charging time mainly depends on light conditions (G) producing insufficient time to fully charge the capacitor as the irradiance levels decrease. Nevertheless, this equation does not allow explanation of the behavior close to the I_{sc} region, which is mainly a function of the sweep speed and switching dynamic (I-V tracer specific-parameters), being more evident as G increases (see Supplementary Information Fig. S1).

3.2. Success rates (SR) indexes

In order to evaluate the performance of the I-V curve concerning the missing data, the regions affected by this missing data related to I_{sc} and V_{oc} are described in terms of the parameters shown in Fig. 2a. Herein, it is possible to determine the performance of the recorded I-V curve considering two normalized indexes. The first index called success rate of current (I_{SR}) is related to the I_{sc} region considering the ratio between V_{min} and V_{oc} as shown in Eq. (2). The second index called success rate of voltage (V_{SR}) is related to the V_{oc} region considering the ratio between I_{min} and I_{sc} as shown in Eq. (3). Thus, a proper I-V curve (mitigating missing data) is expected when both indexes are close to 100 %.

$$I_{SR} = 100\left(1 - \frac{V_{min}}{V_{oc}}\right) \tag{2}$$

$$V_{SR} = 100\left(1 - \frac{I_{min}}{I_{sc}}\right) \tag{3}$$

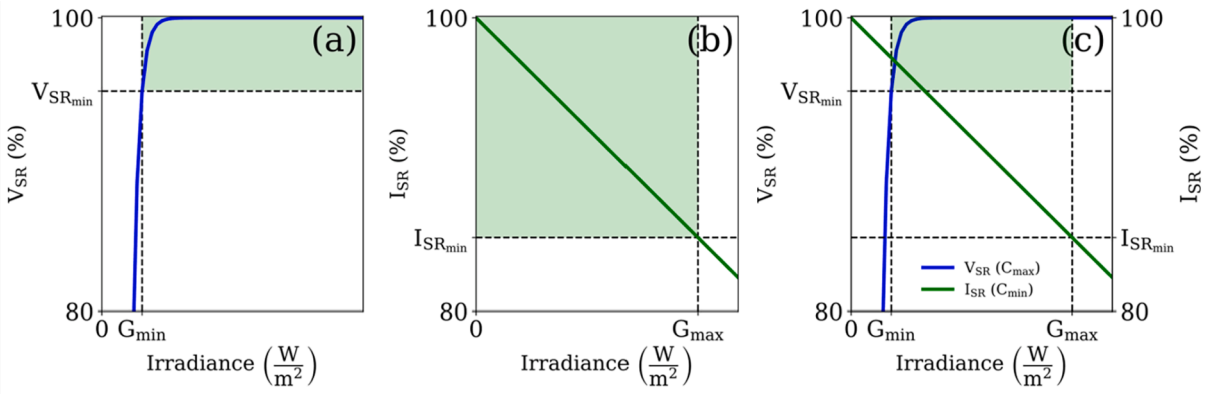

Fig. 4. Definition of target success rates at minimum and maximum irradiances. Panel (a) corresponds to V_{SR}, panel (b) to I_{SR} and panel (c) to the combination of both parameters (V_{SR} and I_{SR}) defined by Eqs. (2) and (3). Green region represents the success area for the parameters. (For interpretation of the references to colour in this figure legend, the reader is referred to the web version of this article.)

It is worth noting that both indexes depend on the irradiance levels (G), as is depicted in Fig. 2b. Accordingly, high irradiance levels are conditions that facilitate the complete capacitor charge, registering the V_{oc} value and improving V_{SR}. Nevertheless, these conditions increase the data loss at the beginning of the capacitor charge (I_{sc} region) because of the switching behavior. In contrast, low irradiance levels are conditions that constrain the capacitor charging process (V_{oc} region). Thus, the V_{oc} value could not be registered. However, under these conditions, current values close to I_{sc} are registered, improving I_{SR}.

3.3. Capacitor charging model

In order to estimate both indexes (I_{SR} and V_{SR}) as a function of G considering the behavior of the DUT and capacitive tracer during the tracing I-V curve process, the two-Step model proposed in the literature (Chen et al., 2020; Spertino et al., 2015) was adapted to consider the dependence of the circuital model with G (Fig. 3a). Therefore, in Step 1, the PV device is assumed as a constant current source charging the capacitor up to a voltage equal to the maximum-power point voltage (V_{mpp}) at the time t_{mpp}, Fig. 3b. In Step 2, the PV device is a constant voltage source in series with a resistor, producing an exponential decay behavior for the current, Fig. 3c.

The circuital model involves the electrical parameters of the DUT such as V_{oc}, I_{sc}, V_{mpp} and I_{mpp}, which are functions of weather conditions (G and temperature). It is possible for design purposes to express I_{sc} and I_{mpp} as a function of irradiance (Eqs. (4) and (5)). Where G is the irradiance in W/m^2, and the subindex STC corresponds to Standard Test Condition (STC). On the other hand, we neglect the effect of G in the DUT voltage (V_{oc} and V_{mpp}).

$$I_{SC}(G) = \frac{Isc_{stc}}{1000} G \tag{4}$$

$$I_{mpp}(G) = \frac{Impp_{stc}}{1000} G \tag{5}$$

Notice that in Step 1 the capacitor voltage increases linearly with time (Fig. 3b). Therefore, I_{sc} at the target irradiance condition (G) is estimated to calculate the time at which the capacitor rises the V_{mpp} value in Step 1 (t_{mpp}), following Eq. (6).

$$t_{mpp}(G) = \frac{CV_{mpp}}{I_{sc}(G)} \tag{6}$$

It is possible in Step 2 to calculate the equivalent resistance R(G) by calculating the inverse of the slope between the maximum power point (V_{mpp}, I_{mpp}) and the open-circuit point (V_{oc}, 0) at the target G, following Eq. (7).

$$R(G) = \frac{V_{oc} - V_{mpp}}{I_{mpp}(G)} \tag{7}$$

Finally, the resulting piecewise expression for the capacitor current in both steps as a function of time (Eq. (8)) is estimated by solving the equivalent circuits taking into account the initial and continuity conditions.

$$i(t) = \begin{cases} I_{sc}(G) & t < t_{mpp}(G) \\ I_{sc}(G) e^{\frac{-(t - t_{mpp}(G))}{RC}} & t > t_{mpp}(G) \end{cases} \tag{8}$$

3.4. Estimation of V_{SR} and I_{SR}

The I_{SR} can be affected by the time delay (t_{delay}) to start the measurement process and charge the capacitor, affecting the I_{sc} region of the I-V curve. Hence, this time must consider the sampling period (t_{sample}) by the acquisition system and commutation delay of the switch (t_{switch}). Thus, t_{delay} can be calculated as follows Eq. (9).

$$t_{delay} = Max\left(t_{sample}, t_{switch}\right) \tag{9}$$

t_{delay} must be smaller than t_{mpp} ($t_{delay} < t_{mpp}$) for guaranteeing a constant charge current in Step 1 (Eq. (8)). Thus, a linear behavior of the capacitor voltage as a function of the time is obtained (Eq. (10)), allowing estimation of the minimum measured voltage (V_{min}) as shown in Eq. (11) (see Fig. 3b), considering the DUT and I-V tracer.

$$V = \frac{I_{sc}(G)}{C} t \tag{10}$$

$$V_{min} = t_{delay} \frac{I_{sc}(G)}{C} = t_{delay} \frac{Isc_{stc} G}{1000C} \tag{11}$$

Finally, I_{SR} (Eq. (12)) is estimated by replacing V_{min} in Eq. (2) to express I_{SR} in terms of G and DUT characteristics related to Step 1, describing the behavior of the I-V curve in the I_{sc} region.

$$I_{SR} = 100\left(1 - \frac{V_{min}}{V_{oc}}\right) = 100\left(1 - \frac{t_{delay} Isc_{stc} G}{1000 C V_{oc}}\right) \tag{12}$$

On the other hand, the V_{oc} region of the I-V curve can be affected by the charging time. Thus, the total acquisition time ($t_{measure}$) can be calculated as the product of the t_{sample} and the maximum number of samples ($n_{samples}$) settled by the acquisition system following Eq. (13).

$$t_{measure} = n_{samples} t_{sample} \tag{13}$$

Accordingly, considering that $t_{measure}$ is greater than t_{mpp}, Eq. (8) related to Step 2 is employed for estimating I_{min} at $t_{measure}$, Eq. (14).

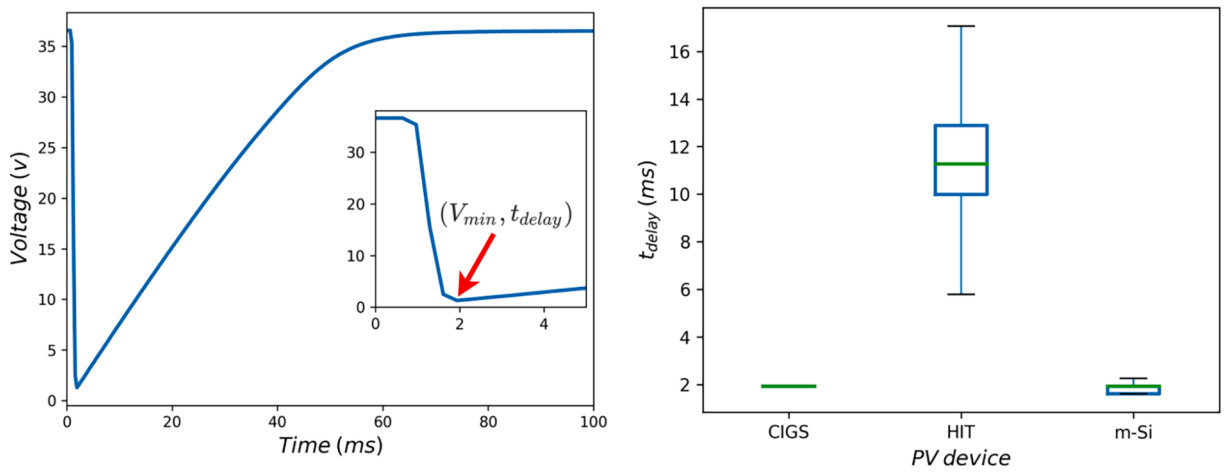

Fig. 5. Switching time (t_{switch}) estimation. Panel (a) corresponds to voltage signal during the I-V curve tracing in outdoor tests. The inset corresponds to the initial behavior of voltage related to the switching process. Panel (b) corresponds to estimated t_{switch} distribution in a form of boxplot considering one year of outdoor testing.

$$I_{min} = I_{sc}(G)e^{\frac{-\left(t_{measure} - t_{mpp}(G)\right)}{R(G)C}} \tag{14}$$

Then, the V_{SR} (Eq. (15)) is calculated by replacing I_{min} in Eq. (3) to express the index in terms of G and corresponding times of Step 2 (see Fig. 3c), describing the I-V curve behavior in the V_{oc} region.

$$V_{SR}(G) = 100\left(1 - \frac{I_{min}(G)}{I_{sc}(G)}\right) = 100\left(1 - e^{\frac{-\left(t_{measure} - t_{mpp}(G)\right)}{R(G)C}}\right) \tag{15}$$

Notice that for t_{mpp} greater than $t_{measure}$, a negative value for V_{SR} is estimated. In those cases, the I-V curve tracer is not able to register the V_{mpp} value.

3.5. Capacitance sizing design

Once I_{SR} and V_{SR} are described in terms of G and the parameters related to the I-V curve tracer, DUT and acquisition system (Eqs. (12) and (15) respectively), it is possible to define acceptable or target values for the success rates to design an appropriate capacitor size. Therefore, defining the SR targets values as V_{SRmin} (Fig. 4a) and I_{SRmin} (Fig. 4b), the operative irradiance range ($G_{min} < G < G_{max}$) for the tracer is constrained (Fig. 4c). In this regard, the capacitances correlated to the I_{sc} and V_{oc} regions could be estimated from Eqs. (12) and (15) respectively. Thus, the maximum capacitance (C_{max}) value is estimated from V_{SR} considering the minimum irradiance (G_{min}) following Eq. (16). The minimum capacitance (C_{min}) value is estimated from I_{SR} considering the maximum irradiance (G_{max}), following Eq. (17). Therefore, both capacitances limit the required operative capacitance range ($C_{min} < C < C_{max}$) for the tracer to guarantee the I-V curves quality concerning the operative irradiance range defined by the target conditions.

It is worth noting that it is also possible to tune-up the design by selecting different target indexes for current and voltage based on the required application or define the irradiance range of interest to estimate the SR values (I_{SR} and V_{SR}) and calculate the capacitor size. Finally, it is highlighted that the proposed design process for sizing the capacitance was validated by the equations involved in two-Step model and by simulation using for instance the one-diode model to include the transient behavior during the capacitance charging process, as is shown in Supporting Information section S2.

$$C_{max} = \frac{t_{measure}}{V_{mpp}/I_{sc}(G_{min}) - R(Gmin)ln(1 - V_{SRmin}/100)} \tag{16}$$

$$C_{min} = \frac{t_{delay} Isc_{stc} G_{max}}{1000\left(1 - \frac{I_{SRmin}}{100}\right)Voc} \tag{17}$$

4. Results

This section shows the validation of the proposed design methodology for selecting the capacitor values to improve the quality of recording I-V curve in outdoor tests. Therefore, three modules of different technologies (Table S1) were monitored in natural sunlight without a tracker (Table S2) (6°15′ 38″N 75°34′ 05″W, facing south at a fixed tilt angle of 13°) by adjusting the corresponding capacitance of the I-V tracers (Table S3). The I-V curves and environmental variables (irradiance, device temperature and ambient temperature) were recorded every minute during light-hours, as was performed in previous work (Padilla et al., 2022; Velilla et al., 2021, 2019a, 2019b). In this way, the outdoor data allowed estimating the t_{delay} of the evaluated Panasonic VBHN330SJ47 (HIT), Miasolé FLEX–02 120 N (CIGS) and Znshine solar ZX55(17.8)M (m-Si) modules (Table S1). These values were used as input in the proposed modeling for estimating the capacitance range of the tracer considering the target indexes V_{SR} and I_{SR} and corresponding irradiance range.

4.1. Time delay estimation

Fig. 5a shows in a general way the voltage signal during the capacitor charging process for tracing the I-V curve. The time delay (t_{delay}) corresponds to the maximum time between t_{switch} and sampling period (t_{sample}) according to Eq. (9). It corresponds to the time to reach the minimum voltage (V_{min}) once the switch is closed, changing the voltage from V_{oc} to V_{min} (transitory state), as is shown in the inset. Therefore, the recorded data during the t_{delay} are not considered in the I-V curve (missing data), affecting the I_{sc} region as was shown in Fig. 2b.

In this regard, t_{delay} was estimated as the required time to register the minimum voltage (V_{min}) in outdoor tests for the evaluated PV devices, considering that t_{switch} is greater than t_{sample} (See Table S2 and S4). Fig. 5b shows the estimated t_{delay} in the form of a boxplot, observing that median values of t_{delay} approach 11.27 ms for HIT and 1.932 ms for other modules. Besides, the data distribution suggested that t_{delay} is almost constant during the outdoor tests for CIGS and m-Si modules, indicating that t_{delay} mainly depends on the switching process or commutation delay (t_{switch}) according to Eq. (9). On the contrary, the estimated t_{delay} distribution for HIT module indicates that t_{delay} changed during the tests, which could be explained because this switch can operate at high voltages (up to 250 V). Nevertheless, results allowed validation of t_{delay} because they are in the range reported by the manufacturers, concerning the typical and maximum values for t_{delay} (see Supporting Information section S.3.1). Finally, it is worth noting that

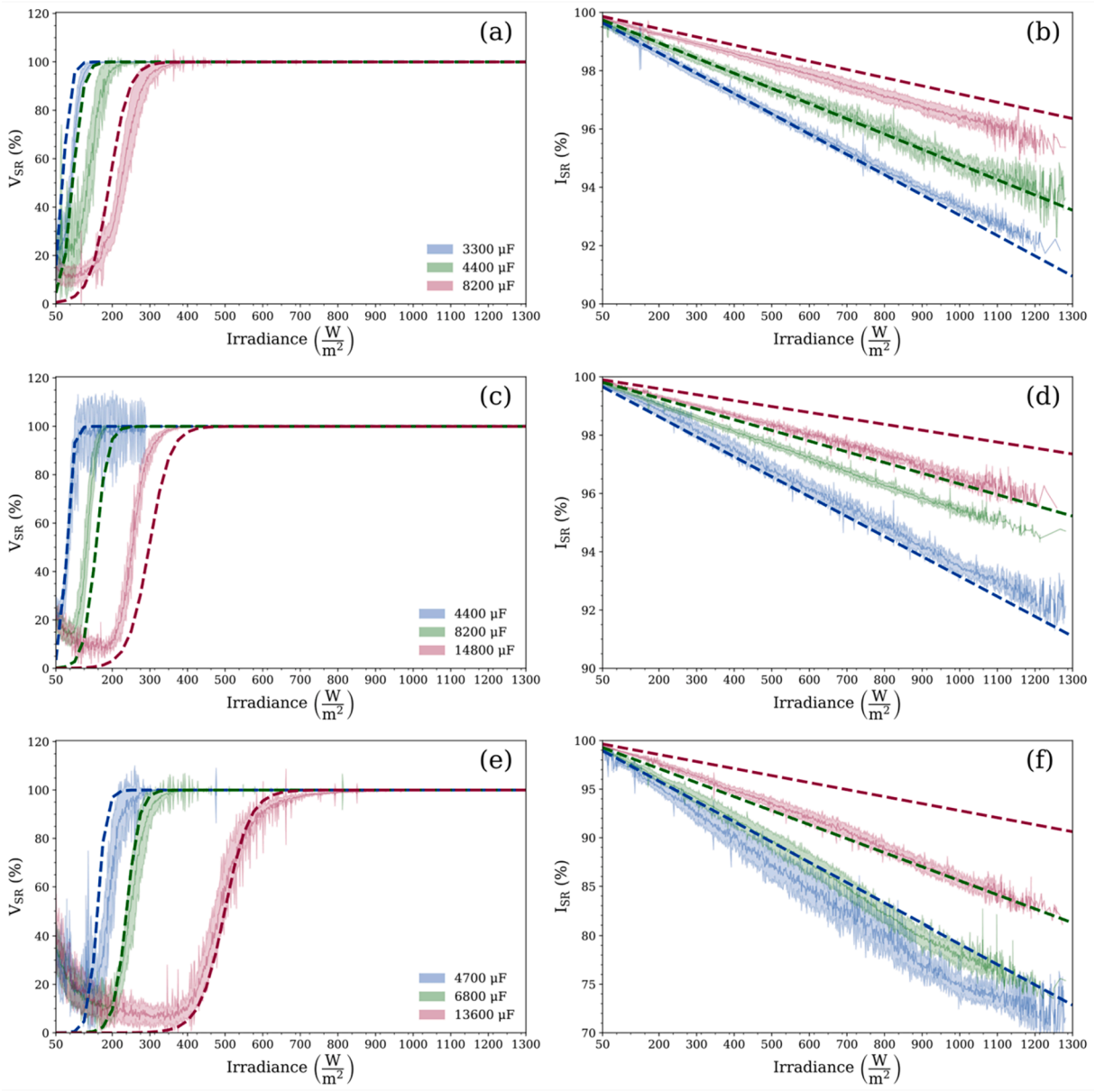

Fig. 6. Impact of irradiance and capacitance on V_{SR} and I_{SR}. Panels (a-b) correspond to CIGS - Miasolé module, (c-d) to m-Si – Znshine module, and (e-f) to HIT - Panasonic module. The dashed lines correspond to the results following the proposed capacitor sizing design, Eq. (15) for V_{SR} and Eq. (12) for I_{SR}. The contour is a visual guide of the corresponding recorded outdoor data, considering one standard deviation with respect to the median values. The insets show the installed capacitance in the tracer.

t_{delay} must be estimated by testing because it is required to mitigate the missing data in the I_{sc} region, according to Eq. (12).

4.2. Capacitance size impact on performance indexes

Different capacitance values were installed in the tracers during the outdoor tests to compare the outdoor performance of I-V curves concerning the proposed capacitance sizing design (proposed modeling). Thus, V_{SR} and I_{SR} were estimated for the DUTs considering the outdoor records corresponding to the I-V curves. In the case of the proposed modeling, V_{SR} and I_{SR} were estimated for the DUTs as a function of G following Eqs. (12) and (15), considering the estimated t_{delay} median values (Fig. 5b), an acquisition time ($t_{measure}$) of 322 ms, DUT parameters (see Table S2), and corresponding installed capacitance value in the tracers.

Fig. 6 shows, in a general way, the agreement between the outdoor tests and proposed modeling. Results allowed observing the impact of irradiance and capacitance on V_{SR} and I_{SR}, characterized by a sigmoidal and linear behavior concerning irradiance, respectively. These behaviors suggest an irradiance range to guarantee the quality of I-V curves concerning the capacitance value, as shown in Fig. 4. V_{SR} indicates a value of G (G_{min}) for improving the index (100 %). Thus, in order to reduce the likelihood of missing data in the I_{sc} region, lower C values must be considered to improve the index by reducing G_{min}. On the contrary, to reduce the likelihood of missing data in the V_{oc} region, greater C values must be considered to improve I_{SR} by increasing the irradiance range (G_{max}). Besides, Fig. 6 demonstrates the dependence of V_{SR} and I_{SR} on the DUT parameters (P_{max}, V_{oc} and I_{sc}), highlighting the principal role of the DUT parameters in the capacitance sizing design.

It is worth noting that differences between the outdoor and proposed modeling can be explained mainly because of the tolerance of the electrolytic capacitors (±20 % at 120 Hz/+20 °C)[1]. This tolerance could

Table 1
Capacitance range estimation according to target conditions, DUT and I-V curve tracer characteristics.

DUT	I-V tracer		Estimated indexes		Capacitance values	
	t_{delay} (ms)	$t_{measure}$ (ms)	V_{SRmin} (%)	I_{SRmin} (%)	C_{min} (uF)	C_{max} (uF)
CIGS	1.932	322	93	93	3280	5420
m-Si	1.932				4140	7030
HIT	11.27				14,020	4290
				75	3930	

affect the estimation of V_{SR} and I_{SR}, as was shown in Fig. S5 of supporting information, considering the lower (dashed lines) and upper (dotted lines) capacitance limits.

4.3. Capacitor sizing design

Eqs. (16) and (17) were followed for capacitance sizing estimation of tracers considering the DUTs parameters and estimated t_{delay} (Fig. 5b). Table 1 shows the calculated values to guarantee the quality of I-V curve in the target irradiance range between 200 and 1000 W/m^2 ($G_{min} < G < G_{max}$).

Notice that HIT calculations were repeated twice because of the long t_{delay} of the corresponding I-V tracer (the switch was slower because of the high V_{oc} constraints). Thus, it was impossible to find a valid capacitance range for target values of 93 % for V_{SRmin} and I_{SRmin}, therefore I_{SRmin} was settled to 93 %. It emphasizes the relevance of using fast commutation switches in the design of capacitive I-V curve tracers in order to guarantee good performance in the I_{sc} region of the curves.

Fig. 7 shows the I-V curve performance regarding V_{SR} and I_{SR} indexes in outdoor tests considering the estimated capacitance shown in Table 1.

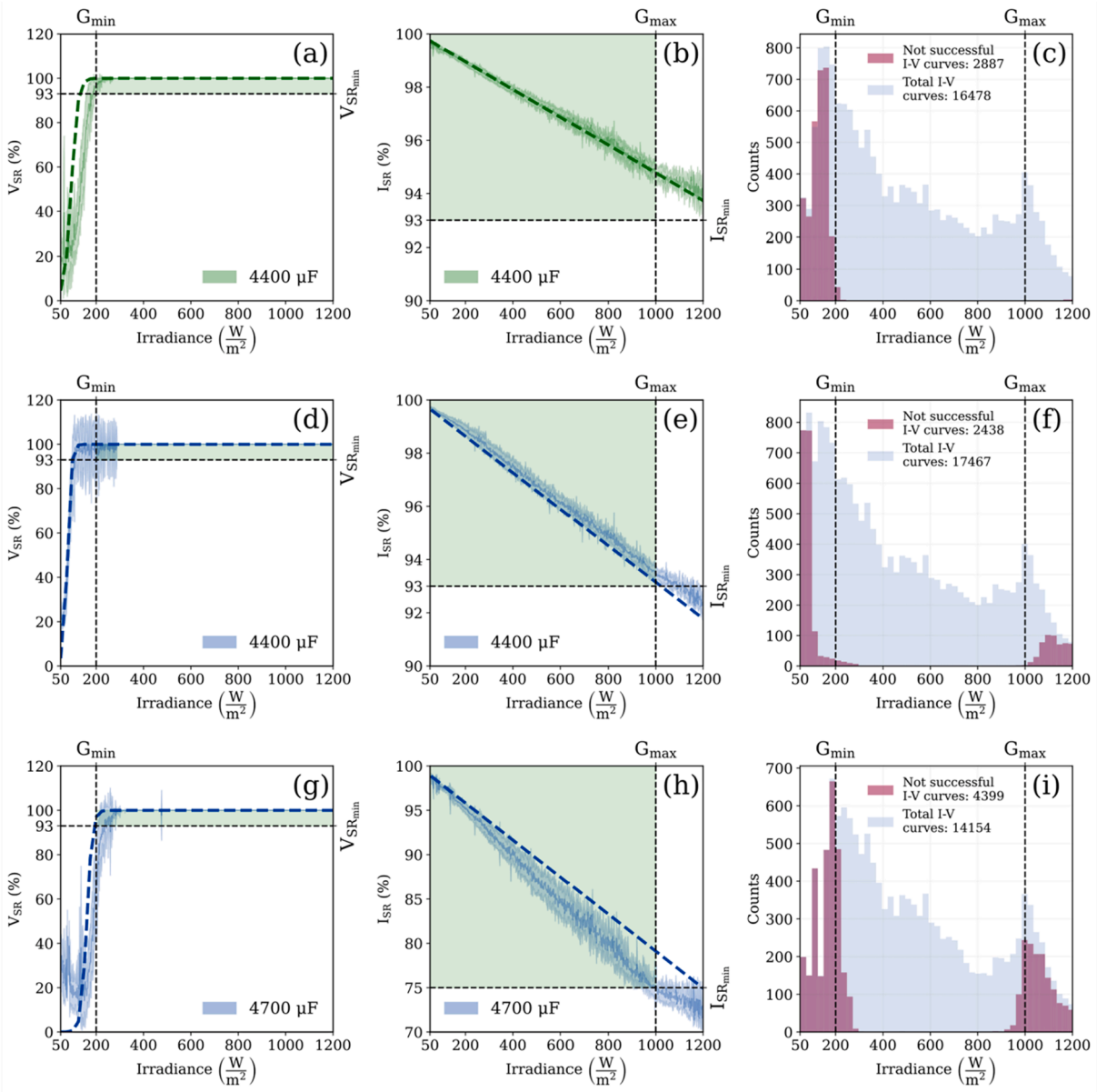

Fig. 7. Capacitor Sizing Verification. Panels (a-c) correspond to CIGS - Miasolé module, (d-f) to m-Si - Znshine and panels (g-i) to HIT - Panasonic module. In panels (a, b, d, e, g, h) the dashed lines correspond to the proposed equations, Eq. (15) for V_{SR} and Eq. (12) for I_{SR} using the estimated t_{delay} corresponding to each DUT (Fig. 5b), the contour area corresponds to real data standard deviation with respect to median values and the green area represents the success area. The insets show the installed capacitance in the tracer. The colors of V_{SR} and I_{SR} plots are correlated with the colors shown in Fig. 6. (For interpretation of the references to colour in this figure legend, the reader is referred to the web version of this article.)

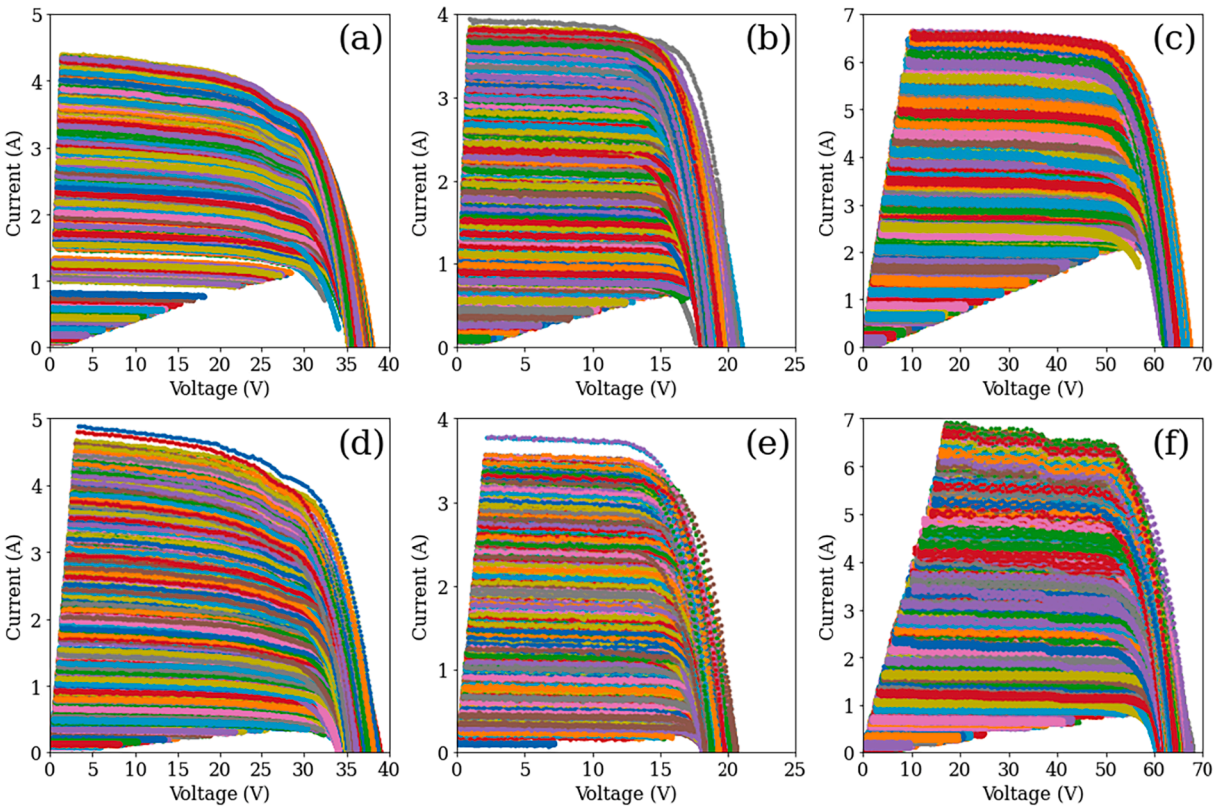

Fig. 8. Impact of capacitance sizing in the I-V curves in outdoor conditions. Panels (a-c) correspond to I-V curves of modules using larger capacitor values. Panels (d-f) correspond to I-V curves of modules using the estimated capacitors. Panels (a and d) correspond to CIGS - Miasolé module, (b and e) to m-Si - Znshine and (c and f) to HIT - Panasonic module. Panels (a and b) correspond to capacitor value of 14,800 μF, panel (d and e) to 4400 μF, panel (c) 13,600 μF and panel (f) 4700 μF.

Accordingly, capacitors of 4400 μF were installed in the tracer for monitoring the CIGS and m-Si modules. It is worth noting that for the HIT module it was necessary to install in the tracer a capacitor of 4700 μF (out of the calculated range) because of the available commercial capacitors. In this regard, the behavior of V_{SR} and I_{SR} indexes (Fig. 7a, b, d, e, g, h) allows validating the agreement between the capacitor sizing design (Eq. (15) for V_{SR} and Eq. (12) for I_{SR}) and outdoor tests considering the target values for G (G_{min} and G_{max}), because the defined minimum target values for V_{SRmin} and I_{SRmin} (Table 1) were properly reached in the target irradiance ranges. This fact can be observed in a better way considering the indexes distribution regarding the irradiance in the form of histograms (Fig. 7c, f, i), indicating that most success measurements are in the target irradiance range. Therefore, the selected capacitance values effectively guarantee the quality of the I-V curve according to the indexes for the target values in outdoor conditions.

Fig. 8 shows the impact of the capacitor values in the I-V curves behavior in outdoor tests by comparing larger capacitor values (Fig. 8a, b and c) regarding the estimated capacitor values shown in Table 1 (Fig. 8d, e, and f). These results highlight the improvement of the proposed design methodology for capacitor sizing because it allows mitigating incomplete I-V curves, observing a noticed improvement in the V_{oc} regions (without significantly affecting the I_{sc} region). This fact indicates that the capacitor charging time was improved concerning the target irradiance range. In the case of HIT - Panasonic module (Fig. 8c, f), although is also observed the improving in the V_{oc} regions, it is worth noting that due to the t_{delay} restriction, the I_{sc} region was affected.

5. Conclusions

In this paper, a capacitor sizing design for I-V tracing in outdoor conditions was proposed considering two performance indexes (V_{SR} and I_{SR}). The indexes were correlated with the performance and quality of I-V curves measurements in the I_{sc} and V_{oc} regions. The indexes were estimated from a circuital model to consider the capacitor charging process dependence with irradiance considering the DUT and I-V curve tracer characteristics. In this way, by defining the target values for both indexes, an irradiance range is limited allowing estimation of an appropriate capacitance range for guaranteeing the constraints regarding the completeness of the I-V curve in the I_{sc} and V_{oc} regions.

The proposed capacitor sizing design was tested and validated by simulation and extensive outdoor measurements using three PV devices of different technologies (CIGS, m-Si and HIT). Results demonstrate that the design considerations and simplifications from the circuital model are appropriated, allowing to tune-up the design for different measurement scenarios, mitigating the incomplete I-V curves in outdoor tests.

Finally, it was shown the relevance of t_{delay} (due to switch commutation) in the design process, which plays a principal role at the beginning of the capacitor charging process affecting the I_{sc} region. Indicating that fast commutation devices must be considered for I-V tracers' development. In this regard, it is worth noting that the switching delay time can be influenced by different factors (temperature, electrical operation point, parasitic elements, etc.). Thus, for an appropriate I-V tracer design, it is required to perform an on-site characterization of t_{delay}, as was shown in this work. However, the maximum values reported by manufacturers in the datasheet can be used in the design as a first approximation.

Declaration of Competing Interest

The authors declare that they have no known competing financial interests or personal relationships that could have appeared to influence the work reported in this paper.

Acknowledgements

Esteban Velilla thanks Colombia's Ministry of Science, Technology and Innovation (MINCIENCIAS) for national doctoral scholarship number 727-2015 (contract no. FP44842-124-2017). Besides, the authors gratefully acknowledge the financial support provided by the Colombia Scientific Program within the framework of the call Ecosistema Científico (contract no. FP44842—218-2018).

Appendix A. Supplementary material

Supplementary data to this article can be found online at https://doi.org/10.1016/j.solener.2022.08.021.

References

Chen, Z., Lin, W., Wu, L., Long, C., Lin, P., Cheng, S., 2018. A capacitor based fast I-V characteristics tester for photovoltaic arrays. Energy Procedia 145, 381–387. https://doi.org/10.1016/j.egypro.2018.04.032.

Chen, Z., Lin, Y., Wu, L., Cheng, S., Lin, P., 2020. Development of a capacitor charging based quick I-V curve tracer with automatic parameter extraction for photovoltaic arrays. Energy Convers. Manag. 226, 113521. https://doi.org/10.1016/j.enconman.2020.113521.

Duran, E., Piliougine, M., Sidrach-de-Cardona, M., Galan, J., Andujar, J.M., 2008. Different methods to obtain the I–V curve of PV modules: A review. In: 2008 33rd IEEE Photovolatic Specialists Conference. IEEE, pp. 1–6. https://doi.org/10.1109/PVSC.2008.4922578.

García-Valverde, R., Chaouki-Almagro, S., Corazza, M., Espinosa, N., Hösel, M., Søndergaard, R.R., Jørgensen, M., Villarejo, J.A., Krebs, F.C., 2016. Portable and wireless IV-curve tracer for >5kV organic photovoltaic modules. Sol. Energy Mater. Sol. Cells 151, 60–65. https://doi.org/10.1016/j.solmat.2016.02.012.

Mahmoud, M.M., 2006. Transient analysis of a PV power generator charging a capacitor for measurement of the I-V characteristics. Renew. Energy 31 (13), 2198–2206. https://doi.org/10.1016/j.renene.2005.09.019.

Morales-Aragonés, J.I., Alonso-García, M.D.C., Gallardo-Saavedra, S., Alonso-Gómez, V., Balenzategui, J.L., Redondo-Plaza, A., Hernández-Callejo, L., 2021. Online Distributed Measurement of Dark I-V Curves in Photovoltaic Plants. Appl. Sci. 11 (4), 1924. https://doi.org/10.3390/app11041924.

Padilla, A., Londoño, C., Jaramillo, F., Tovar, I., Cano, J.B., Velilla, E., 2022. Photovoltaic performance assess by correcting the I-V curves in outdoor tests. Sol. Energy 237, 11–18. https://doi.org/10.1016/j.solener.2022.03.064.

Reischauer, I.W., Rix, A.J., 2019. Design of a low cost multi-module capacitive IV curve tracer for PV module mismatch characterisation. In: 2019 Southern African Universities Power Engineering Conference/Robotics and Mechatronics/Pattern Recognition Association of South Africa (SAUPEC/RobMech/PRASA). IEEE, pp. 340–346. https://doi.org/10.1109/RoboMech.2019.8704809.

Sayyad, J.K., Nasikkar, P.S., 2020. Capacitor Load Based I-V Curve Tracer for Performance Characterisation of the Solar Photovoltaic System. Appl. Sol. Energy 56, 168–177. https://doi.org/10.3103/S0003701X2003010X.

Spertino, F., Ahmad, J., Ciocia, A., Di Leo, P., Murtaza, A.F., Chiaberge, M., 2015. Capacitor charging method for I-V curve tracer and MPPT in photovoltaic systems. Sol. Energy 119, 461–473. https://doi.org/10.1016/j.solener.2015.06.032.

Velilla, E., Restrepo, S., Jaramillo, F., 2017. Cluster analysis of commercial photovoltaic modules based on the electrical performance at standard test conditions. Sol. Energy 144, 335–341. https://doi.org/10.1016/j.solener.2017.01.037.

Velilla, E., Cano, J.B., Jaramillo, F., 2019a. Monitoring system to evaluate the outdoor performance of solar devices considering the power rating conditions. Sol. Energy 194, 79–85. https://doi.org/10.1016/j.solener.2019.10.051.

Velilla Hernández, E., Bernardo Cano Quintero, J., Felipe Montoya, J., Mora-Seró, I., Jaramillo Isaza, F., 2022. Outdoor Performance of Perovskite Photovoltaic Technology. In: Thin Films Photovoltaics. IntechOpen. https://doi.org/10.5772/intechopen.100437.

Velilla, E., Ramirez, D., Uribe, J.-I., Montoya, J.F., Jaramillo, F., 2019b. Outdoor performance of perovskite solar technology: Silicon comparison and competitive advantages at different irradiances. Sol. Energy Mater. Sol. Cells 191, 15–20. https://doi.org/10.1016/j.solmat.2018.10.018.

Velilla, E., Jaramillo, F., Mora-Seró, I., 2021. High-throughput analysis of the ideality factor to evaluate the outdoor performance of perovskite solar minimodules. Nat. Energy 6 (1), 54–62. https://doi.org/10.1038/s41560-020-00747-9.

Warner, T.H., Cox, C.H., 1982. A high power current-voltage curve tracer employing a capacitive load. Sol. Cells 7 (1-2), 175–181. https://doi.org/10.1016/0379-6787(82)90102-8.

Zhu, Y., Xiao, W., 2020. A comprehensive review of topologies for photovoltaic I-V curve tracer. Sol. Energy 196, 346–357. https://doi.org/10.1016/j.solener.2019.12.020.

Anexo 2:

Supporting information of Capacitive tracer design to mitigate incomplete I-V curves in outdoor tests

Capacitive Tracer Design to Mitigate Incomplete I-V Curves in Outdoor Tests

Londoño C.D, Cano J.B, Velilla E.

Corresponding author: bernardo.cano@udea.edu.co

S.1 Impact of irradiance and capacitance value on I-V curve performance

Figure S1 shows I-V curves recorded at outdoor conditions for three different capacitance value used by the I-V tracer. It is observed the effects on the I-V curves performance due to the capacitor value. For higher capacitance values, the V_{SR} index (V_{oc} region) increases and the I_{SR} index (I_{sc} region) decreases and vice versa.

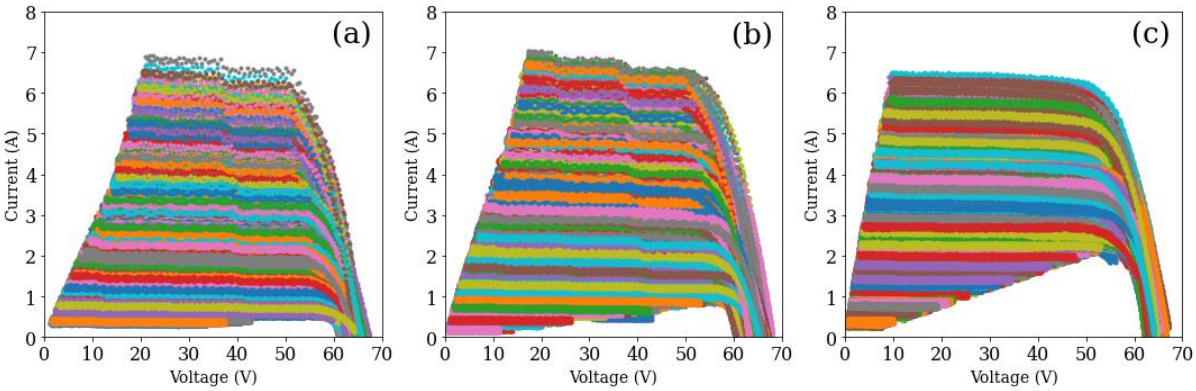

Figure S1. **I-V curve performance in outdoor conditions and different capacitor values.** Curves correspond to HIT module. Panel (a) corresponds to 3200 µF capacitance value, panel (b) to 4700 µF and panel (c) to 13600 µF.

S.2 Simulations

Figure S2 shows the graphical representation of the simulation model. It presents the solar panel, capacitive load and the switch. The switch is controlled by the booleanStep block, guaranteeing its closure at $t = 0$ seconds. The irradiance block allows to set the constant irradiance for the simulation, while the ModuleData block allows modifying the main panel characteristics (V_{oc}, I_{sc}, V_{mpp}, I_{mpp} and temperature coefficients).

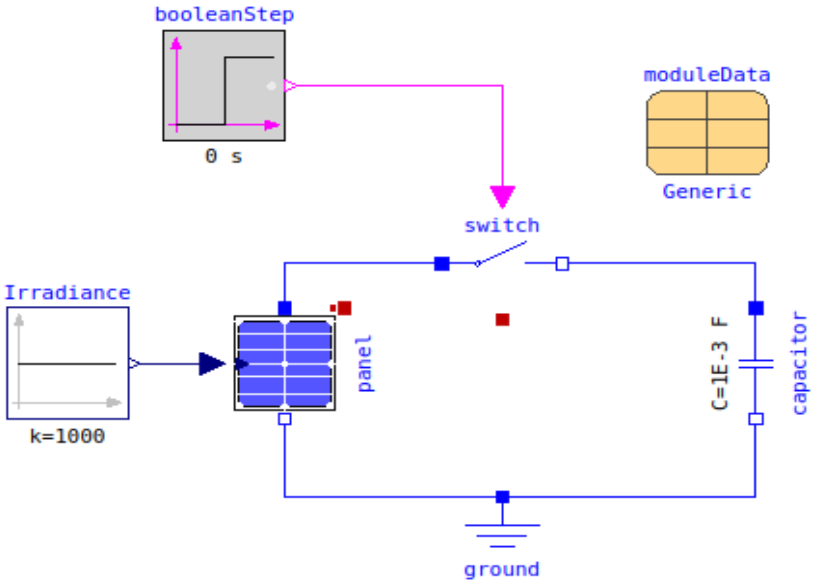

Figure S2. Graphical model for OpenModelica simulation.

Table S1 shows the main parameters used for the simulations. The irradiance has been varied over a range from 200 to 1200 W/m^2. Python scripting was used to modify the simulation parameters.

Table S1. Solar panel models and I-V tracer characteristics for simulation.

Parameter	Values
Irradiance	200 - 1200 W/m^2
Capacitance	1.5mF - 14.8mF
Solar panels	CIGS - Miasolé FLEX–02 120N I_{sc} = 4.53A, V_{oc} = 38.1V, I_{mpp} = 3.93A, V_{mpp} = 30.5V.
	m-Si - Znshine solar ZX55(17.8)M I_{sc} = 3.34A, V_{oc} = 22.25V, I_{mpp} = 3.09A, V_{mpp} = 17.8V.
	HIT - Panasonic VBHN330SJ47 I_{sc} = 6.07A, V_{oc} = 69.7V, I_{mpp} = 5.7A, V_{mpp} = 58V.
Sampling	Up to 1000 samples at a sampling rate of 0.322 ms/sample
t_{delay}	1.5ms (except for HIT with 5ms). According to typical values of solid-state relay in the datasheet.

S.2.1 Simulation results

Equations 12 and **15** allow estimating the I_{SR} and V_{SR} indexes, respectively, as a function of irradiance, electrical panel and tracer characteristics. They also are the basis for the capacitor sizing equations (**Equation 16** and **17**). In this section, simulations are used to verify if **Equations 12** and **15** are valid approximations to the solar panel behavior.

Simulations were carried out using the OpenModelica integrated modeling and simulation environment (Fritzson et al., 2020) and the Photovoltaics Library (Brkic et al., 2019). Scripting and data processing were done in Python using the OMPython package (Kalaiarasi Ganeson et al., 2012). Three different solar panels were evaluated (**Table S1**) with different irradiance levels and capacitance values. In each case the V_{SR} and I_{SR} indexes were calculated.

Figure S3 shows the results of I_{SR} as a function of the irradiance for the different solar panels. Simulation results and theoretical calculations from **Equation 12** are plotted in the same axes. It can be seen that the relationship between I_{SR} and irradiance is linear for the evaluated range of irradiance and capacitance. Also, there is a good approximation between the theoretical and the simulated behavior of the solar panels.

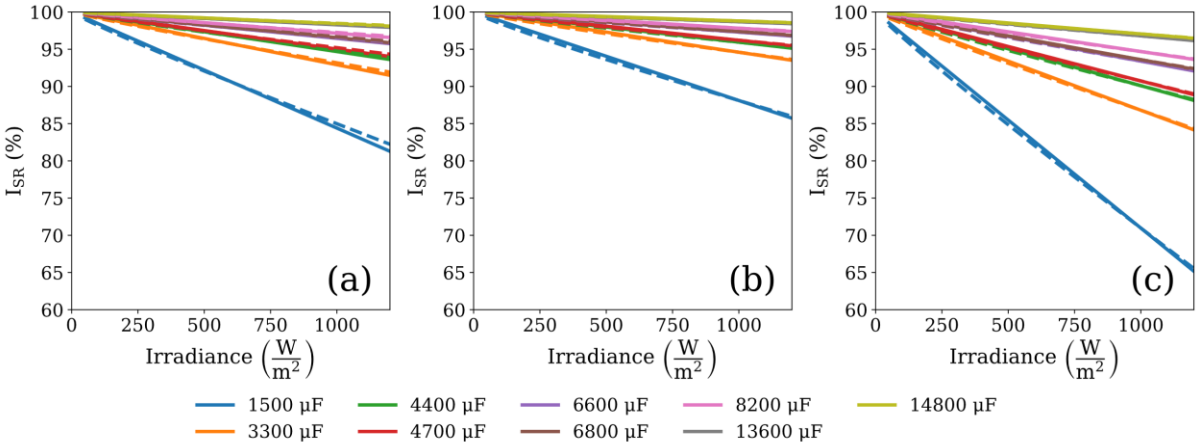

Figure S3. **Theoretical (solid line) and simulation (dashed line) results for I_{SR} as a function of irradiance for different solar panels**. Panel (a) corresponds to m-Si module, (b) to CIGS module and (c) to HIT module. The theoretical I_{SR} was generated according to **Equation 12**.

Figure S4 shows the results for the V_{SR} index. Notice that the exponential shape predicted on the **Equation 15** is confirmed by the simulation results. There is a good approximation between the theoretical calculations and simulated data, allowing us to verify the validity of the assumptions. As stated before, **Equation 15** can predict negative values for the V_{SR} index, this is evident in **Figure S3** where the theoretical curve does not decrease to the zero value of V_{SR} at zero irradiance.

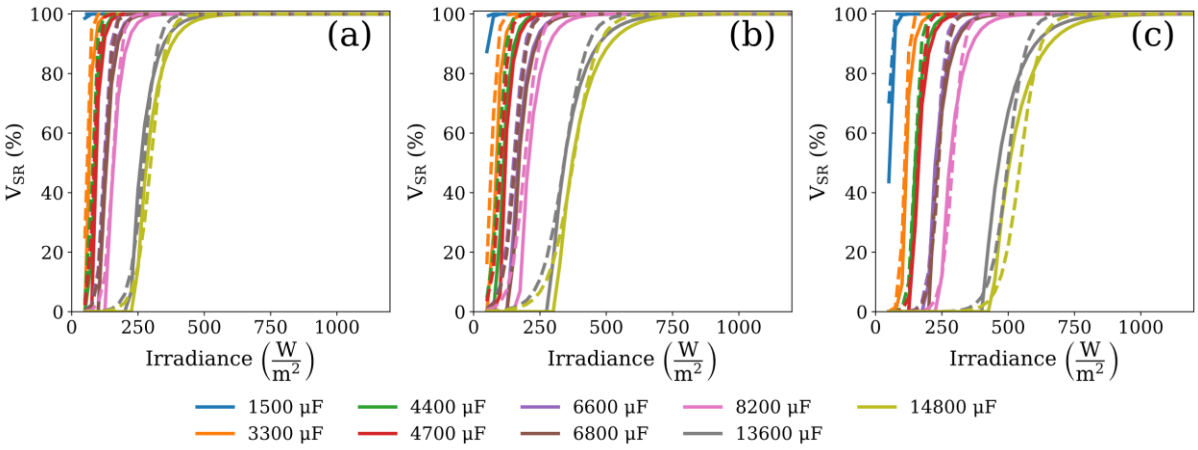

Figure S4. **Theoretical (solid line) and simulation (dashed line) results for V_{SR} as a function of irradiance for different solar panels**. Panel (a) corresponds to m-Si module, (b) to CIGS module and (c) to HIT module. The theoretical V_{SR} was generated according to **Equation 15**.

It can be concluded that the proposed equations (**Equation 12** and **15**) allow a good approximation to the simulated values (which uses the one-diode model for the solar panels) being a practical tool for easy design of the capacitor values.

S.3 Experimental verification

Solar panels in outdoor conditions were used to verify the design methodology. Solar panels references are the same listed in **Table S1**. Solar panels are located at the coordinates (6° 15′ 38″ N 75° 34′ 05″W) corresponding to the terrace of the University Research Center SIU (Sede de Investigaciones Universitarias - Universidad de Antioquia), facing south, with a fixed tilt angle of 13°. I-V curve tracers, irradiance sensors, communications, data storage and processing are the same described at (Velilla et al., 2021, 2019) **Table S2** shows the main characteristics of I-V tracer and monitoring system. For HIT module has been necessary to use different voltage sensor and switch (with higher commutation delay) due to its higher V_{oc} and V_{mpp} values.

Table S2. Main characteristics of I-V tracers and system monitoring.

I-V tracer	**Type**	Capacitive load
	t_{sample}	0.322ms
	$t_{measure}$	322ms (1000 samples)
	Current sensor	0-5A (Tracer for all panels bar HIT) 0-12.5 A (Tracer for HIT panel) Hall efect sensor.
	Voltage sensor	0-35 V (Tracer for all panels bar HIT) 0-65 V (Tracer for HIT panel) Isolated amplifier.
Sensors	**Irradiance**	Spektron 210 (TRITEC international)
	Ambient Temperature	PT-1000 (TRITEC international)

The monitoring system was formed by a calibrated cells TRITEC International (Spektron 210) irradiance sensor located coplanar with the DUTs. Also, a pyranometer MS-60S by Eko instruments (with an uncertainty of 0.77 % and coverage factor of 1.96) was used to validate the irradiance measurements. The ambient and device temperature were registered by TRITEC International sensors (PT-1000 with a tolerance of ± 0.8 °C). Ambient temperature was measured near to the irradiance sensors, and device temperature was measured at the back part of the devices. A Fronius sensor box (Fronius International GMBH) was used as a data-logger for irradiance and temperature sensors. The voltage and current sensors (**Table S2**) of the I-V curve tracers were calibrated using certified equipment (Fluke 5522 A-SC) according to procedure CEM-EL-001, obtaining a maximum extended measurement uncertainty of 4.4 mV for voltage and 7.2 mA for current, considering a coverage factor and probability of 2 and 95 % respectively.

I-V curve tracer's capacitance was changed through several values, from March 01 to December 31 of 2021. **Table S3** resumes the capacitance values used on each panel.

Table S3. Capacitance values and time used on experimental verification.

Panel	Technology	Capacitance values and time					
		(µF)	Weeks	(µF)	Weeks	(µF)	Weeks
Miasolé FLEX–02 120N	CIGS	3300	8	4400	5	8200	20
Znshine solar ZX55(17.8)M	m-Si	4400	5	8200	20	14800	8
Panasonic VBHN330SJ47	HIT	4700	5	6800	20	13600	8

During the exposition time, an I-V curve is captured every minute from 6:00 AM to 6:59 PM. At each curve, the I_{min}, V_{min}, V_{SR}, and I_{SR} parameters were calculated, additionally to the traditional V_{oc}, I_{sc}, V_{mpp}, and I_{mpp} parameters. Also, irradiance and ambient temperature were recorded for each measurement.

S.3.1 Estimated and Datasheet t_{switch} Values

Table S4 shows a comparison between estimated and reported manufacture t_{switch} values. The estimated value was generated from I-V curve records on outdoor conditions.

Table S4. Estimated values for t_{switch} vs datasheet values

PV Device	Switch reference	t_{switch}		
		Datasheet (typical)	Datasheet (maximum)	Estimated (median)
m-Si	CPC1907	2.7ms	5ms	1.932ms
CIGS				
HIT	CPC1727	5.5ms	20ms	11.27ms

S.3.2 Capacitance uncertainty

With the aim of showing the capacitance uncertainty influence on V_{SR} and I_{SR} indexes, **Figure S5** was generated, where a capacitance uncertainty of ±20% was considered (similar to commercial values).

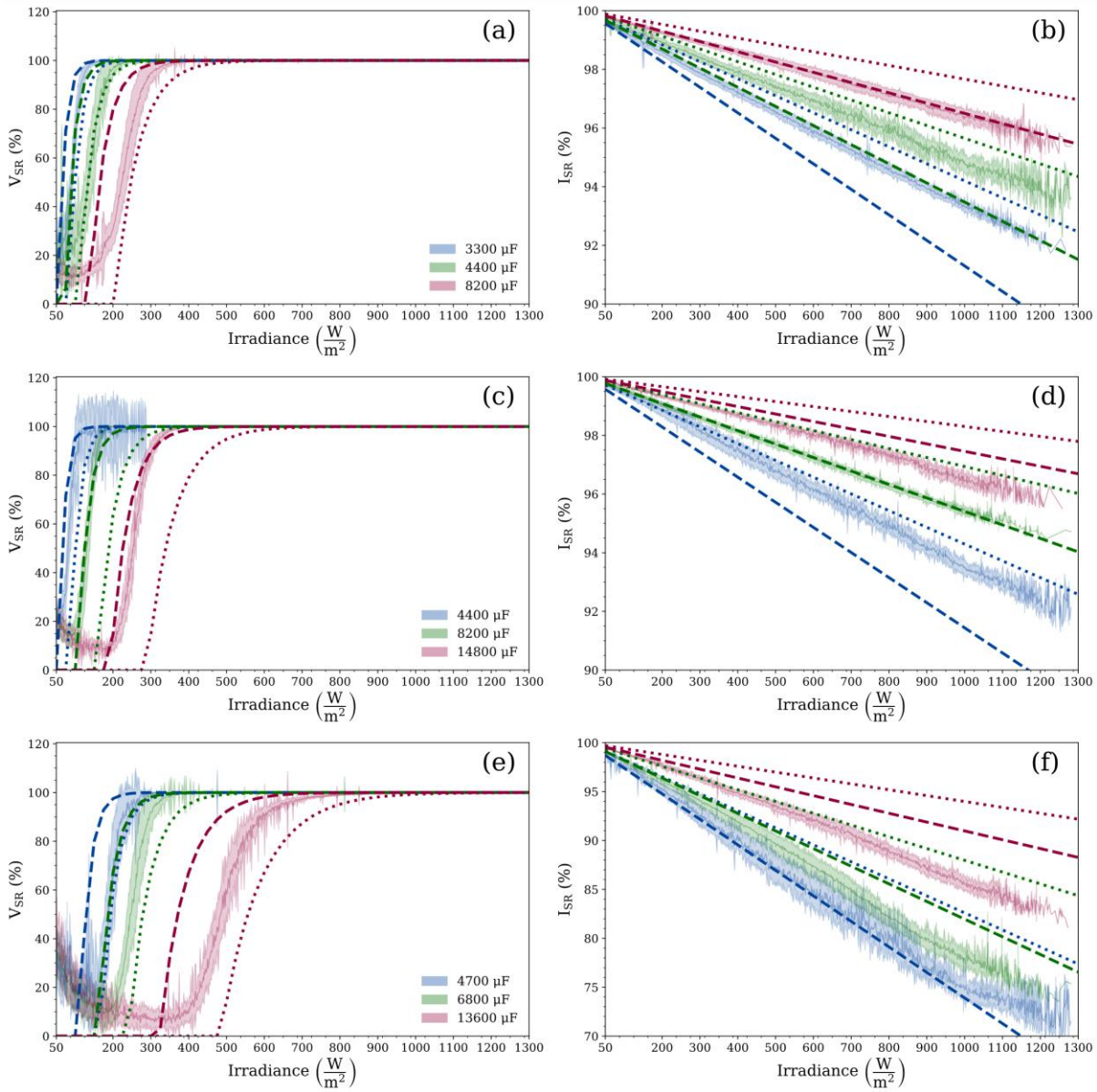

Figure S5. Impact of uncertainty capacitance value on the indexes. V_{SR} and I_{SR} for different capacitor values. Panels (a-b) correspond to the CIGS - Miasolé module, (c-d) to the m-Si - Znshine, and panels (e-f) to the HIT - Panasonic module. The dotted lines correspond to the proposed design equations with +20% of capacitance, the dashed lines correspond to the proposed design equations with -20% of capacitance, **Equation 15** for V_{SR} and **Equation 12** for I_{SR} using the estimated t_{delay} found for each panel (**Table S4**). The contour area corresponds to real data standard deviation with respect to median values. The insets shown the installed capacitance in the tracer.

S.3.3 Heat maps

In order to simultaneously observe how the V_{SR} and I_{SR} are affected by irradiance and the selected capacitance, **Figure S6** shows a heat map of these values for real and simulated data. In a general way, it can be observed that there is concordance between both cases. These maps are very useful as they allow a quick way to size the capacitor for the desired irradiance conditions for a particular photovoltaic panel.

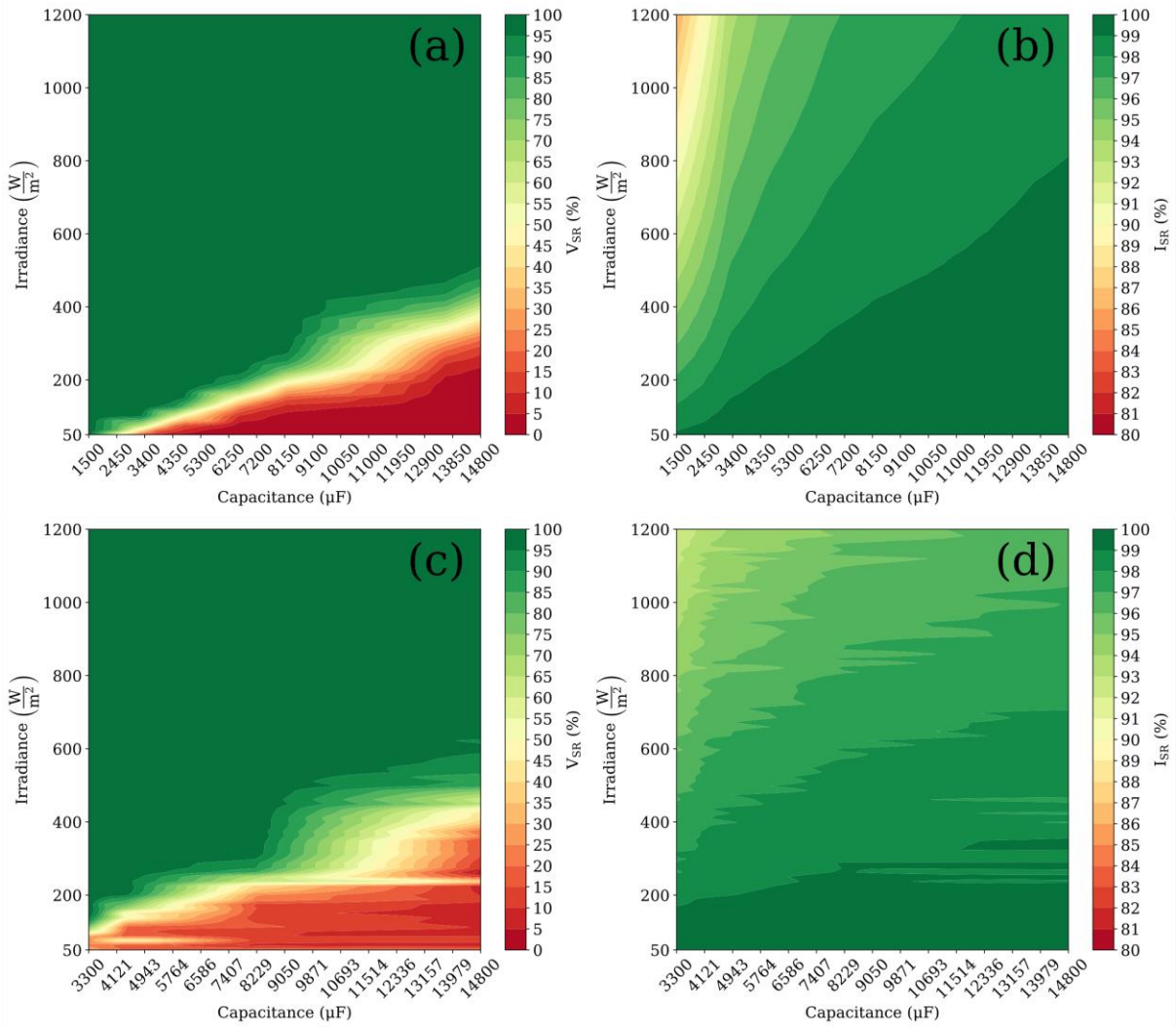

Figure S6. Success rate as a function of irradiance and capacitance for CIGS panel. Panels (a-c) correspond to V_{SR} and (b-d) to I_{SR}. Panels (a-b) correspond to simulated data in OpenModelica and panels (c-d) correspond to real outdoor data.

References

Brkic, J., Ceran, M., Elmoghazy, M., Kavlak, R., Haumer, A., Kral, C., 2019. Open Source PhotoVoltaics Library for Systemic Investigations. Proc. 13th Int. Model. Conf. Regensburg, Ger. March 4–6, 2019 157, 41–50. https://doi.org/10.3384/ecp1915741

Fritzson, P., Pop, A., Abdelhak, K., Asghar, A., Bachmann, B., Braun, W., Bouskela, D., Braun, R., Buffoni, L., Casella, F., Castro, R., Franke, R., Fritzson, D., Gebremedhin, M., Heuermann, A., Lie, B., Mengist, A., Mikelsons, L., Moudgalya, K., Ochel, L., Palanisamy, A., Ruge, V., Schamai, W., Sjolund, M., Thiele, B., Tinnerholm, J., Ostlund, P., 2020. The OpenModelica integrated environment for modeling, simulation, and model-based development. Model. Identif. Control 41, 241–285. https://doi.org/10.4173/MIC.2020.4.1

Kalaiarasi Ganeson, A., Fritzon, P., Rogovchenko, O., Asghar, A., Sjölund, M., Pfeiffer, A., 2012. An OpenModelica Python Interface and its use in PySimulator. Proc. 9th Int. Model. Conf. Sept. 3-5, 2012, Munich, Ger. 76, 537–548. https://doi.org/10.3384/ecp12076537

Velilla, E., Cano, J.B., Jaramillo, F., 2019. Monitoring system to evaluate the outdoor performance of solar devices considering the power rating conditions. Sol. Energy 194, 79–85. https://doi.org/10.1016/J.SOLENER.2019.10.051

Velilla, E., Jaramillo, F., Mora-Seró, I., 2021. High-throughput analysis of the ideality factor to evaluate the outdoor performance of perovskite solar minimodules. Nat. Energy 6, 54–62. https://doi.org/10.1038/s41560-020-00747-9

Anexo 3:

Outdoor and synthetic performance data for PV devices concerning the weather conditions and capacitor values of I-V tracer

https://doi.org/10.1016/j.dib.2023.109007

Data in Brief 47 (2023) 109007

Contents lists available at ScienceDirect

Data in Brief

journal homepage: www.elsevier.com/locate/dib

Data Article

Outdoor and synthetic performance data for PV devices concerning the weather conditions and capacitor values of I-V tracer

C.D. Londoño [a], J.B. Cano [a,*], F. Jaramillo [b], J.A. Valencia [a], E. Velilla [a,b]

[a] *Grupo en Manejo Eficiente de la Energía, GIMEL, Universidad de Antioquia UdeA, Calle 70 No. 52-21, Medellín, Colombia*

[b] *Centro de Investigación, Innovación y Desarrollo de Materiales – CIDEMAT, Universidad de Antioquia UdeA, Calle 70 No. 52-21, Medellín, Colombia*

ARTICLE INFO

Article history:
Received 26 October 2022
Revised 15 February 2023
Accepted 16 February 2023
Available online 23 February 2023

Dataset link: Outdoor and Synthetic Data of PV devices Performance Concerning the Weather Conditions and Capacitor Values of I-V Tracer (Original data)

Keywords:
Outdoor tests
Photovoltaic devices performance
I-V curves
Capacitive I-V tracers
Weather conditions

ABSTRACT

This article presents the outdoor and synthetic performance data concerning the main electrical parameters estimated from the I-V curve for three photovoltaic technologies (HIT, m-Si and CIGS) and the weather conditions (irradiance, ambient and panel temperature). Synthetic data were generated by simulating in OpenModelica software the impact of weather conditions on device performance, considering an irradiance range between 50 and 1300 W/m^2. The outdoor data corresponds to the performance of the evaluated PV modules in outdoor tests in Medellin-Colombia for ten months using capacitive I-V tracers. In both cases, different capacitor values were considered to evaluate the effect on the I-V curve behavior of devices.

DOI of original article: 10.1016/j.solener.2022.08.021

* Corresponding author.
E-mail address: bernardo.cano@udea.edu.co (J.B. Cano).

https://doi.org/10.1016/j.dib.2023.109007

Specifications Table

Subject	Renewable Energy, Sustainability and the Environment
Specific subject area	Solar energy, characterization of photovoltaic devices in outdoor and simulating conditions through I-V curves estimated by capacitive technique using different capacitor values
Type of data	Table OpenModelica photovoltaic panel model Python script
How the data were acquired	• The real data were obtained by measuring the electrical performance (I-V curves) for different PV modules in outdoor conditions and eather conditions. Capacitive I-V tracers (details on tracer specifications can be found in [1] and [2]) were used to record the I-V curve of each solar panel. From the curves, the electrical variables concerning the device performance were estimated: short circuit current (I_{sc}), open circuit voltage (V_{oc}), maximum power (P_{max}) and voltage and current at maximum power point (V_{mpp}, I_{mpp}). Ambient and solar panel temperatures were recorded by using PT1000 thermistors (TRITEC International). Solar irradiance was measured by using calibrated cells (Spektron 210 - TRITEC International) coplanar with the solar panel array. Also, a pyranometer class B was used to validate the irradiance values. All variables were sampled at a rate of 1 sample/minute during the light-hours (6:00AM to 6:00PM). • The synthetic data were obtained by simulating the solar panels behavior in OpenModelica software through python scripting. In both cases (outdoor and synthetic data) different values of capacitance were used for the I-V tracer.
Data format	Raw
Description of data collection	Data correspond to the electrical variables of three modules of different technologies, Panasonic VBHN330SJ47 (HIT), Znshine solar ZX55(17.8)M (m-Si), and Miasolé FLEX–02 120 N (CIGS) in outdoor and simulating conditions. For outdoor data, the panels were located in natural sunlight without a tracker, facing south at a fixed tilt angle of 13°. Different capacitance values were used in outdoor tests and simulation process to estimate the device performance.
Data source location	Institution: Universidad de Antioquia (UdeA) City/Town/Region: Medellin Country: Colombia Latitude and longitude for collected samples/data: **6°15′ 38″N 75°34′ 05″W**
Data accessibility	Data is hosted on Mendeley Data [3]. Data identification number: 10.17632/k8y3nxxyp5.2 Direct URL to data: https://data.mendeley.com/datasets/k8y3nxxyp5/2 The source code for generating the simulated data is include in the link above.
Related research article	Londoño, C. D., Cano, J. B., Velilla, E., Capacitive tracer design to mitigate incomplete IV curves in outdoor tests. Sol. Energy. *243* (2022), 361–369. 10.1016/j.solener.2022.08.021

Value of the Data

- The dataset contains the electrical performance estimated from the I-V curve for three different commercial photovoltaic technologies (HIT, m-Si, CIGS) concerning the weather conditions. Synthetic data were generated in an electrical simulation program (OpenModelica). The data are highly valuable to research, monitor and compare the behavior of these technologies and devices under the same conditions.
- These data can benefit researchers and companies working on the characterization and validation of photovoltaic technologies in outdoor conditions as well as other applications related to Deep Learning and solar panel modeling.
- These data can be used to reproduce previous results in order to validate the proposed design approach for the capacitive I-V tracers [4]. In addition, because the data correspond to the outdoor performance of PV devices, the data can be used for comparing the PV devices' behavior under real operation conditions or selecting proper conditions regarding the weather conditions.

Table 1
List of column names, units of measurement and descriptions of data provided in the outdoor dataset (*"BD_DIB_Outdoor_Solar_Panels_Electrical_Parameters.xlsx"*).

Column Name	Units	Description
Panel	–	Technology / panel device
C	µF	Capacitance used in the I-V tracer
datetime	yyyy-mm-dd HH:MM:SS	Measurement date and time
Irradiance	W/m^2	Global irradiance coplanar to tilt angle of the devices
T panel	°C	Panel temperature
T amb	°C	Ambient temperature
Voc	V	Open circuit voltage
Isc	A	Short circuit current
Pmax	W	Maximum power
Vmpp	V	Voltage at the maximum power point
Impp	A	Current at the maximum power point
Vmin	V	Minimum voltage measured in I-V curve
Imin	A	Minimum current measured in I-V curve
Voc_Success	%	Success rate of voltage, defined by $100(1-\frac{I_{min}}{I_{sc}})$
Isc_Success	%	Success rate of current, defined by $100(1-\frac{V_{min}}{V_{oc}})$

Objective

Incomplete I-V curves of PV devices were observed in outdoor tests when capacitive tracers were used to trace the I-V curve. This behavior was also observed by simulating the PV devices considering similar weather conditions and the circuital elements involved in the capacitive technique. In this regard, the synthetic data allows validating the outdoor behavior and the proposed methodology for sizing the capacitance of the tracer [4]. Therefore, both datasets are useful for researchers to understand, compare and model the performance of devices under real weather conditions. In addition, datasets can be used for validating testing techniques to be implemented in I-V tracers.

1. Data Description

The file "*BD_DIB_Outdoor_Solar_Panels_Electrical_Parameters.xlsx*" contained in the Mendeley Data repository [3], it is related to the outdoor dataset with the electrical parameters of three different photovoltaic panels (Panasonic VBHN330SJ47 (HIT), Znshine solar ZX55(17.8)M (m-Si), and Miasolé FLEX–02 120 N (CIGS)) and weather conditions related to the place where these devices were installed (Fig. 1). In Table 1 are listed the details relating to the data. This table comprises the column names as they appear in the data CSV file, the unit of measurement, and a brief description of the data in each column.

The file "*BD_DIB_Synthetic_Solar_Panels_Electrical_Parameters.xlsx*" contained in the Mendeley Data repository [3], it is related to the synthetic dataset with the electrical parameters for three different photovoltaic panels (Panasonic VBHN330SJ47 (HIT), Znshine solar ZX55(17.8)M (m-Si), and Miasolé FLEX–02 120 N (CIGS)) estimated in OpenModelica [5] software version 1.19.2. In Table 2 are listed the details relating to the data. This table comprises the column names as they appear in the data CSV file, the unit of measurement, and a brief description of the data in each column.

The file *"IVTraceCapacitor.mo"* contained in the Mendeley Data repository [3], it is the OpenModelica [5] photovoltaic panel model that allows to model the behavior of the photovoltaic modules. The parameters of modules at Standard Test Conditions are show in Table 3.

The file *"Generate_Synthetic_Data_OpenModelica.py"* contained in the Mendeley Data repository [3], it is a python script related to the simulation process carried out to estimate the synthetic dataset data. This script is summarized in the flowchart shown in the Fig. 2.

Fig. 1. Laboratory for performance characterization of photovoltaic devices in outdoor conditions, Sede de Investigación Universitaria – SIU, Universidad de Antioquia, Medellín, Colombia.

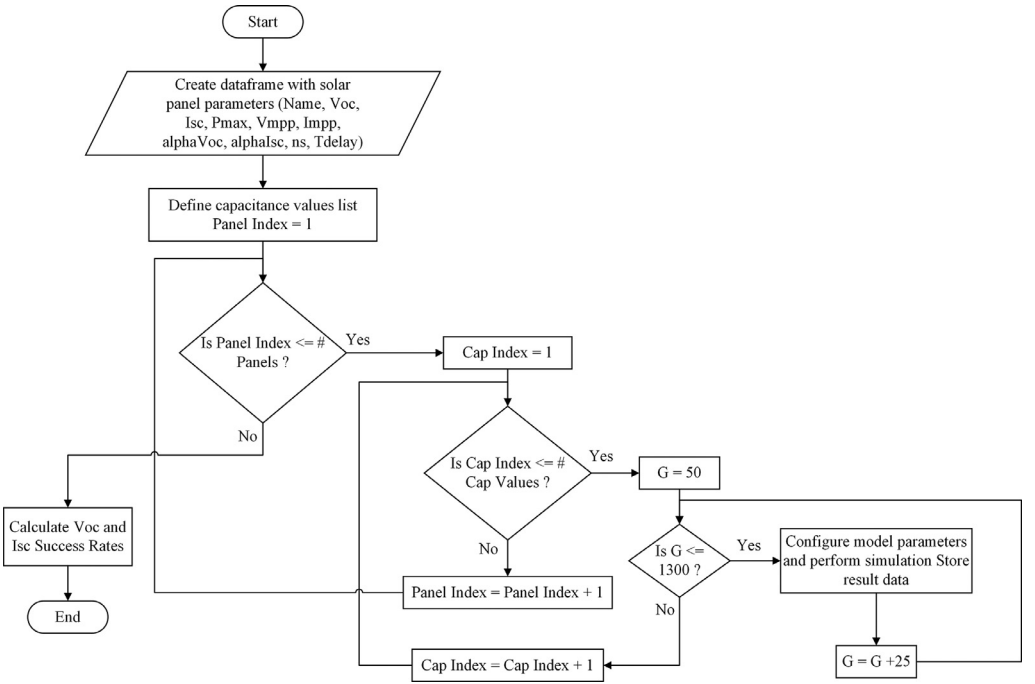

Fig. 2. Flowchart of simulating process in OpenModelica [5] using the python script *"Generate_Synthetic_Data_OpenModelica.py"*.

Table 2
List of column names, units of measurement and descriptions of data provided in the simulating dataset (*"BD_DIB_Synthetic_Solar_Panels_Electrical_Parameters.xlsx"*).

Column Name	Units	Description
Panel	–	Technology / panel device
C	µF	Capacitance used in the I-V tracer
Irradiance	W/m^2	Global irradiance coplanar to tilt angle of the devices
Voc	V	Open circuit voltage
Isc	A	Short circuit current
Pmax	W	Maximum power
Vmpp	V	Voltage at the maximum power point
Impp	A	Current at the maximum power point
Vmin	V	Minimum voltage measured in I-V curve
Imin	A	Minimum current measured in I-V curve
Voc_Success	%	Success rate of voltage, defined by $100(1-\frac{I_{min}}{I_{sc}})$
Isc_Success	%	Success rate of current, defined by $100(1-\frac{V_{min}}{V_{oc}})$
Tmpp	ms	Time to reach the maximum power point
TVoc	ms	Time to reach the maximum open circuit point

Table 3
Parameters of photovoltaic modules.

Panel Technology	Manufacturer	Series	Electrical Parameters at Standard Test Conditions (STC)					Dimensions (mm)	
			P_{max} (W)	V_{mpp} (V)	I_{mpp} (A)	V_{oc} (V)	I_{sc} (A)	Length	Width
CIGS	Miasolé	FLEX–02 120N	120	30.50	3.93	38.10	4.53	2598	370
m-Si	Znshine solar	ZX55(17.8)M	55	17.80	3.09	22.25	3.34	837	541
HIT	Panasonic	VBHN330SJ47	330	58.00	5.70	69.70	6.07	1590	1053

Table 4
Main parameters for simulating processes in OpenModelica.

Parameter	Values
Irradiance Range	50–1300 W/m^2 with steps of 25 W/m^2
Capacitances	1500 µF, 3300 µF, 4400 µF, 4700 µF, 6600 µF, 6800 µF, 8200 µF, 13,600 µF, 14,800 µF
Solar Panels Parameters	CIGS - Miasolé FLEX–02 120 N I_{sc} = 4.53A, V_{oc} = 38.1 V, I_{mpp} = 3.93A, V_{mpp} = 30.5 V, alphaVoc = −0.0028, alphaIsc = 0.00008, ns = 60 m-Si - Znshine solar ZX55(17.8)M I_{sc} = 3.34A, V_{oc} = 22.25 V, I_{mpp} = 3.09A, V_{mpp} = 17.8 V, alphaVoc = −0.0028, alphaIsc = 0.00008, ns = 24 HIT - Panasonic VBHN330SJ47 I_{sc} = 6.07A, V_{oc} = 69.7 V, I_{mpp} = 5.7A, V_{mpp} = 58 V, alphaVoc = −0.0028, alphaIsc = 0.00008, ns = 96
Sampling	Up to 1000 samples at a sampling rate of 0.322 ms/sample
t_{delay}	1.5 ms (except for HIT with 5 ms). According to typical values of solid-state relay in the datasheet.

The experimental setup used to obtain the data is described in the next section. In this regard, Fig. 3 shows the weather condition sensors, Fig. 4 shows the developed I-V curve tracers and Fig. 5 shows the implemented monitoring system. Concerning the synthetic data, Table 4 shows the main parameters considered in OpenModelica to perform the simulations following the flowchart shown in Fig. 2 and the circuit diagram of Fig. 6.

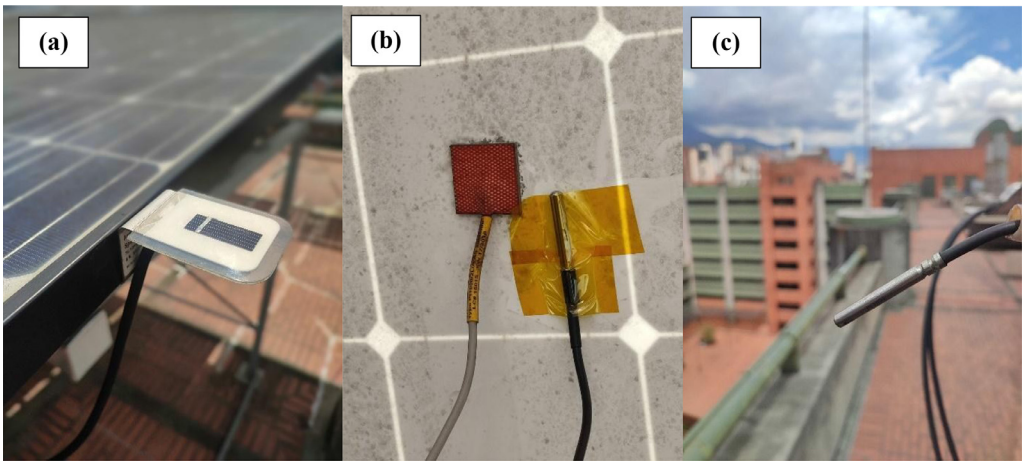

Fig. 3. Sensors for measuring weather conditions. Panel (a) corresponds to irradiance sensor, panel (b) to panel temperature sensor and panel (c) to ambient temperature sensor.

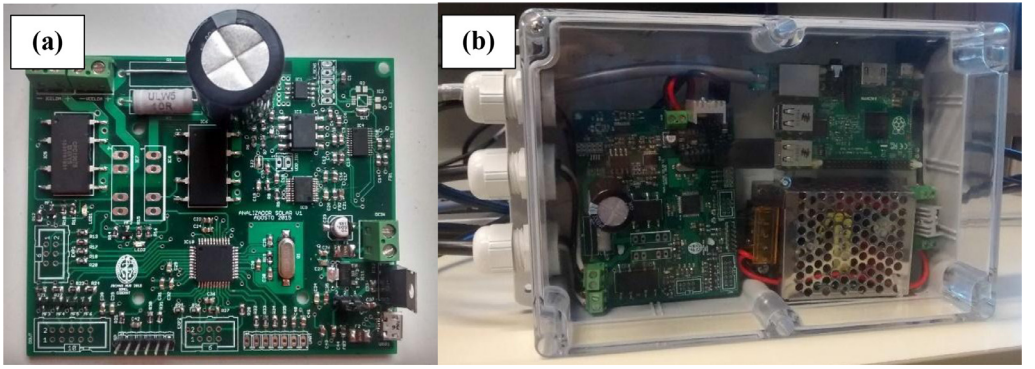

Fig. 4. Capacitive I-V tracer. Panel (a) corresponds to the designed electronic circuit to trace the I-V curve considering the capacitive technique. Panel (b) shows the developed prototype to record the I-V curves in outdoor conditions using an embedded computer to automate the process.

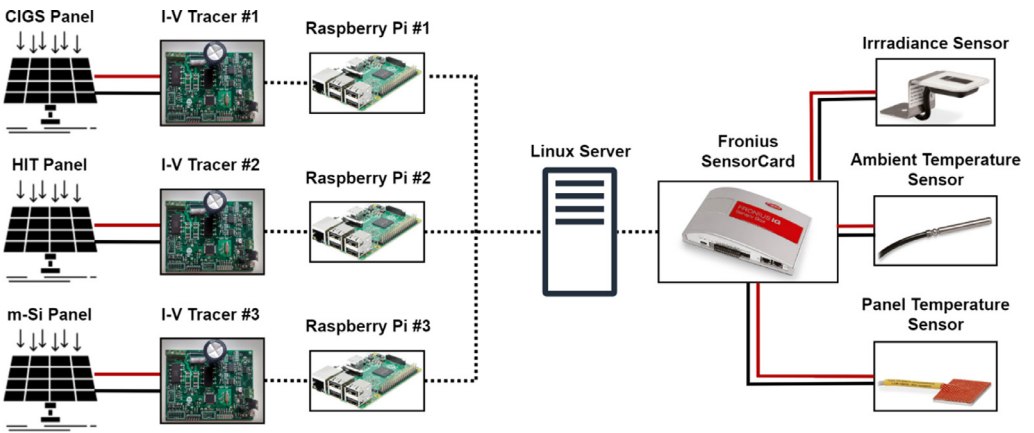

Fig. 5. Schematic diagram of the experimental setup for measuring real I-V curves in outdoor conditions and weather variables.

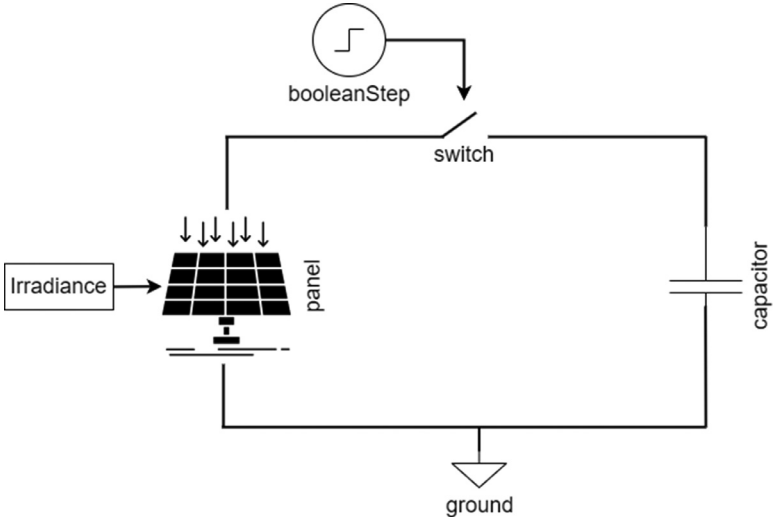

Fig. 6. Circuit diagram used in OpenModelica by python scripting.

2. Experimental Design, Materials and Methods

This section presents the methodologies, methods and elements used for the information acquisition process of the real data in outdoor conditions and the data obtained through simulation.

2.1. Outdoor Data

The outdoor data has been obtained using the facilities of the Universidad de Antioquia for photovoltaic outdoor device characterization, located in Medellín, Colombia (6°15′ 38″N 75°34′ 05″W). Fig. 1 shows the entire experimental set-up for monitoring the PV devices, where it can be observed photovoltaic devices under test, sensors for measuring weather variables and electronic power devices for connecting panels to the grid.

Fig. 3 shows the sensor used for measuring temperature and irradiance. Panel and ambient temperature were measured by PT1000 thermistors (TRITEC International). In the panel temperature case, the thermistor was located in the back side of the panel. Global irradiance was measured by using a calibrated cell (Spektron 210 - TRITEC International) located parallel to the tilt angle of the panels. The three sensors of Fig. 3 were connected to a Fronius SensorCard (Fronius International GmbH). These variables were measured every minute and were synchronized regarding the I-V tracers records.

2.2. Photovoltaic Modules

Table 3 shows the characteristics of the three photovoltaic modules used in the development of this work.

2.3. I-V Tracers

Fig. 4 shows the equipment used to measure the I-V curves of the solar panels that were evaluated. The I-V tracers (Fig. 4a) use the capacitive technique that consists in tracing the I-V curve by measuring the charge of the capacitor connected to the device under test. For more details about the characteristics of these device consult [1,2]

The capacitance values installed in the I-V tracers during the exposure time for each evaluated solar panel were as follows: for Miasolé FLEX–02 120 N (CIGS) panel 3300, 4400, 8200 and 14,800 µF, for Znshine solar ZX55(17.8)M (m-Si) panel 1000, 4400, 8200 and 14,800 µF and for Panasonic VBHN330SJ47 (HIT) panel 3200, 4700, 6800 and 13,600 µF. The capacitance values were changed with the aim of validating the capacitance design methodology proposed in [4].

2.4. Experimental Setup

Fig. 5 shows a schematic diagram of the experimental setup used in the development of this work. Each panel is connected to an I-V tracer (with its corresponding capacitor) whit the corresponding raspberry pi to record the I-V curve data and send the data to the main computer (linux server). Ambient and panel temperature and irradiance sensors were connected to a Fronius SensorCard to record the weather data. Each I-V curve and weather variables were measured simultaneously every minute during daylight hours (6:00AM to 6:00PM).

2.5. Synthetic Data

The synthetic data were generated by using OpenModelica simulation software. Fig. 6 shows the circuit diagram representation of the simulation model. The solar panel, capacitive load and the switch are present in the process. The simulation model contains different blocks that allow modification and set parameters by python scripting (using the OMPython package [6]). The booleanStep block controls the switch, guaranteeing its closure at $t = 0\ s$. The irradiance block allows to set a constant irradiance for the simulation, while the ModuleData block allows to modify the main panel characteristics (V_{oc}, I_{sc}, V_{mpp}, I_{mpp} and temperature coefficients). Solar panel models were taken from the Photovoltaics library described at [7] and parameterized using the datasheet information for each panel.

.The simulation process in OpenModelica was automatized by using a Python script according to the flowchart shown in Fig. 2. By the end of the simulation a dataset with the parameters was generated as shown in the Table 2. The source code and the OpenModelica model file ".om" can be download from the repository listed in the Specifications table/ data accessibility section [3].

Table 4 shows the parameters used for the simulation by python scripting using the OpenModelica library.

Declaration of Competing Interest

The authors declare that they have no known competing financial interests or personal relationships that could have appeared to influence the work reported in this paper.

Data Availability

Outdoor and Synthetic Data of PV devices Performance Concerning the Weather Conditions and Capacitor Values of I-V Tracer (Original data) (Mendeley Data).

CRediT Author Statement

C.D. Londoño: Methodology, Software, Investigation, Writing – original draft; **J.B. Cano:** Conceptualization, Methodology, Software, Investigation, Writing – review & editing, Supervision; **F. Jaramillo:** Investigation, Writing – review & editing, Supervision; **J.A. Valencia:** Validation, Supervision, Writing – review & editing; **E. Velilla:** Conceptualization, Methodology, Software, Validation, Supervision, Writing – review & editing.

Ethics Statement

This work did not involve human subjects, animal experiments and data collected from social media platforms.

Acknowledgment

Esteban Velilla thanks Colombia's Administrative Department of Science, Technology and Innovation (MINCIENCIAS) for national doctoral scholarship number 727–2015 (contract no. FP44842–124–2017).

Besides, the authors gratefully acknowledge the financial support provided by the Colombia Scientific Program within the framework of the call Ecosistema Científico (contract no. FP44842—218–2018).

References

[1] E. Velilla, J.B. Cano, F. Jaramillo, Monitoring system to evaluate the outdoor performance of solar devices considering the power rating conditions, Sol. Energy 194 (2019) 79–85, doi:10.1016/j.solener.2019.10.051.
[2] A. Padilla, C. Londoño, F. Jaramillo, I. Tovar, J.B. Cano, E. Velilla, Photovoltaic performance assess by correcting the I-V curves in outdoor tests, Sol. Energy 237 (2022) 11–18, doi:10.1016/j.solener.2022.03.064.
[3] C. Londoño, J. Cano, F. Jaramillo, J. Valencia, E. Velilla, Outdoor and synthetic data of PV devices performance concerning the weather conditions and capacitor values of I-V tracer, Mendeley Data (2022), doi:10.17632/k8y3nxxyp5.2.
[4] C.D. Londoño, J.B. Cano, E. Velilla, Capacitive tracer design to mitigate incomplete I-V curves in outdoor tests, Sol. Energy 243 (2022) 361–369, doi:10.1016/j.solener.2022.08.021.
[5] P. Fritzson, A. Pop, K. Abdelhak, A. Asghar, B. Bachmann, W. Braun, D. Bouskela, R. Braun, L. Buffoni, F. Casella, R. Castro, R. Franke, D. Fritzson, M. Gebremedhin, A. Heuermann, B. Lie, A. Mengist, L. Mikelsons, K. Moudgalya, L. Ochel, A. Palanisamy, V. Ruge, W. Schamai, M. Sjolund, B. Thiele, J. Tinnerholm, P. Ostlund, The OpenModelica integrated environment for modeling, simulation, and model-based development, Model. Identif. Control 41 (2020) 241–285, doi:10.4173/MIC.2020.4.1.
[6] A. Kalaiarasi Ganeson, P. Fritzon, O. Rogovchenko, A. Asghar, M. Sjölund, A. Pfeiffer, An OpenModelica python interface and its use in PySimulator, in: Proceedings of the 9th International MODELICA Conference; September 3-5; 2012; Munich; Germany, 76, 2012, pp. 537–548, doi:10.3384/ecp12076537.
[7] J. Brkic, M. Ceran, M. Elmoghazy, R. Kavlak, A. Haumer, C. Kral, Open source photovoltaics library for systemic investigations, in: Proceedings of the 13th International Modelica Conference, Regensburg, Germany, March 4–6, 2019, 157, 2019, pp. 41–50, doi:10.3384/ecp1915741.

Anexo 4:

Photovoltaic performance assess by correcting the I-V curves in outdoor tests

https://doi.org/10.1016/j.solener.2022.03.064

Solar Energy 237 (2022) 11–18

Contents lists available at ScienceDirect

Solar Energy

journal homepage: www.elsevier.com/locate/solener

Photovoltaic performance assess by correcting the I-V curves in outdoor tests

A. Padilla [a], C. Londoño [b], F. Jaramillo [c], I. Tovar [a], J.B. Cano [b,*], E. Velilla [b,c]

[a] Grupo Interdisciplinario de Investigación en Energía y Medio Ambiente, - GIIMA, Universidad Autónoma del Caribe, Código Postal 080020, Barranquilla, Colombia
[b] Grupo en Manejo Eficiente de la Energía, GIMEL, Universidad de Antioquia UdeA, Calle 70 No. 52-21, Medellín, Colombia
[c] Centro de Investigación, Innovación y Desarrollo de Materiales – CIDEMAT, Universidad de Antioquia UdeA, Calle 70 No. 52-21, Medellín, Colombia

ARTICLE INFO

Keywords:
Outdoor tests
Photovoltaic performance
I-V curves
STC
NOCT
Temperature coefficients

ABSTRACT

The photovoltaic performance is conventionally defined at Standard Test Conditions (STC), considering mainly an irradiance of 1000 W/m^2 and device temperature of 25 °C. Nevertheless, outdoor conditions involve additional variables, including their transient behavior, affecting the performance. Therefore, measuring the performance at STC in outdoor tests is not always possible. In order to estimate the performance at STC or other power rating conditions such as the Nominal Operating Cell Temperature (NOCT), this work translated the outdoor performance at the target conditions by combining three different I-V curves and corresponding weather data for three photovoltaic technologies. Hence, a random process was proposed to generate the dataset to be translated, ensuring reliability in the estimation due to the significant number of considered weather conditions combinations, covering a wide range of the outdoor performance behavior as a function of irradiance and temperature. Besides, the dataset was filtered using an irradiance and extrapolation range, improving the estimation by calculating relative error of less than 8% at STC and NOCT concerning the datasheet values. Finally, the procedure was extended to estimate the temperature coefficients allowing a complete performance validation concerning the datasheet.

1. Introduction

The outdoor performance of photovoltaic devices is a function of variables such as irradiance, temperature, relative humidity, wind speed, etc. (Quansah and Adaramola, 2019), including the transient behavior of these variables during the exposure. Therefore, these conditions change during the operation, affecting the device performance and could result in various degradation mechanisms such as discoloration, delamination, hot spot, among others (Ndiaye et al., 2013), finally affecting the lifetime. Related to outdoor tests, five power rating conditions (PRC), including STC and NOCT, are suggested to evaluate the impact of weather variables on performance and complete the characterization of the devices (IEC 61853-1, 2011). However, despite STC being conventionally included in the datasheet and used to define the device performance, these conditions rarely occur outdoors; therefore, it is not easy to measure the performance under these conditions in tests with natural sunlight (Velilla et al., 2019a). In this regard, it is essential to develop numerical tools to estimate the performance, verify the module status concerning the datasheet, compare photovoltaic modules under specific conditions (Velilla et al., 2019b), investigate the performance evolution, and estimate, for instance, the lifetime (Jordan et al., 2018; Phinikarides et al., 2014).

The standard IEC 60891 provides three procedures for correcting the performance measured at specific temperature and irradiance conditions to the target conditions. Procedure 1 corresponds to the voltage and current temperature coefficients. Procedure 2 is based on the one-diode model, including the temperature coefficients and an additional coefficient related to the series resistance. Procedure 3 is based on the interpolation or extrapolation of the I-V curves to estimate the target performance at specific irradiance and temperature conditions. Although these procedures are generally suitable for indoor measurements because the variables can be controlled (temperature and irradiance), these coefficients have been estimated in outdoor tests. For instance, the three procedures were compared for predicting photovoltaic energy production for an m-Si module (Duck et al., 2013), showing that the estimated performance depends on the most frequent irradiance and temperature conditions during the tests. Moreover, even though the three procedures were also used for evaluating thin-film technologies at

* Corresponding author.
E-mail address: bernardo.cano@udea.edu.co (J.B. Cano).

https://doi.org/10.1016/j.solener.2022.03.064
Received 26 July 2021; Received in revised form 22 March 2022; Accepted 27 March 2022
Available online 2 April 2022

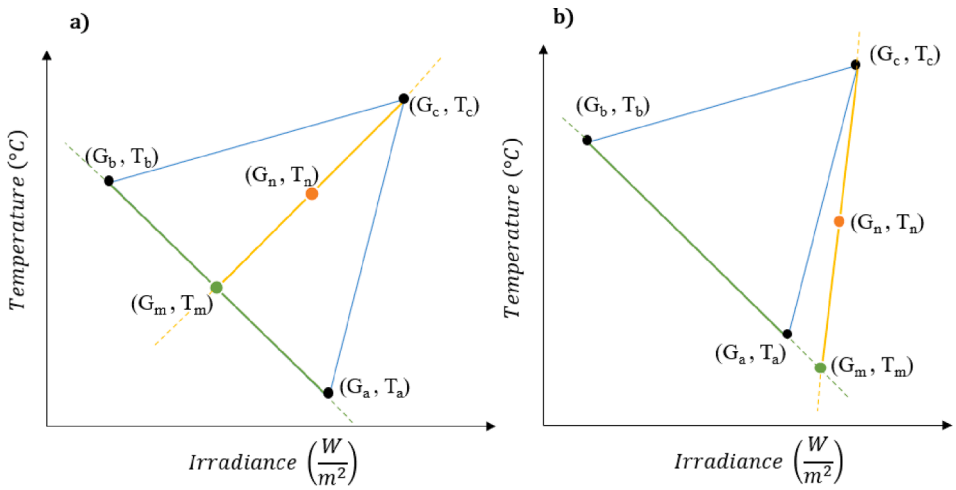

Fig. 1. Schematic diagram for the correction process. Panel (a) corresponds to the interpolation case and (b) corresponds to the extrapolation case. Points a, b and c correspond to the irradiance and temperature conditions of the three I-V curves. Subindex n corresponds to the target conditions, and subindex m corresponds to the auxiliary point in the translation.

STC, lower error deviations concerning the datasheet values were calculated following procedure 3 (Priya et al., 2015). Nevertheless, the precision of this procedure depends on the quality and quantity of the I-V curves involved in the estimation (Vemula et al., 2013). In this regard, the importance of the extensive I-V curve measurements to cover a wide range of irradiance and temperature conditions in the translation process was highlighted (Lad et al., 2010), due that under outdoor conditions, it is not easy to measure curves that can be used as references in the translation process (Tsuno et al., 2006). Therefore, longer testing times are required to record appropriate reference curves (Hishikawa et al., 2019).

It is worth noting that Procedure 1 and 2 require the temperature coefficients, which may generate uncertainty because their values depend on the incident spectrum and considered irradiance levels in the estimation (IEC 60891, 2009). This dependency could restrict the applicability of these procedures to some photovoltaic technologies (Marion et al., 2004). On the contrary, Procedure 3 is a general method applicable to all technologies. Therefore, in this work, to mitigate these drawbacks in the translation method, I-V curves of devices and weather conditions of three commercial modules (m-Si, HIT, and CIGS) exposed in natural sunlight without a tracker were recorded every minute during the light-hours. The data were processed using the linear determination method to moderate the atypical data. Moreover, a random process was proposed to generate the dataset and cover a wide range of irradiance and temperature conditions in the estimation by combining three I-V curves and corresponding weather data. This methodology ensures the estimation reliability at the target conditions (for instance, at STC or NOCT) by calculating less than 8% relative errors regarding the datasheet values.

2. Performance estimation

This section describes the procedures to estimate the performance and temperature coefficients of PV devices, which are conventionally reported in the datasheet by manufacturers.

2.1. Temperature coefficients

Linear regression between the electrical parameters and the device temperature is performed to estimate these coefficients, corresponding the slope of the fitted equation to the temperature coefficient, α for the short circuit current (I_{sc}) and β for the open-circuit voltage (V_{oc}). It is worth noting that these coefficients are valid for the irradiance levels considered in the estimation (IEC 60891, 2009). Therefore, current (I) and voltage (V) are corrected at the target conditions following Equation (1) and (2), respectively.

$$I_2 = I_1 + I_{SC}\bullet\left(\frac{G_2}{G_1} - 1\right) + \alpha\bullet(T_2 - T_1) \tag{1}$$

$$V_2 = V_1 - R_S\bullet(I_2 - I_1) - K\bullet I_2\bullet(T_2 - T_1) + \beta\bullet(T_2 - T_1) \tag{2}$$

Where G is the irradiance and T is the device temperature. Subindex 1 is related to the measured conditions and subindex 2 is related to the target conditions. R_s is the internal resistance of the device and K is a curve correction factor.

2.2. I-V curves corrections

The I-V curves corrections allow estimating the performance at the target conditions defined by the irradiance and temperature conditions. In the event that irradiance and temperature change simultaneously during the test, as is expected in outdoor tests, at least three I-V curves are required to perform the correction. In this context, the temperature and irradiance conditions of the three curves correspond to the vertices of the triangle shown in Fig. 1**a**: (G_a, T_a), (G_b, T_b) and (G_c, T_c). The point (G_n, T_n) corresponds to the irradiance and temperature for the target conditions. Therefore, the process is performed in two steps to correct the data to the target conditions. The first step translates the electrical parameters to condition (G_m, T_m); hence the conditions (G_a, T_a) and (G_b, T_b) are considered to calculate the line equation connecting both points. Similarly, the second step translates the parameters to the target conditions (G_n, T_n) considering the line equation defined by the points (G_c, T_c) and (G_m, T_m). The related line in each step is shown in green and orange, respectively, in Fig. 1.

It is noted that the point (G_m, T_m) is the intersection point between the line defined by the points (G_a, T_a) and (G_b, T_b), and the line defined by the points (G_n, T_n) and (G_c, T_c). Therefore, based on the relationship between the irradiances values in both steps (Equation (3) and Equation (4)), when a_1 takes a value between 0 and 1 indicates that the point (G_m, T_m) is between (G_a, T_a) and (G_b, T_b), involving an interpolation process in the correction. On the contrary, other values indicate that the point is not between them, as shown in Fig. 1**b**, indicating an extrapolation process. Similarly happens to the constant a_2.

$$a_1 = \frac{G_m - G_a}{G_b - G_a} \tag{3}$$

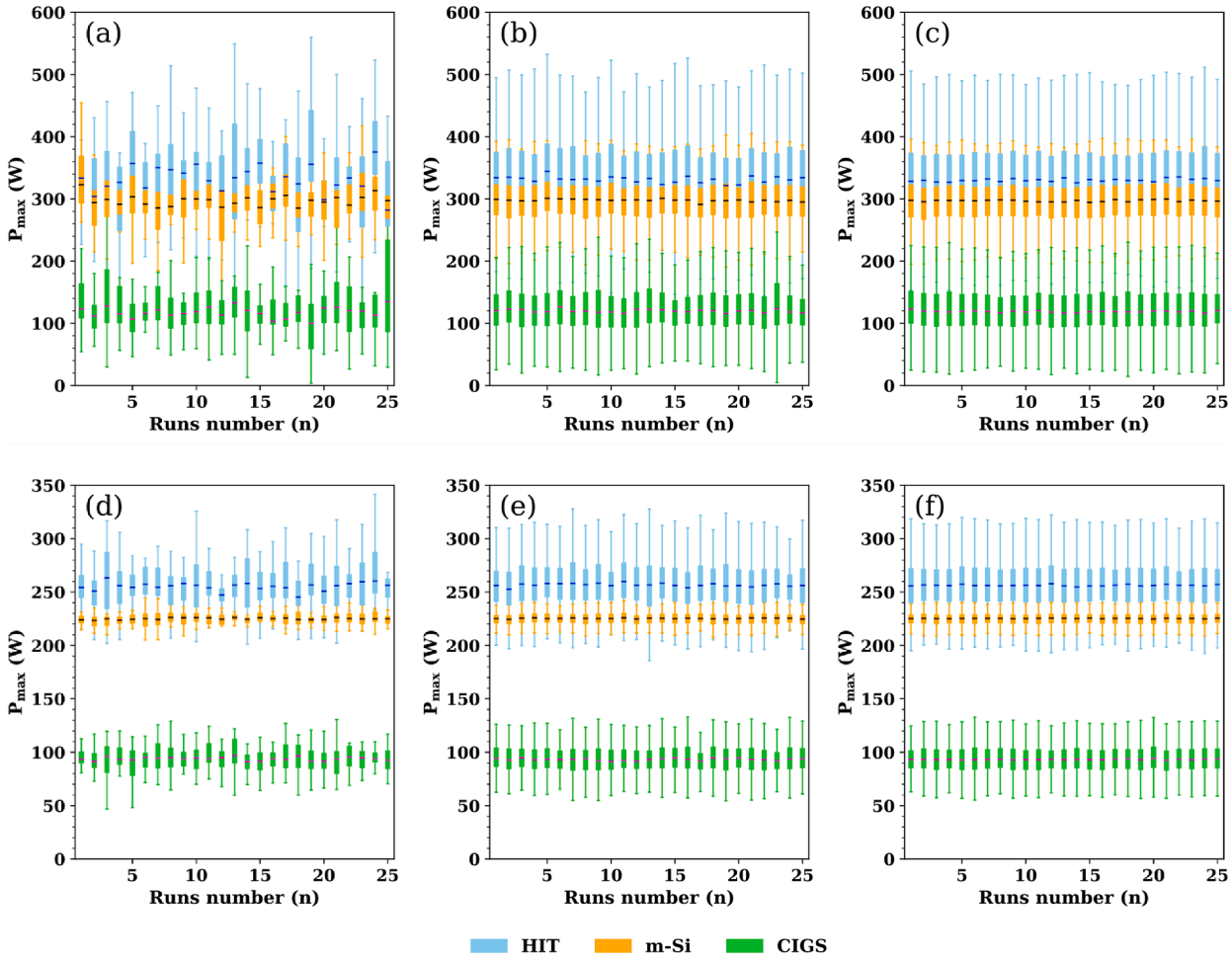

Fig. 2. Effect of the I-V curves selection in the performance estimation. Panels (a-c) correspond to STC, and (d-f) to NOCT. (a and d) correspond to 30 combinations, (b and e) to 300 combinations, and (c and f) to 1000 combinations. Results for HIT are shown in blue, for m-Si in orange, and for CIGS in green.

$$a_2 = \frac{G_n - G_m}{G_c - G_m} \tag{4}$$

Finally, using the estimated a_1 and a_2, the electrical parameters are corrected at the target conditions (G_n, T_n) following Equations (5)–(8).

$$I_m = a_1(I_b - I_a) + I_a \tag{5}$$

$$V_m = a_1(V_b - V_a) + V_a \tag{6}$$

$$I_n = a_2(I_c - I_m) + I_m \tag{7}$$

$$V_n = a_2(V_c - V_m) + V_m \tag{8}$$

3. Results and discussion

The estimation reliability of both procedures was assessed by testing three modules of different technologies in natural sunlight without a tracker facing south at a fixed tilt angle of 13° (6°15′ 38″N 75°34′ 05″W). The evaluated modules were a Panasonic VBHN330SJ47 (HIT), Sharp NU-RC290 (m-Si), and Miasolé FLEX–02 120N (CIGS).

The I-V curves of the modules, irradiance, ambient temperature and device temperature were recorded every minute during the light-hours using the monitoring system for photovoltaic devices described in (Velilla et al., 2019a). The monitoring system included calibrated cells by TRITEC International (Spektron 210), located coplanar with the modules. Besides, a pyranometer MS-60S by Eko instruments (with an uncertainty of 0.77 % and coverage factor of 1.96) was used to validate the irradiance measurements. Temperature sensors by TRITEC International (PT-1000 with a tolerance of ± 0.8 °C) were used for measuring the ambient and panel temperatures. In the case of ambient temperature, the sensors were located close to the irradiance sensors, in the case of the device temperature, the surface sensors were located on the back part of the devices. Fronius sensor box (Fronius International GMBH) was used as a data-logger for irradiance and temperature sensors. Solar panel analyzers (SPA) were used for the I-V curve tracing. SPA were designed for a fast I-V curve tracing considering a capacitive load technique, a sampling period of 0.3 ms for each curve point, and a maximum of 1000 points for each curve. The voltage and current sensors of the SPA were calibrated using certified equipment (Fluke 5522 A-SC) according to procedure CEM-EL-001 (see Supplementary data relate to the calibration results, Fig S1 and Table S1), obtaining a maximum extended measurement uncertainty of 4.4 mV for voltage and 7.2 mA for current, considering a coverage factor and probability of 2 and 95 % respectively.

The outdoor data were processed following the methodology proposed in previous works (Velilla et al., 2021, 2019a, 2019b). Briefly, from the I-V curves, the main parameters such as the maximum power (P_{max}), I_{sc} and V_{oc} were extracted and correlated with the corresponding weather conditions (G, T). The data were filtered using the linear relationship between the irradiance and P_{max} (linear determination method) to mitigate atypical data and transient effects of irradiance changes during the measurements. Then, the data that approach this behavior (within a error of ± 5 %) are chosen to obtain the impact of weather variables on the performance, estimate the temperature coefficients and

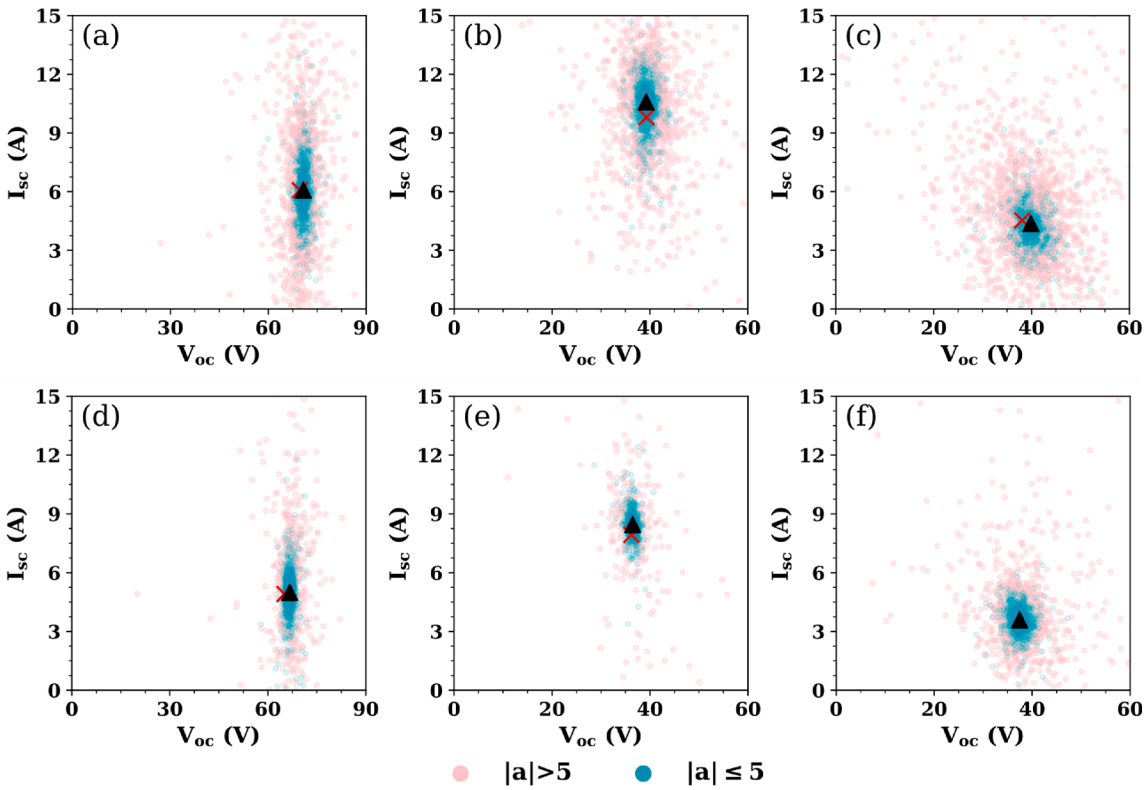

Fig. 3. Interpolation and extrapolation cases in the translation process. Panels (a-c) correspond to corrected results for I_{sc} and V_{oc} at STC, and (d-f) at NOCT. (a and c) correspond to HIT, (b and d) to m-Si, and (c and e) to CIGS. Blue dots correspond to results considering $|a| < 5$, and red points to $|a| > 5$. The red cross indicates the datasheet value and black triangle the estimated performance.

translate the performance to the target conditions (**see Supplementary data Fig S2**).

3.1. Performance estimation using the I-V curves correction

Procedure 3 of IEC 60891 is helpful to estimate the performance because this procedure could be applied to most photovoltaic technologies and it does not require correction parameters as input, such as the *k* factor required in the case of procedure 2 to estimate the temperature coefficients (Equation (2)), reducing the uncertainties in the estimation. Nevertheless, an interpolation or extrapolation process is involved in the procedure depending on the choice of the measured irradiance and temperature conditions (G, T), as is shown in Fig. 1. Then, the maximum power could be estimated as the product between the corrected voltage and current at the maximum power point ($P_{max} = V_{mpp}\, I_{mpp}$) following Equation (5)–(8). Besides, the maximum power value at the target conditions could be estimated using a similar approach to translate the voltage and current, as suggested by the following standard (Equation (9)–(10)). Therefore, Supplementary data shows the estimated performance at the power rating conditions suggested by IEC 61853, calculating similar values using both approaches (Tables S2-S4). In this regard, the linear interpolation in terms of power reduced one translation process because only one parameter is translated (P_{max}) instead of the two parameters V_{mpp} and I_{mpp}. Therefore, this approach reduces the error from the numerical point of view because fewer calculation processes are required, as evidenced by the standard deviation reduction (Tables S2-S4). Thus, the following results related to power are estimated according to Equation (9)–(10).

$$P_m = a_1(P_b - P_a) + P_a \tag{9}$$

$$P_n = a_2(P_c - P_m) + P_m \tag{10}$$

Accordingly, a random process is proposed to generate the dataset to correct the performance at the target conditions in outdoor tests. This dataset is constructed using the outdoor performance obtained following the methodology mentioned in previous works and correlated with the most frequent impact of weather variables on the performance during the exposure (Velilla et al., 2021, 2019b). Thus, each case considered in the dataset consists of the three (G, T) chosen conditions and corresponding I-V curves data (P_{max}, I_{sc}, and V_{oc}), see Supplementary data Fig. S2. This process generates a significant number of triangles covering a wide range of the performance behavior measured during the outdoor tests as a function of the weather variables. Moreover, this process was constrained to ensure different (G, T) combinations in the estimation process. Thus, the average performance at the target condition is defined as the median value of the corrected performance in order to mitigate outliers. Fig. 2 shows in the form of a boxplot the effect of 30, 300, and 1000 random combinations for correcting the P_{max} at STC and NOCT for the three modules using the data recorded for one month of exposure. Besides, the random process to generate the dataset considering the I-V curves and (G, T) conditions was performed several times (runs number, n) to explore different combinations and validate the estimation stability.

Based on the behavior shown in Fig. 2, it is noted that using few combinations, the median values vary significantly for each execution (run). Nevertheless, as the number of combinations increases, the median values tend to be the same value independently of the runs. Similar behavior was observed for correcting other electrical parameters (I_{sc} and V_{oc}) at STC and NOCT (**see Supplementary data Fig. 3–4**). In addition, the data dispersion showed in the boxplot allowed observing that NOCT estimation (Fig. 2**. d-f**) is less sensitive to the number of combinations and runs number than the STC estimation (Fig. 2**. a-c**). Therefore, 1000 combinations in the estimation process are sufficient in order to cover a wide range of the performance behavior measured during the outdoor tests and ensure the estimation at the target conditions.

On the other hand, it is expected that the accuracy of the correction

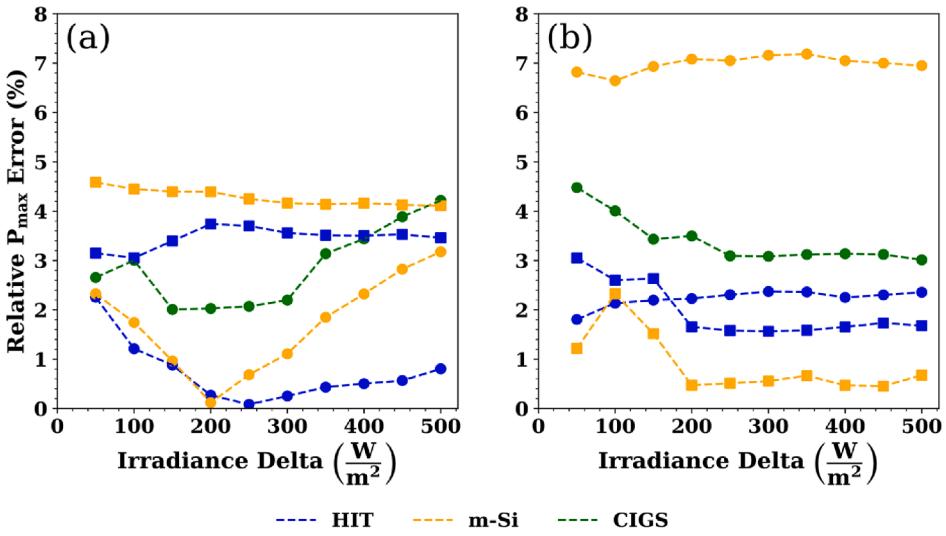

Fig. 4. Relative error for the estimated P_{max} using different irradiance deltas. Panel (a) corresponds to device temperature, and (b) to ambient temperature. The circle markers correspond to STC and the square markers to NOCT. Results for HIT are shown in blue, for m-Si in orange, and for CIGS in green. Relative errors for CIGS at NOCT are not calculated because this condition was not reported in the datasheet.

depends on the interpolation or extrapolation process involved in the procedure as a result of the generated (G, T) conditions. These conditions define if the target conditions are inside of the triangle delimited by the three (G, T) conditions, indicating an interpolation process (Fig. 1**a**), other cases indicating an extrapolation process (Fig. 1**b**). In this sense, Fig. 3 shows the corrected performance at STC and NOCT for I_{sc} and V_{oc}, considering the data corresponding to irradiance levels higher than 500 W/m^2. Therefore, an extrapolation range between −5 and 5 ($|a| < 5$) for a_1 and a_2 was proposed in order to minimize the extrapolation cases (red dots) and reduce the dispersion in the estimated values (blue dots). Consequently, the performance (black triangle) was calculated as the median value of the data in the selected range (blue dots). Hence, using this extrapolation range improved the performance estimation concerning the datasheet values (red cross).

In this regard, Fig. 3 allows observation of the estimation dispersion mainly affected by the extrapolation processes. The data were processed by irradiance ranges to mitigate the extrapolation cases using an irradiance delta (dG) to select the data close to the target irradiance (G ± dG). For instance, if the target condition is STC (1000 W/m^2), and a dG of 100 W/m^2 is considered, the data measured between 900 and 1100 W/m^2 are used to generate the (G,T) combinations and select the corresponding I-V curves. Fig. 4 shows the effect of varying dG between 50

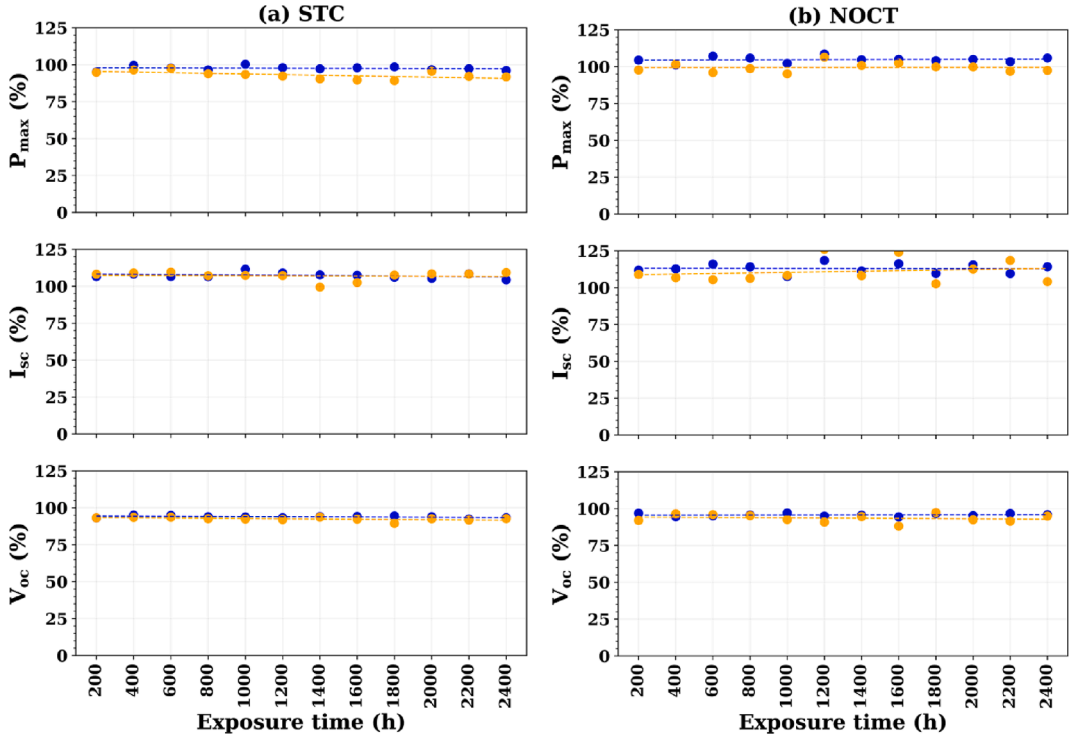

Fig. 5. Estimated PRCs over the exposure time. The electrical parameters were estimated using the ambient temperature and an irradiance delta of 200 W/m^2. Panel (a) corresponds to STC and (b) to NOCT. The dot points corresponded to the estimated data and lines corresponded to the fit (blue color to HIT and orange color to m-Si).

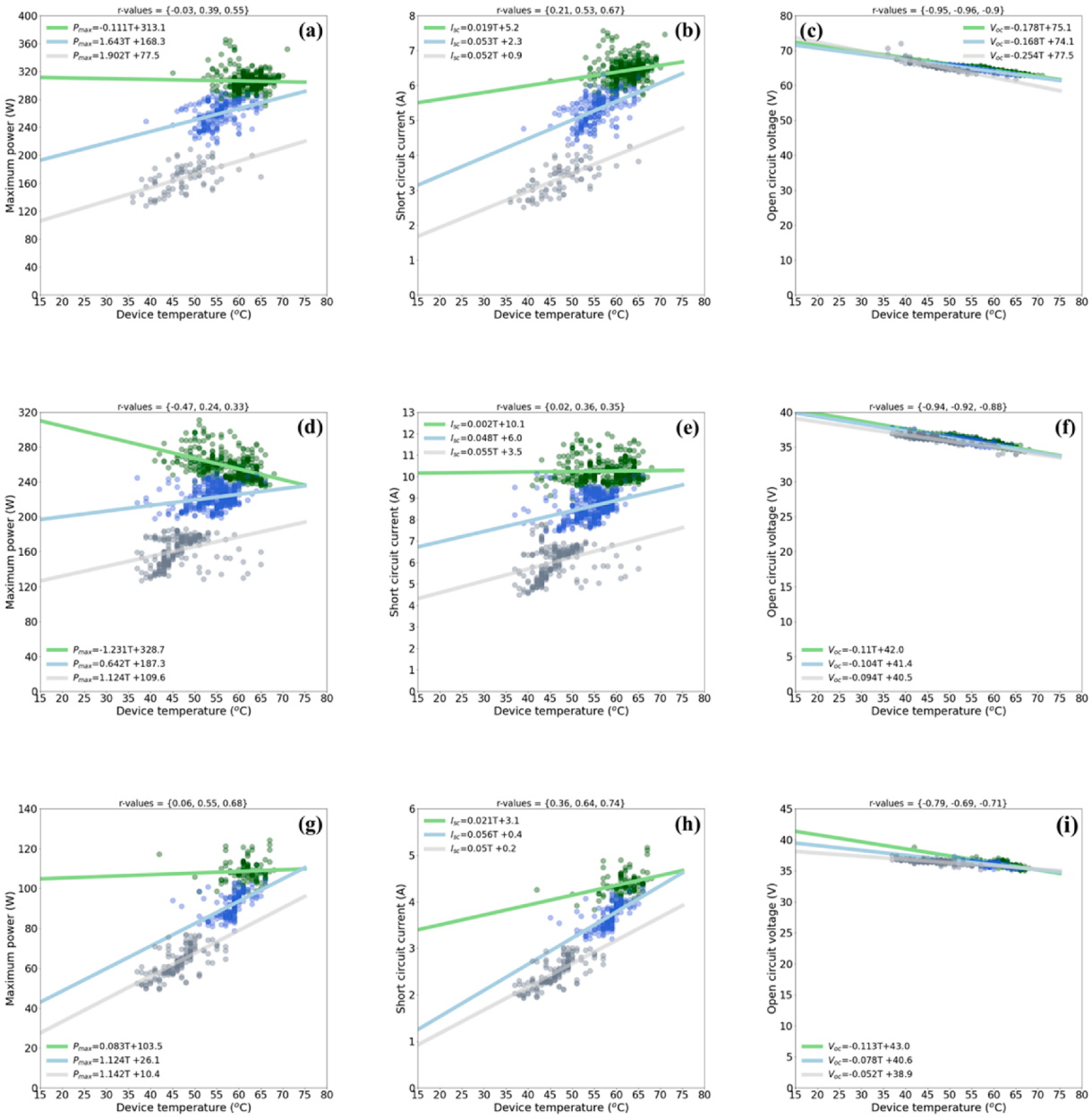

Fig. 6. Estimation of the temperature coefficients. Panels (a-c) correspond to HIT module, (d-f) to m-Si module, and (g-i) to CIGS module. The color dot points correspond to the measured data, and color lines correspond to the fits. The colors are correlated to the irradiance levels used in the estimation (green to 1000, blue to 800, and gray to 500 W/m^2). The fitted equations are shown in the inset. At the top are shown the r-values of the fits.

and 500 on the P_{max} estimation at STC and NOCT regarding the datasheet values. In a general way, the results indicated that a dG of 200 W/m^2 is adequate to minimize the relative error in the estimation for both power rating conditions, even using the device temperature (Fig. 4**a**) and ambient temperature (Fig. 4**b**). It is also noted that using the device temperature, the correction at STC is improved (circle markers). On the other hand, using the ambient temperature the corrections at NOCT are improved, highlighting the role of both temperatures in the estimation of PRCs.

Moreover, when P_{max}, I_{sc}, and V_{oc} are estimated considering a dG of 200 W/m^2 (**see Supplementary data Fig. 5–6**), the dispersion on the estimated values is reduced regardless of the number of runs (n). These results indicated the principal role of the irradiance range in the estimation, which constrains the search region in order to generate (G, T) combinations close to the target. Therefore, the complete procedure (including the random process, the extrapolation range, and the irradiance delta) improved the performance estimation by calculating relative error percentages of less than 8% for the PRCs in outdoor tests for the considered photovoltaic technologies (m-Si, HIT, and CIGS).

To analyze the effect of weather conditions on the performance estimation during the considered exposure time, the outdoor data were processed by batches using 200 h of exposure and corresponding measurements, ambient temperature, $|a| < 5$, and a dG of 200 W/m^2. Fig. 5 depicts estimation for P_{max}, I_{sc}, and V_{oc} at STC and NOCT, which were normalized regarding the datasheet values (see **Table S5**). The results highlighted three main facts related to the implemented procedure. The first is related to the almost constant behavior trend of the variables, suggesting that a proper estimation can be performed regardless of the season or the weather conditions involved during the test. The second is related to the behavior change of this trend, which can be correlated to soiling effects to define the cleaning maintenance of the modules. Moreover, this trend can be used to perform other analyses such as

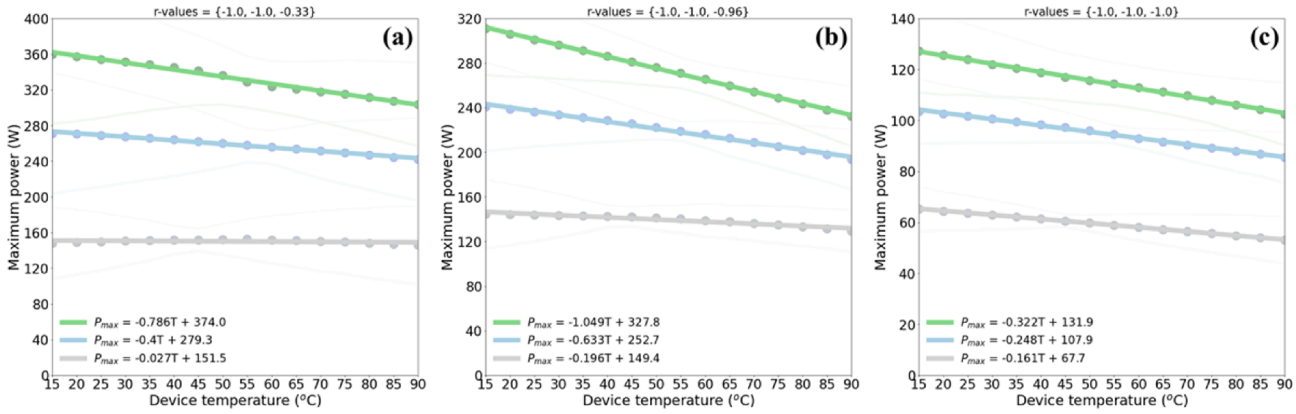

Fig. 7. Estimated temperature coefficients for P_{max} using the translation procedure. Panels (a) correspond to HIT module, (b) to m-Si module, and (c) to CIGS module. The color dot points correspond to the translated data, and color lines correspond to the fit. The colors are correlated to the irradiance levels used in the estimation (green to 1000, blue to 800, and gray to 500 W/m^2). The fitted equations are shown in the inset.

lifetime considering long-term data. The third is related to the PRC, in this case, STC and NOCT allow the validation of the performance concerning the datasheet and comparison of different technologies evaluated under outdoor conditions.

3.2. Temperature coefficients estimation

Fig. 6 shows the behavior of the principal electrical variables extracted from the I-V curves as a function of the device temperature (dots points) in order to estimate the temperature coefficients, as the slope of the linear regressions (solid lines). The fitted equations were calculated by considering the measurements for 200 h of exposure and selecting the data close to three irradiance levels with a deviation of 10% concerning each irradiance level (1000, 800 and 500 W/m^2). It was observed the almost constant behavior of the temperature coefficient of V_{oc} with irradiance levels, calculating similar coefficients values regarding the datasheet using the device and ambient temperature (Fig. 2, **Fig S7** and **Table S6** of Supplementary data). On the contrary, the temperature coefficients values for power and short circuit current showed differences concerning the considered temperature and irradiance levels. These differences in the estimated coefficient could be associated with the device temperature control, equipment used for measuring weather and electrical data, fitting process, etc (Mihaylov et al., 2016). Nevertheless, the estimated values and behaviors depicted in Fig. 6 represent the actual temperature coefficients for the operative conditions because the device temperature was not controlled during the outdoor tests.

On the other hand, the reversal of the sign in the temperature coefficients for power depicted in Fig. 6 and Fig S7, was observed in the literature for different photovoltaic technologies in outdoor tests and correlated with the spectral effect, incidence angle, and dews (Whitaker et al., 1992), suggesting that additional corrections are required to estimate the parameters in uncontrolled tests (Paudyal and Imenes, 2021). Thus, to estimate the temperature coefficients in a broad range of conditions, including conditions not recorded during the tests, the outdoor data were translated to the irradiance levels shown in Fig. 6 considering the device temperatures ranging between 15 and 85 °C and dG of 200 W/m^2. Fig. 7 shows the estimated temperature coefficient for power, **Fig. S8** and **Fig. S9** show the results for I_{sc} and V_{oc}, respectively. It is noted that the estimation accuracy is guaranteed because the calculated r-values approach −1 (values shown on the top of the figures and in Table S7). Besides, considering the translated data, the estimated slopes by the linear regressions allowed calculating temperature coefficients that approach the datasheet values. These results highlight the central role of the translation process in outdoor tests to validate the data reported by manufacturers in the datasheet or to track the performance, diagnose faults or establish maintenance guidelines.

4. Conclusions

This paper estimated the performance of three PV modules (m-Si, HIT, and CIGS) at STC and NOCT in outdoor tests by correcting the I-V curves data. Therefore, a random process was proposed to generate the dataset and estimate the performance at the target conditions by combining three different weather data (G, T) and the corresponding parameters extracted from the I-V curves. Furthermore, the dataset was filtered using an irradiance range (dG) and extrapolation range (a) to constrain the search region and mitigate the extrapolation cases. These factors allowed the dispersion reduction in the estimated values, calculating a relative error of less than 8% at STC and NOCT concerning the datasheet.

Accordingly, the random process was carried out several times (runs) in order to explore different (G, T) combinations measured during the outdoor tests. It ensured in each execution a significant number of (G, T) combinations covering a wide range of the performance behavior as a function of the weather variables. Then, the performance was calculated as the median value of the translated data to avoid the effect of the outliers. Therefore, a robust numerical tool was obtained to estimate a reliable performance by combining these factors with the proposed extrapolation range (a) and irradiance delta (dG).

On the other hand, despite the correction of the I-V curves allowing estimating the outdoor performance at both power rating conditions conventionally included in the datasheet of commercial modules, the results showed less dispersion on the estimation at NOCT than at STC, as was shown in Fig. 2. These facts highlighted the role of NOCT in outdoor tests because under outdoor conditions is more likely to measure weather conditions approaching NOCT, reducing the extrapolation cases in the estimation. Besides, based on the irradiance delta analysis shown in Fig. 4, it is observed that a dG of 200 W/m^2 is adequate to reduce the error between the estimated performance and datasheet values.

Finally, the implemented procedure to translate the outdoor performance to the target conditions was successfully extended to calculate the temperature coefficients. Thus, the procedure allows the complete performance characterization of the devices regarding the datasheet and could be used to track the performance evolution, implement a real-time diagnosis, or estimate the lifetime.

Declaration of Competing Interest

The authors declare that they have no known competing financial interests or personal relationships that could have appeared to influence the work reported in this paper.

Acknowledgements

Esteban Velilla thanks Colombia's Ministry of Science, Technology and Innovation (MINCIENCIAS) for national doctoral scholarship number 727-2015 (contract no. FP44842-124-2017). We gratefully acknowledge the financial support provided by the Colombia Scientific Program within the framework of the call Ecosistema Científico (contract no. FP44842—218-2018).

Appendix A. Supplementary data

Supplementary data to this article can be found online at https://doi.org/10.1016/j.solener.2022.03.064.

References

Duck, B.C., Fell, C.J., Marion, B., Emery, K., 2013. Comparing standard translation methods for predicting photovoltaic energy production. In: In: 2013 IEEE 39th Photovoltaic Specialists Conference (PVSC). IEEE, pp. 0763–0768. https://doi.org/10.1109/PVSC.2013.6744261.

Hishikawa, Y., Takenouchi, T., Higa, M., Yamagoe, K., Ohshima, H., Yoshita, M., 2019. Translation of solar cell performance for irradiance and temperature from a single I-V curve without advance information of translation parameters. IEEE J. Photovoltaics 9, 1195–1201. https://doi.org/10.1109/JPHOTOV.2019.2924388.

IEC 60891, 2009. Photovoltaic devices – Procedures for temperature and irradiance corrections to measured I-V, International Electrotechnical Committee.

IEC 61853-1, 2011. Photovoltaic (PV) module performance testing and energy rating - Part 1: Irradiance and temperature performance measurements and power rating, International Electrotechnical Committee.

Jordan, D.C., Deline, C., Kurtz, S.R., Kimball, G.M., Anderson, M., 2018. Robust PV degradation methodology and application. IEEE J. Photovoltaics 8, 525–531. https://doi.org/10.1109/JPHOTOV.2017.2779779.

Lad, R., Wohlgemuth, J., TamizhMani, G., 2010. Outdoor energy ratings and spectral effects of photovoltaic modules. In: 2010 35th IEEE Photovoltaic Specialists Conference. IEEE, pp. 002827–002832. https://doi.org/10.1109/PVSC.2010.5616859.

Marion, B., Rummel, S., Anderberg, A., 2004. Current-voltage curve translation by bilinear interpolation. Prog. Photovoltaics Res. Appl. 12, 593–607. https://doi.org/10.1002/pip.551.

Mihaylov, B., Betts, T.R., Pozza, A., Mullejans, H., Gottschalg, R., 2016. Uncertainty estimation of temperature coefficient measurements of PV modules. IEEE J. Photovoltaics 6, 1554–1563. https://doi.org/10.1109/JPHOTOV.2016.2598259.

Ndiaye, A., Charki, A., Kobi, A., Kébé, C.M.F., Ndiaye, P.A., Sambou, V., 2013. Degradations of silicon photovoltaic modules: a literature review. Sol. Energy 96, 140–151. https://doi.org/10.1016/j.solener.2013.07.005.

Paudyal, B.R., Imenes, A.G., 2021. Investigation of temperature coefficients of PV modules through field measured data. Sol. Energy 224, 425–439. https://doi.org/10.1016/j.solener.2021.06.013.

Phinikarides, A., Kindyni, N., Makrides, G., Georghiou, G.E., 2014. Review of photovoltaic degradation rate methodologies. Renew. Sustain. Energy Rev. 40, 143–152. https://doi.org/10.1016/j.rser.2014.07.155.

Priya, S.S., Sastry, O.S., Bora, B., Kumar, A., 2015. Comparison of curve correction procedure of current and voltage as per IEC 60891 for thin film technology. In: 2015 IEEE 42nd Photovoltaic Specialist Conference (PVSC). IEEE, pp. 1–4. https://doi.org/10.1109/PVSC.2015.7355843.

Quansah, D.A., Adaramola, M.S., 2019. Assessment of early degradation and performance loss in five co-located solar photovoltaic module technologies installed in Ghana using performance ratio time-series regression. Renew. Energy 131, 900–910. https://doi.org/10.1016/j.renene.2018.07.117.

Tsuno, Y., Hishikawa, Y., Kurokawa, K., 2006. Translation equations for temperature and irradiance of the I-V curves of various PV cells and modules. In: In: 2006 IEEE 4th World Conference on Photovoltaic Energy Conference. IEEE, pp. 2246–2249. https://doi.org/10.1109/WCPEC.2006.279619.

Velilla, E., Cano, J.B., Jaramillo, F., 2019a. Monitoring system to evaluate the outdoor performance of solar devices considering the power rating conditions. Sol. Energy 194, 79–85. https://doi.org/10.1016/j.solener.2019.10.051.

Velilla, E., Jaramillo, F., Mora-Seró, I., 2021. High-throughput analysis of the ideality factor to evaluate the outdoor performance of perovskite solar minimodules. Nat. Energy 6, 54–62. https://doi.org/10.1038/s41560-020-00747-9.

Velilla, E., Ramirez, D., Uribe, J.-I., Montoya, J.F., Jaramillo, F., 2019b. Outdoor performance of perovskite solar technology: silicon comparison and competitive advantages at different irradiances. Sol. Energy Mater. Sol. Cells 191, 15–20. https://doi.org/10.1016/j.solmat.2018.10.018.

Vemula, M.G., John, J.J., Kuitche, J., Tamizhmani, G., 2013. Power rating of photovoltaic modules per IEC 61853–1 standard using a new outdoor test method. In: In: 2013 IEEE 39th Photovoltaic Specialists Conference (PVSC). IEEE, pp. 0724–0728. https://doi.org/10.1109/PVSC.2013.6744253.

Whitaker, C.M., Townsend, T.U., Wenger, H.J., Iliceto, A., Chimento, G., Paletta, F., 1992. Effects of irradiance and other factors on PV temperature coefficients. In: The Conference Record of the Twenty-Second IEEE Photovoltaic Specialists Conference - 1991. IEEE, pp. 608–613. https://doi.org/10.1109/PVSC.1991.169283.

Anexo 5:

Supporting information of Photovoltaic performance assess by correcting the I-V curves in outdoor tests

Supporting information

Photovoltaic Performance Assess by Correcting the I-V Curves from Outdoor Tests Padilla A., Londoño C., Jaramillo, F., Tovar I., Cano J.B, Velilla E.

corresponding author: bernardo.cano@udea.edu.co

Fig S1 and Table S1 are related to the calibration results of the SPA using a Fluke 5522 A-SC as reference equipment.

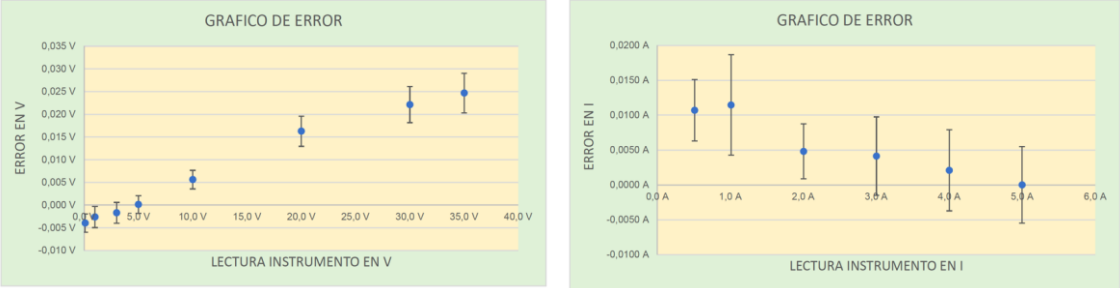

Fig S1. Uncertainty in the SPA Measurements. a) for voltage and b) for current. Results taken from the calibrated certificate No. MT-26651-0410 performed by Laboratorio EPM-Area Metrologia, comparing the SPA measurements with the Fluke 5522 A-SC measurements, according to procedure CEM-EL-001.

INTERVALO	LECTURA INSTRUMENTO	LECTURA PATRON	ERROR	INCERTIDUMBRE
35 V	0,0960 V	0,1000 V	-0,0040 V	0,0020 V
	0,9974 V	1,0000 V	-0,0026 V	0,0023 V
	2,9983 V	3,0000 V	-0,0017 V	0,0023 V
	5,0001 V	5,0000 V	0,0001 V	0,0020 V
	10,0056 V	10,0000 V	0,0056 V	0,0020 V
	20,0163 V	20,0000 V	0,0163 V	0,0033 V
	30,0221 V	30,0000 V	0,0221 V	0,0040 V
	35,0247 V	35,0000 V	0,0247 V	0,0044 V

INTERVALO	LECTURA INSTRUMENTO	LECTURA PATRON	ERROR	INCERTIDUMBRE
5 A	0,5107 A	0,5000 A	0,0107 A	0,0044 A
	1,0115 A	1,0000 A	0,0115 A	0,0072 A
	2,0048 A	2,0000 A	0,0048 A	0,0039 A
	3,0041 A	3,0000 A	0,0041 A	0,0056 A
	4,0021 A	4,0000 A	0,0021 A	0,0058 A
	5,0000 A	5,0000 A	0,0000 A	0,0055 A

Table S1. Numerical uncertainty in the SPA Measurements. a) for voltage and b) for current. Results taken from the calibrated certificate No. MT-26651-0410 performed by Laboratorio EPM-Area Metrologia, comparing the SPA measurements with the Fluke 5522 A-SC measurements, according to procedure CEM-EL-001.

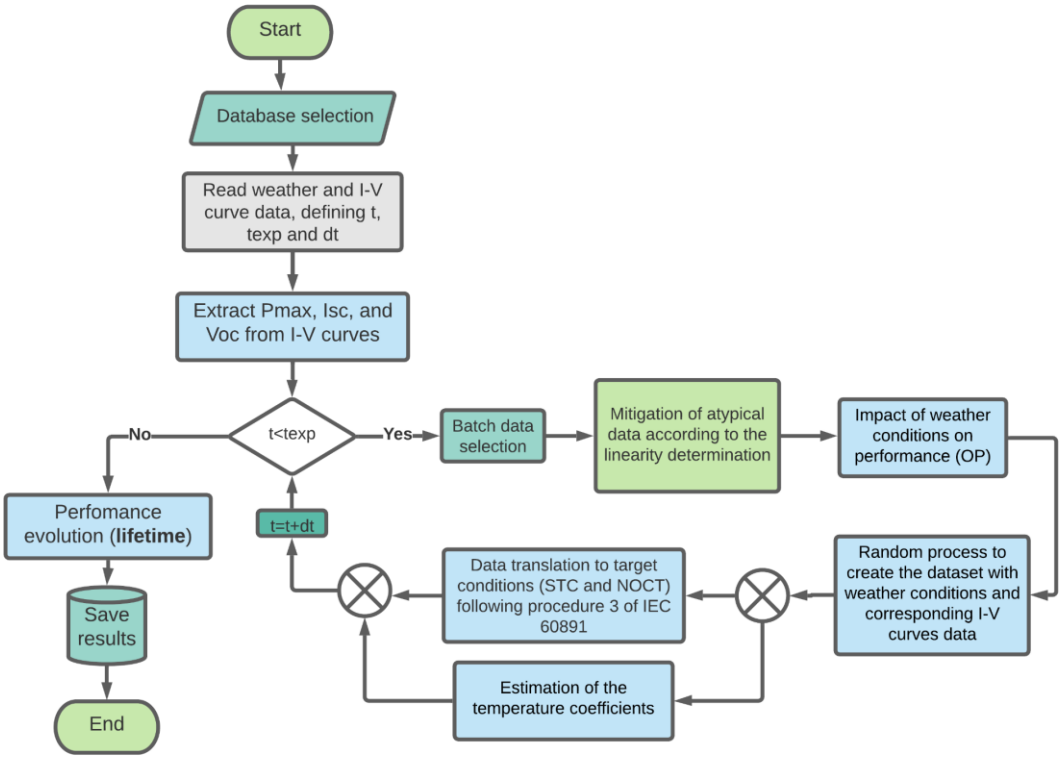

Fig S2. Flowchart to process the I-V curves and weather data recorded in outdoor conditions to perform the proposed analyzes.

Table S2. Power rating conditions (PRC) estimation for the HIT module.

Power rating conditions	Pmax (W)		Pmax (Vmpp*Impp)		Impp (A)		Vmpp (V)		Isc (A)		Voc (V)	
	median	std	median	std	median	std	median	std	median	std	median	std
STC (25,1000)	**331,71**	57,23	**332,09**	64,92	5,61	1,11	59,09	1,48	6,11	1,62	70,94	1,4
NOCT (20*,800)	**257,95**	41,76	**255,96**	43,69	4,66	0,87	54,63	4,46	5,03	1,26	66,08	4,07
LIC (25,200)	**46,53**	3,8	**45,55**	17,49	1,14	0,18	38,98	8,24	1,19	0,3	50,59	12,66
HTC (75,1000)	**309,69**	30,91	**308,37**	28,89	6,28	0,6	49,1	0,79	6,77	0,98	61,76	0,79
LTC (15,500)	**152,72**	37,67	**147,66**	42,63	2,44	0,72	60,31	3,16	2,63	1,05	71,42	8,71

Table S3. Power rating conditions (PRC) estimation for the m-Si module.

Power rating conditions	Pmax (W)		Pmax (Vmpp*Impp)		Impp (A)		Vmpp (V)		Isc (A)		Voc (V)	
	median	std	median	std	median	std	median	std	median	std	median	std
STC (25,1000)	**297,91**	30,29	**299,38**	34,47	9,76	1,18	30,89	1,88	10,39	1,27	39,21	1,47

NOCT (20*,800)	**229,87**	28,29	**228,48**	31,28	7,75	1,18	29,92	3,33	8,36	1,68	37,74	2,49
LIC (25,200)	**58,83**	3,75	**58,85**	4,27	1,89	0,16	31,17	0,87	1,97	0,18	36,8	0,41
HTC (75,1000)	**250,99**	19,17	**248,89**	17,66	9,92	0,75	25,01	1,26	10,83	0,8	33,83	0,97
LTC (15,500)	**143,83**	21,15	**143,55**	34,84	4,43	1,11	32,55	3,11	4,89	1,43	39,05	1,29

Table S4. Power rating conditions (PRC) estimation for the CIGS module.

Power rating conditions	**Pmax (W)**		**Pmax (Vmpp*Impp)**		**Impp (A)**		**Vmpp (V)**		**Isc (A)**		**Voc (V)**	
	median	**std**	**median**	**std**	**median**	**std**	**median**	**std**	**median**	**std**	**median**	**std**
STC (25,1000)	**120,97**	19,71	**120,49**	20,65	3,6	0,61	33,39	2,85	4,12	0,81	40,57	2,69
NOCT (20*,800)	**95,35**	15,01	**95,12**	15,26	3,21	0,55	29,46	2,78	3,7	0,71	36,65	2,75
LIC (25,200)	**25,65**	5,06	**25,49**	5,18	0,86	0,17	29,77	1	1,02	0,2	36,91	2,21
HTC (75,1000)	**113,54**	14,94	**113,01**	14,87	4,02	0,54	28,21	2,24	4,6	0,73	35,65	2,18
LTC (15,500)	**55,59**	14,11	**55,62**	15,17	1,73	0,47	32,3	1,28	2,01	0,54	38,81	1,37

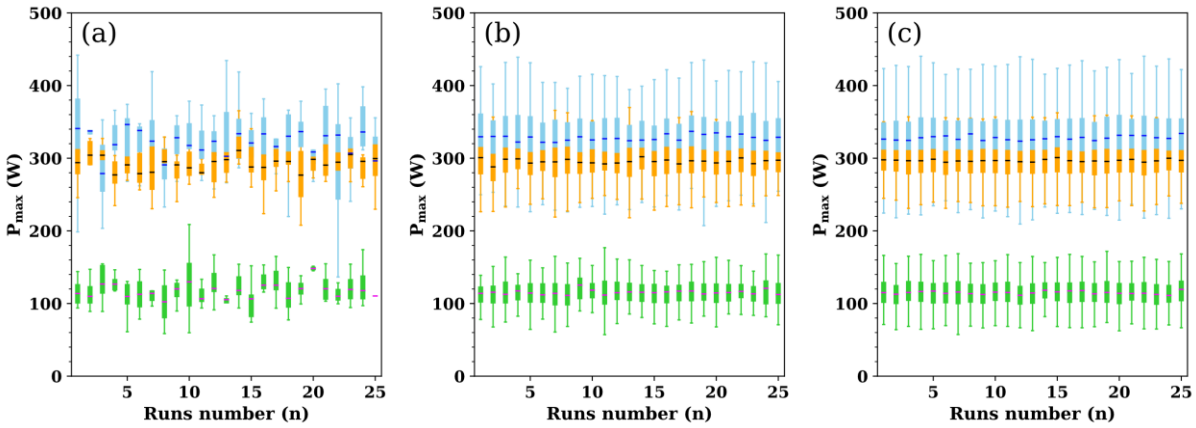

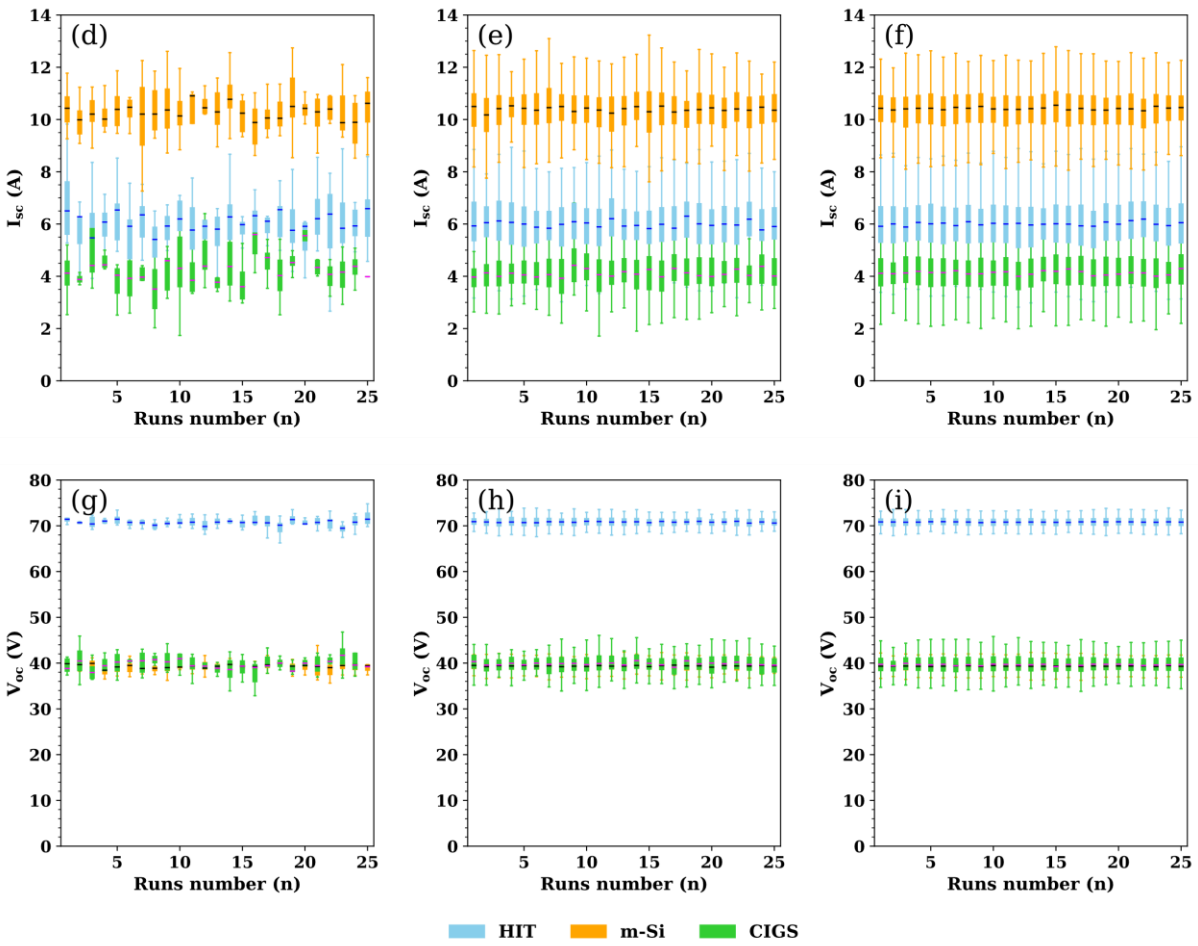

Fig S3. I-V curves selection effect on the performance estimation at STC. Corresponding (a-c) to P_{max}, (d-f) to I_{sc}, and (g-i) to V_{oc}. (a, d and g) correspond to 30 combinations, (b, e, and h) correspond to 300 combinations, and (c, f, and i) correspond to 1000 combinations. Results for the HIT are shown in blue, for the m-Si in orange, and for the CIGS in green.

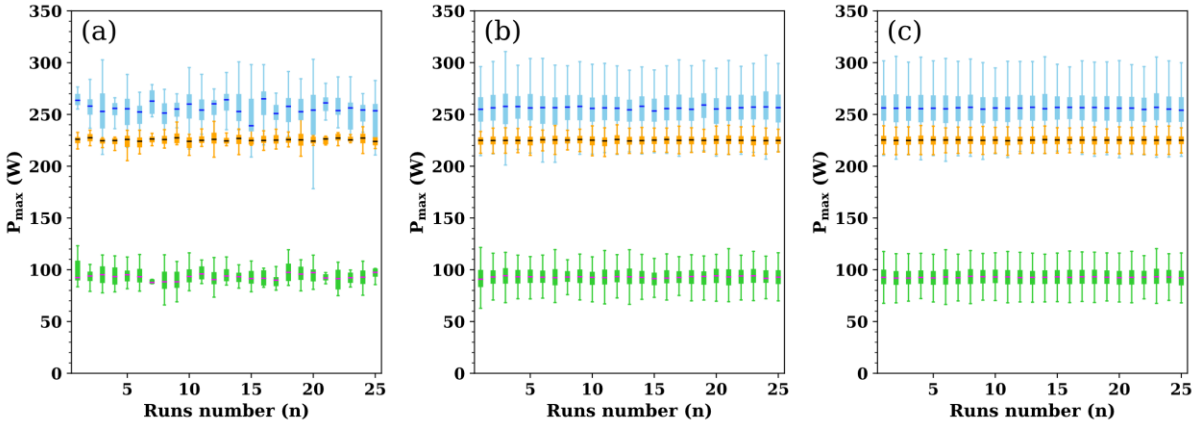

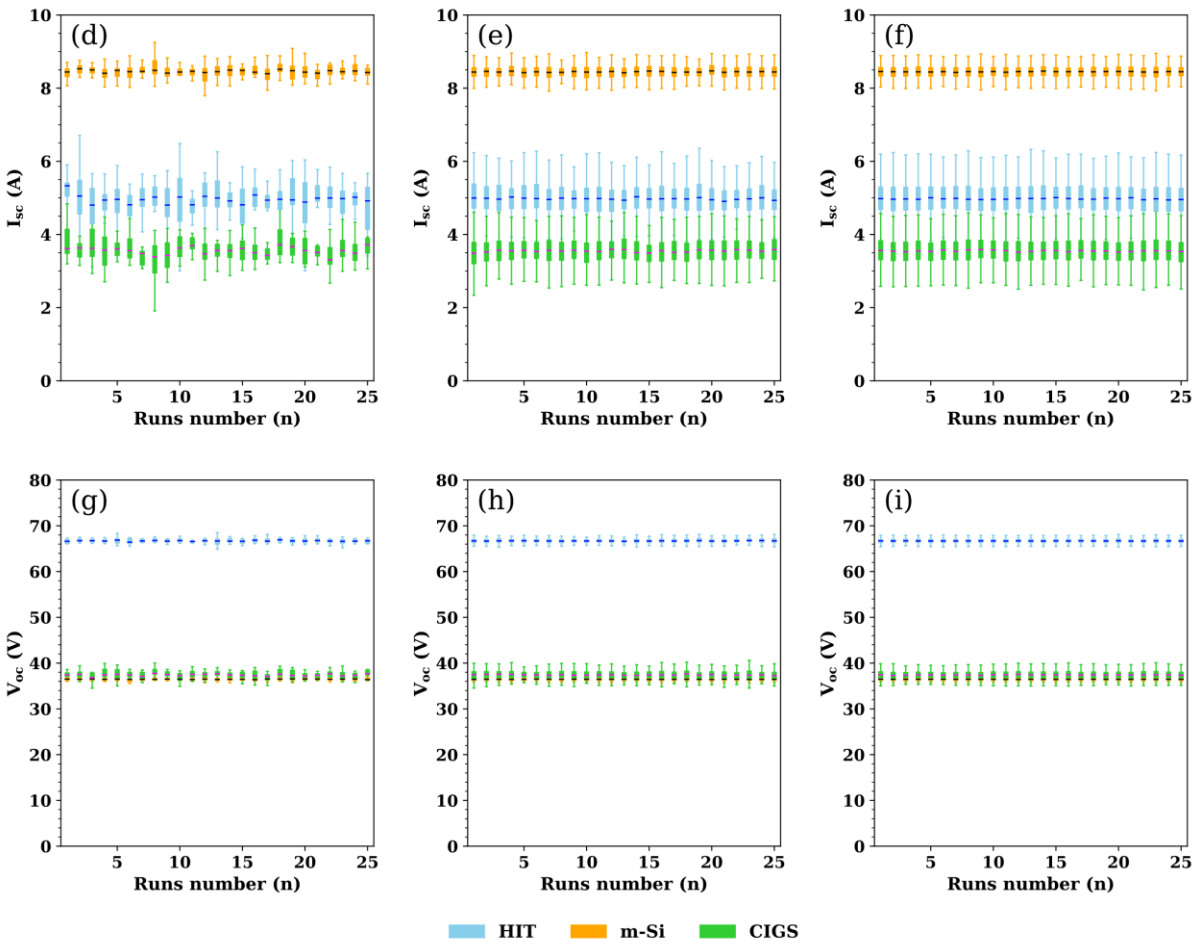

Fig S4. I-V curves selection effect on the performance estimation at NOCT. Corresponding (a-c) to P_{max}, (d-f) to I_{sc}, and (g-i) to V_{oc}. (a, d, and g) correspond to 30 combinations, (b, e, and h) correspond to 300 combinations, and (c, f, and i) correspond to 1000 combinations. Results for the HIT are shown in blue, for the m-Si in orange, and for the CIGS in green.

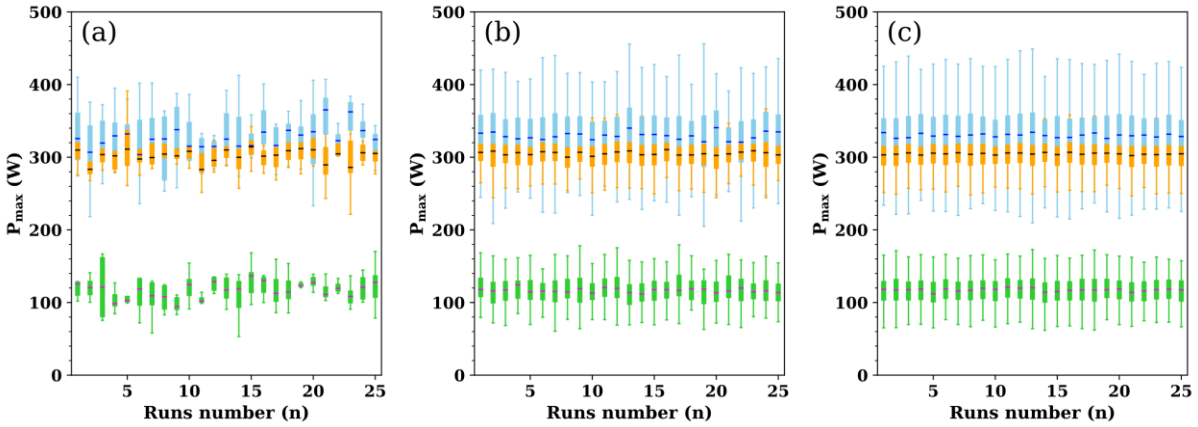

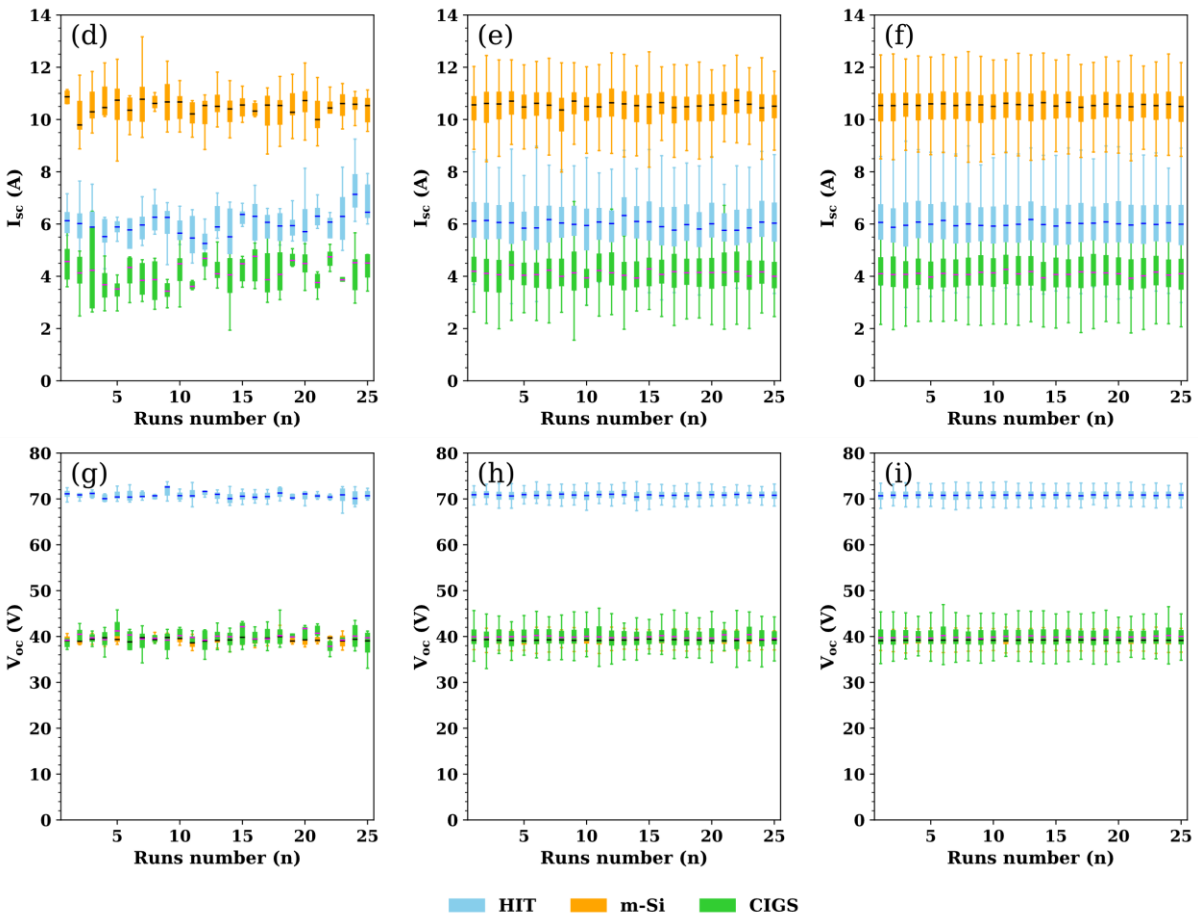

Fig S5. I-V curves selection effect on the performance estimation at STC considering a dG of 200. Corresponding (a-c) to P_{max}, (d-f) to I_{sc}, and (g-i) to V_{oc}. (a, d, and g) correspond to 30 combinations, (b, e, and h) correspond to 300 combinations, and (c, f, and i) correspond to 1000 combinations. Results for the HIT are shown in blue, for the m-Si in orange, and for the CIGS in green.

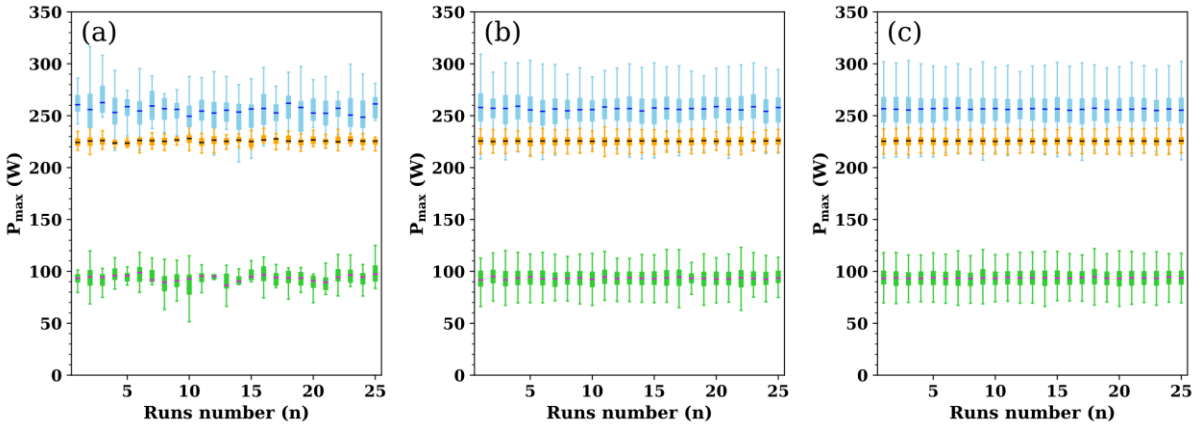

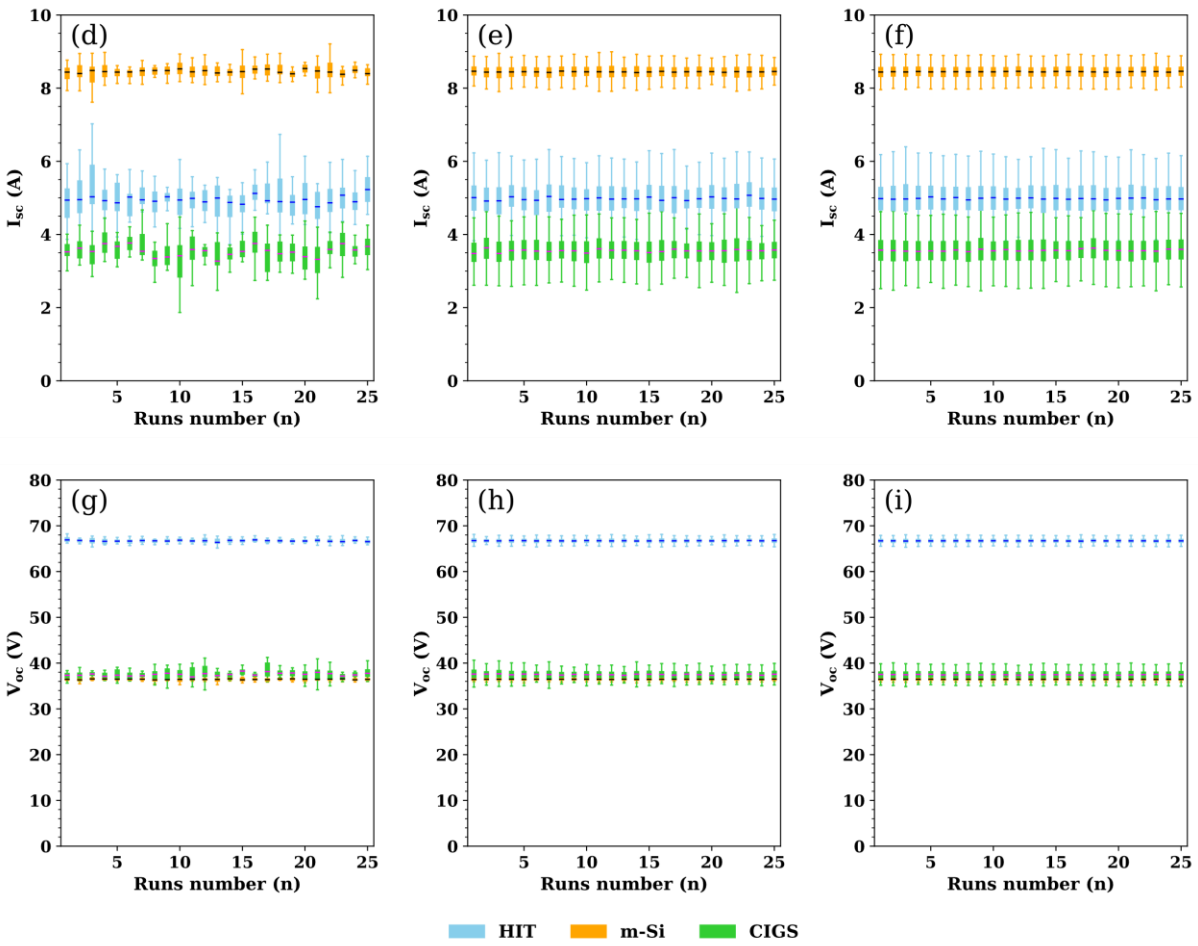

Fig S6. I-V curves selection effect on the performance estimation at NOCT considering a dG of 200. Corresponding (a-c) to P_{max}, (d-f) to I_{sc}, and (g-i) to V_{oc}. (a, d, and g) correspond to 30 combinations, (b, e, and h) correspond to 300 combinations, and (c, f, and i) correspond to 1000 combinations. Results for the HIT are shown in blue, for the m-Si in orange, and for the CIGS in green.

Table S5. Power rating conditions (PRC) of evaluated modules.

	STC			**NOCT**		
Module	P_{max} *(W)*	I_{sc} *(A)*	V_{oc} *(V)*	P_{max} *(W)*	I_{sc} *(A)*	V_{oc} *(V)*
HIT	330	6.07	69.7	247.2	4.91	65.1
m-Si	290	9.8	39.3	212	7.93	36.2
CIGS	120	4.53	38.1			

Table S6. Calculated temperature coefficients using 200 hours of exposure for P_{max} (δ), I_{sc} (α), and V_{oc} (β).

		Device Temperature			Ambient Temperature		
PV Module	Irradiance level (W/m^2)	δ (W/°C)	α (A/°C)	β (V/°C)	δ (W/°C)	α (A/°C)	β (V/°C)
HIT	500	1.902	0.052	-0.178	3.073	0.074	-0.394
	800	1.643	0.053	-0.168	2.733	0.067	-0.082
	1000	0.111	0.019	-0.254	-0.523	0.002	-0.122
	Datasheet	-0.957	0.002	-0.174	-0.957	0.002	-0.174
m-Si	500	1.124	0.055	-0.094	1.185	0.088	-0.063
	800	0.642	0.048	-0.104	1.018	0.068	-0.051
	1000	-1.231	0.002	-0.11	-1.956	-0.035	-0.103
	Datasheet	-1.160	0.0049	-0.112	-1.160	0.0049	-0.112
CIGS	500	1.142	0.05	-0.052	1.046	0.045	-0.063
	800	1.124	0.056	-0.078	1.162	0.058	-0.076
	1000	0.083	0.021	-0.113	1.295	0.07	-0.104
	Datasheet	-0.456	0.0003	-0.106	-0.456	0.0003	-0.106

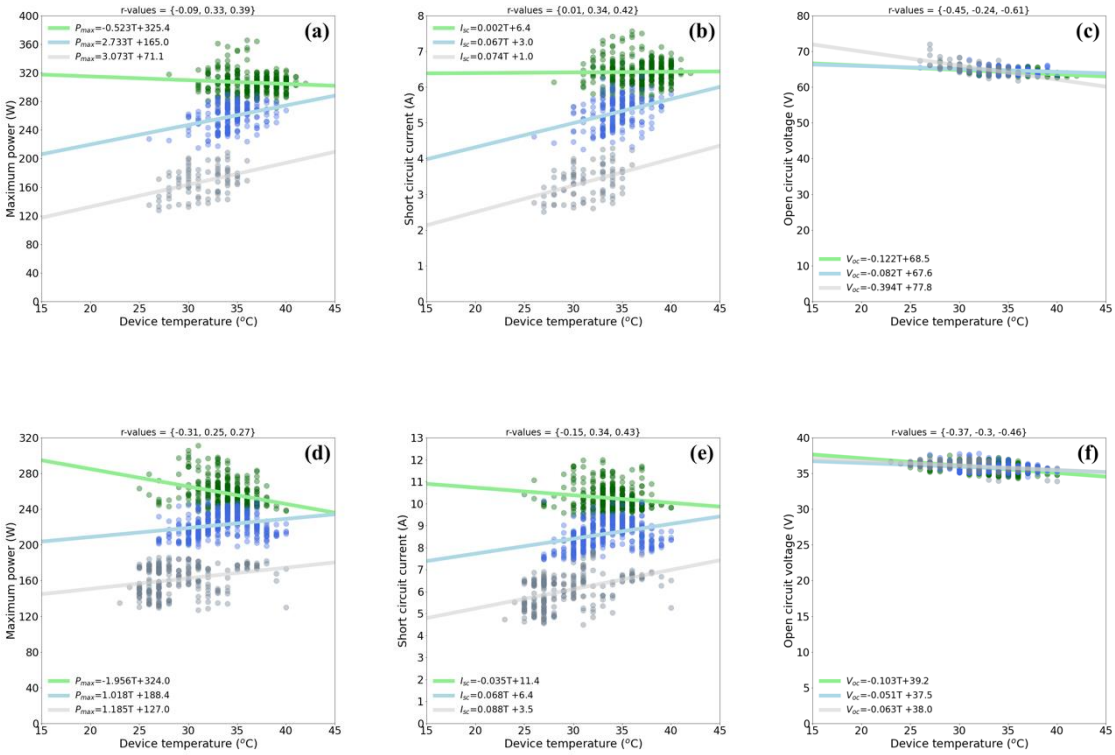

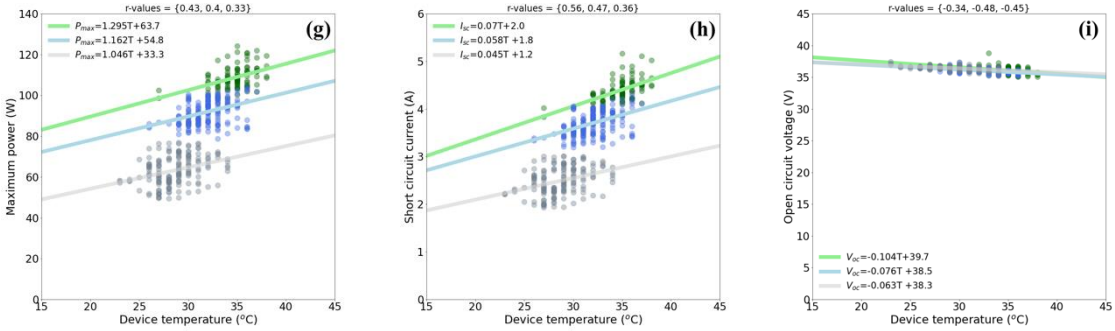

Fig S7. Temperature coefficients as a function of the ambient temperature. Panels (a-c) correspond to the HIT module, (d-f) to the m-Si module, and (g-i) to the CIGS module. Dot points correspond to the measured data, and lines correspond to the fits. The colors are correlated to the irradiance levels used in the estimation (green to 1000, blue to 800, and gray to 500 W/m^2). The fitted equations are shown in the inset. At the top are shown the r-values of the fits.

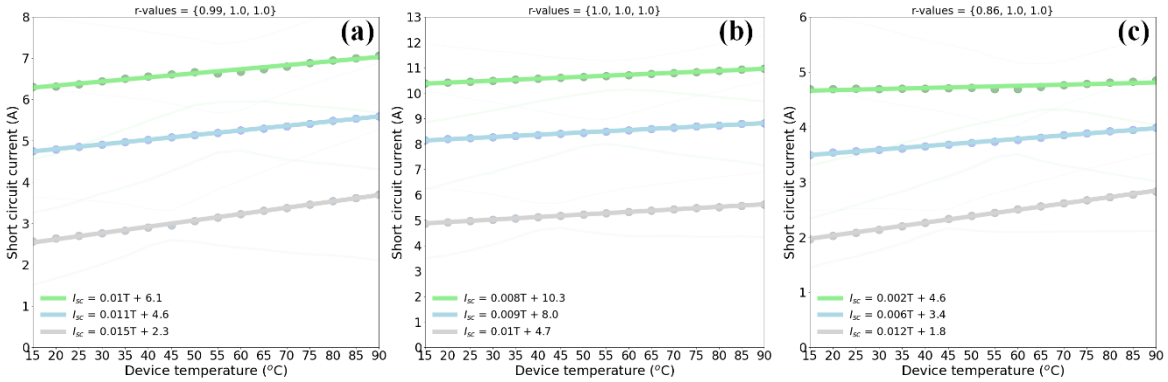

Fig S8. Estimated temperature coefficients for I_{sc} using the translation procedure. Panels (a) correspond to HIT module, (b) to m-Si module, and (c) to CIGS module. The color dot points correspond to the translated data, and color lines correspond to the fit. The colors are correlated to the irradiance levels used in the estimation (green to 1000, blue to 800, and gray to 500 W/m^2). The fitted equations are shown in the inset.

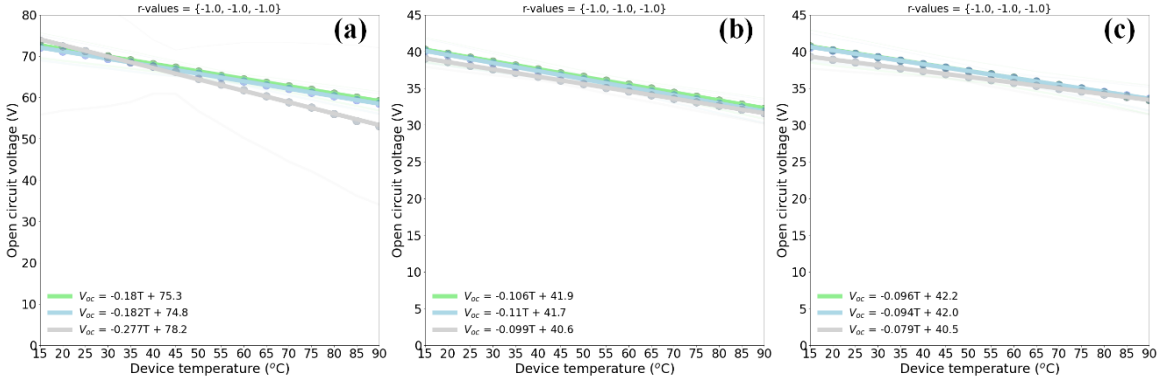

Fig S9. Estimated temperature coefficients for V_{oc} using the translation procedure. Panels (a) correspond to HIT module, (b) to m-Si module, and (c) to CIGS module. The color dot points correspond to the translated data, and color lines correspond to the fit. The colors are correlated to

the irradiance levels used in the estimation (green to 1000, blue to 800, and gray to 500 W/m^2). The fitted equations are shown in the inset.

Table S7. Parameters of the fitting processes using translation procedure for the estimation of P_{max} (δ).

PV Module	G (W/m^2)	Slope (W/^{o}C)	Intercept (W)	r-value
HIT	1000	-0.786	374.024	-0.995
	800	-0.399	279.256	-0.996
m-Si	1000	-1.049	327.766	-0.999
	800	-0.633	252.745	-0.997
CIGS	1000	-0.322	131.880	-0.999
	800	-0.248	107.927	-0.998

Anexo 6:

Photovoltaic Modules Series Resistance Estimation In Outdoor Conditions Using I-V Curves Data (Borrador)

Photovoltaic Modules Series Resistance Estimation In Outdoor Conditions Using I-V Curves Data

César Londoño[a,c], Juan Cano[a], Esteban Velilla[a,b], Jaime Valencia[a]

[a] *Grupo en Manejo Eficiente de la Energía - GIMEL, Universidad de Antioquia UdeA, Calle 70 No. 52-21, Medellín, 050010, Antioquia, Colombia*
[b] *Centro de Investigación, Innovación y Desarrollo de Materiales – CIDEMAT, Calle 70 No. 52-21, Medellín, 050010, Antioquia, Colombia*
[c] *Corresponding author: cesard.londono@udea.edu.co*

Abstract

abstract here.

Keywords: series resistance, outdoor tests, I-V Curves, solar panel
PACS: 0000, 1111
2000 MSC: 0000, 1111

1. Indroduction

Insert Introduction.

2. Methodology

2.1. Suns Voc Method

The Suns Voc Methodology consists into genarate a free-resistance IV curve ()

2.2. Real Time Series Resistance - RTSR

Method for determinate the series resistances of photovoltaic devices that applies the Suns Voc methodology for obtain the series resistance value at every operating point (Deceglie et al., 2015). To apply this method it is necessary to record the panel temperature (T_0), irradiance (E_0), voltage at specific operating point (V_0), current at specific operating point (I_0), open circuit voltage at specific operating point (Voc_0) and short circuit current

at specific operating point (Isc_0). Likewise, it is essential to mesure recents open circuit voltages at lows irradiances.

The I-V curve measured at (E_0, T_0) is translated into a suitable lower irradiance (E'_target) with the same temperature and where the produced current (I_2) is expected to be zero. This translation is carry out with the correction equation for current given in the IEC 60891 procedure 1 (ref IEC 60891 2020):

$$I_2 = I_0 + I_{sc}\left(\frac{E'_{target}}{E_1} - 1\right) + \alpha\,(T_2 - T_0) \tag{1}$$

Since the translation is made over the same temperature ($T_2 = T_0$), the temperature coefficient for current (α) is not involved, and by setting I_2 equals to zero, the previous equation is re arranged to:

$$E'_{target} = E_0\left(1 - \frac{I_0}{I_{sc,0}}\right) \tag{2}$$

The open circuit voltage of the new I-V curve translated at this suitable irradiance (V'_oc) corresponds to the voltage measured at E_o curve but assuming free series resistance ($R_s = 0$) (Suns Voc methodology). The difference between this ideal voltage assuming no series resistance (V'_oc) and the measured voltage (V'_o) is used to find the (R_s) with the ohm law:

$$R_s = \frac{V'_{oc} - V_0}{I_0} \tag{3}$$

To enable the algorithm to adapt to any change of performance in the module and obtain the time series, only the recent recorded points are used to calculate the R_s. In this sense, after E'_target is found for a given operational point (step 3), the database is filtered with only the measurements within a maximum of 10% deviation from the E'_target value, and also, only with the ones recorded in the previous 7 days of the operational point measurement date (step 4). After the filtering, some measurements with different temperatures than T_0 will be presented. Since the method requires to translate the I-V curve at same temperature T_0, a linear regression between V_oc and the temperatures of the filtered database is done (step 5). Using the regression equation, the V'_oc at T_0 is calculated (step 6). Finally, the predicted V'_oc is used to find the R_s of the operational point (step 7). Fig x illustrates an example of the regression process used to calculate the predicted V'_oc (indicated

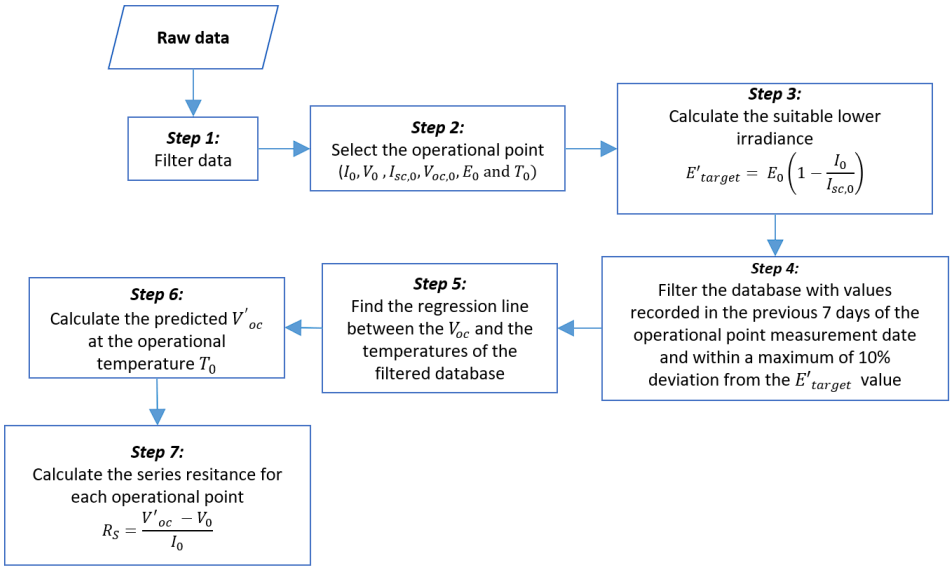

Figure 1: Flow chart for the calculation of the series resistance using the RTSR method

by the red cross) for a given operational point, where the blue points were measurements at the target irradiance but with different temperatures, thus, the regression line is used to predict the V'_oc at the measured temperature T_0 of the selected operational point.

2.3. Correcting I-V Curves

In order to be able to calculate and compare the value of series resistance troguth time, the corrective proposed method based on IEC was used. the behavior have a static operating point in wich the device series resistance

2.4. Proposed Methodology

The proposal ....

3. Results

In this section...

3.1. Data Measurement and Device Parameters

The IV curves were recorded by electronic devices based on capacitor technique to trace the curve (ref capacitor y monitoring). This devices were installed in the Solar Outdoor Laboratory (Figure 2). The IV curves and meteorological variables were measured every minute in time interval from 06:00 to 19:00 and store in a internal server data base which was later consulted.

Figure 2: Solar Outdoor Laboratory for characterization of photvoltaic devices in real operating conditions, Sede de Investigación Universitaria – SIU, Universidad de Antioquia, Medellín, Colombia

Table 1 shows the electrical parameters of the photovoltaic modules used in this work.

Technology	Reference	STC parameters
m-Si	Znshine solar ZX55(17.8)M	$I_{sc} = 3.34A$, $V_{oc} = 22.25V$, $I_{mpp} = 3.09$, $V_{mpp} = 17.8V$
CIGS	Miasolé FLEX–02 120N	$I_{sc} = 4.53A$, $V_{oc} = 38.1V$, $I_{mpp} = 3.93A$, $V_{mpp} = 30.5V$
m-Si	Sharp NU-RC290	$I_{sc} = 9.8A$, $V_{oc} = 39.3V$, $I_{mpp} = 9.25A$, $V_{mpp} = 31.3V$

Table 1: Solar devices under outdoor evaluation.

3.2. Series Resistance Calculation in Outdoor Conditions

Apply method to photovoltaic panels...

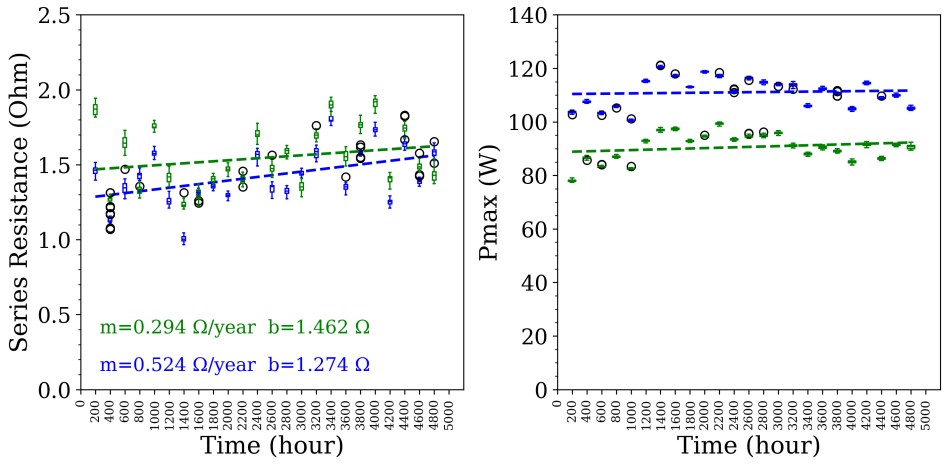

Figure 3: Panel (a) corresponds to Series resistance of CIGS 1 module at NOCT and STC conditions using the proposed methodology and panel (b) corresponds to Pmax estimated by the correcting I-V methodology

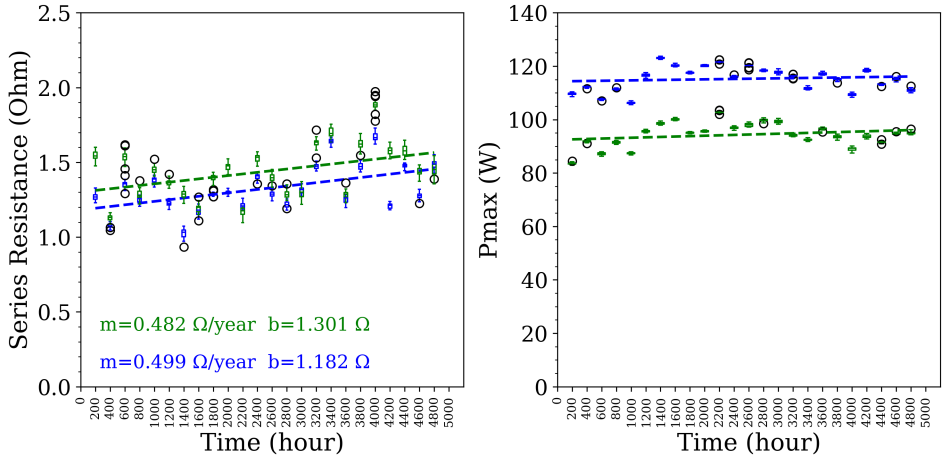

Figure 4: Panel (a) corresponds to Series resistance of CIGS 2 module at NOCT and STC conditions using the proposed methodology and panel (b) corresponds to Pmax estimated by the correcting I-V methodology

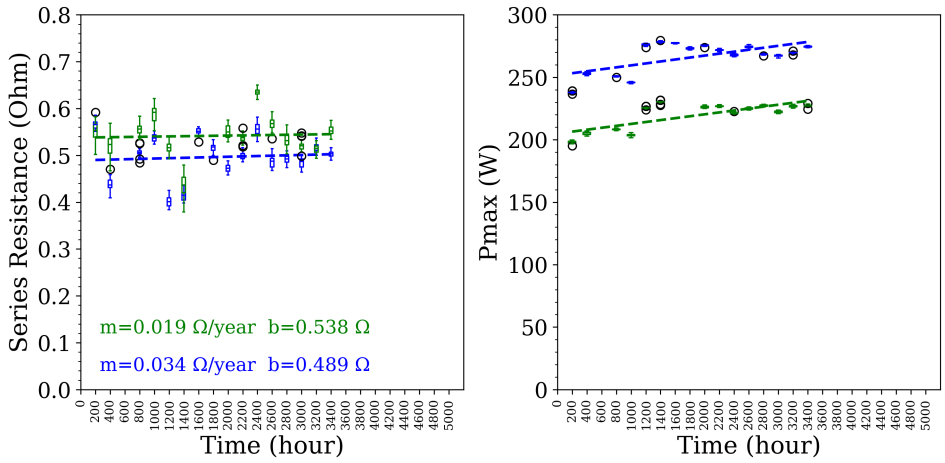

Figure 5: Panel (a) corresponds to Series resistance of Sharp module at NOCT and STC conditions using the proposed methodology and panel (b) corresponds to Pmax estimated by the correcting I-V methodology

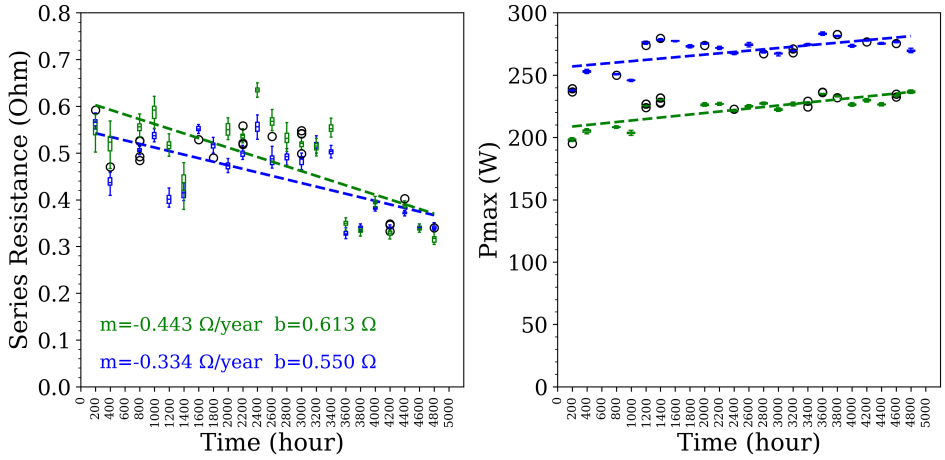

Figure 6: Panel (a) corresponds to Series resistance of Sharp module at NOCT and STC conditions using the proposed methodology and panel (b) corresponds to Pmax estimated by the correcting I-V methodology

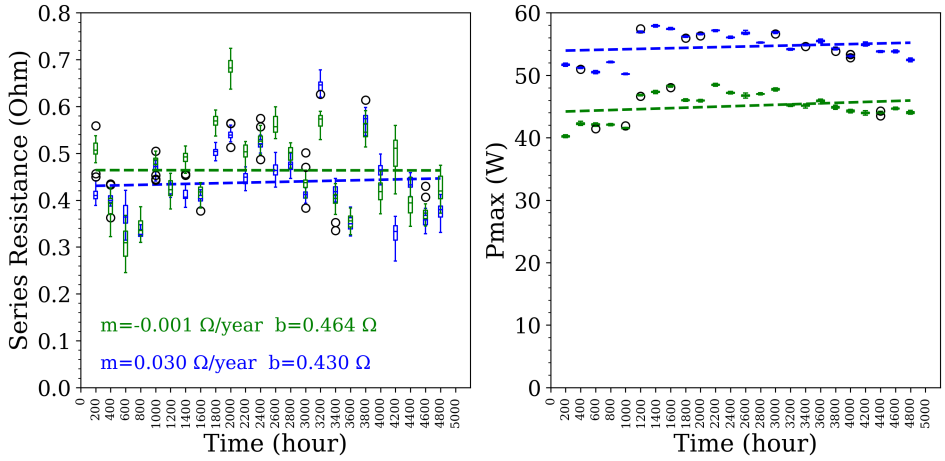

Figure 7: Panel (a) corresponds to Series resistance of Znshine m-Si module at NOCT and STC conditions using the proposed methodology and panel (b) corresponds to Pmax estimated by the correcting I-V methodology

4. Conclusions

Insert conclusions ...